Quantifying the Influence of Salt Marshes on Wave Run-Up on a Dike During Extreme Wave Conditions

An Experimental Study

S.H. Lakerveld

Delft University of Technology

Quantifying the Influence of Salt Marshes on Wave Run-Up on a Dike During Extreme Wave Conditions

An Experimental Study

by

S.H. Lakerveld

to obtain the degree of Master of Science
at the Delft University of Technology,
to be defended publicly on Monday 27th of May, 2024 at 11:00.

Student number:	4366247	
Project duration:	16th of January, 2023 – 27th of May, 2024	
Faculty:	Faculty of Civil Engineering, Delft	
Thesis committee:	Dr. Ir. A. Antonini,	TU Delft, supervisor
	Dr. Ir. B. Hofland,	TU Delft
	Ir. D. Dermentzoglou,	TU Delft
	Ir. J. R. M. Muller,	University of Twente

Cover: Flume setup used in the experiments, from within the flume

Abstract

Due to climate change, sea levels rise and extreme weather events are predicted to have a higher occurrence. Additionally, human activities near the coastline intensify and are expected to rise further in the coming decades, leading to an increase of the (financial) damages and consequences of flooding events. To mitigate these consequences, dikes that protect the lower-lying hinterland from flooding events need to be reinforced. Nature-based alternatives to dike management have gained interest worldwide. Salt marshes have been studied for their wave-attenuating effects and sea level adaptation, and provide a large variation of ecosystem services. Wave energy is dissipated on the salt marsh and the reduces the incoming wave energy at the dike. Vegetated foreshores were found to significantly reduce wave energy during severe storm conditions, with a reduction rate of the significant wave height ranging from 25 to 50% compared to the dissipation by wave breaking and bottom friction alone. The presence of vegetation contributed to wave energy dissipation, even for larger inundation depths and when vegetation was in a winter state. The rate of growth of a salt marsh can vary depending on the supply of sediment and the rate of accumulation of organic matter. In this way it can adjust to hydrodynamic changes, such as sea level rise. This natural adaptation occurring in salt marshes stabilize shorelines, which could be used as a nature-based solution to maintain the flood risk reducing functions, given that enough sediment supply is present.

As many tests have been conducted on the wave attenuation of salt marshes, there is only a handful of tests which have studied the interaction of a salt marshes and dikes. Wave flume studies show that when wave run-up measurements are compared with equations found in literature, they show substantial differences, as the bulk of their measurements have vastly lower relative wave run-up. These differences were contributed to the considerable foreshore, and shallow water conditions. Cases where water depth was lower than vegetation height were especially different, where non-linear interaction between waves, vegetation and dike is higher than for higher water depths / vegetation height ratios. Relative wave run-up height is lower than expected, when applying currently used equations. This results in an overestimation of wave run-up, causing current methods to be too conservative. Dikes are designed using extreme wave conditions that occur for instance once in 10000 years. Hence, it is necessary to determine if these diminishing effects of wave run-up can also be seen using larger water depths and wave heights, which occur during these extreme wave conditions. Moreover, the results measuring wave run-up under the influence of salt marsh vegetation using properly scaled mimics are inconclusive, it is not known if this behavior is test specific or a general trend. Furthermore, both studies do not take into account the cliff which can be formed at the interface of the salt marsh and unvegetated flood planes.

The analysis of wave run-up provides a direct means to understand the interaction between a specific wave climate and a dike, because changes in wave behavior correspond somewhat linearly with changes in run-up behavior. Given that wave run-up significantly influences overtopping behavior, which is integral to assessing the safety of modern dikes, describing wave run-up offers initial insights into the safety assessment of a dike adjacent to a salt marsh. Therefore, a comprehensive understanding of wave run-up behavior affected by high water levels on salt marshes is essential for robust dike design and safety assessments in coastal areas prone to storm surges. Hence, the objective of this thesis is to quantify the effectiveness of a salt marsh system on the run-up on a dike during extreme storm surge conditions and to quantify the differences of wave run-up behavior caused by the wave attenuation of salt marshes in comparison with what is predicted by literature.

To quantify this influence, physical model tests are conducted in a wave flume. The advantage of physical modeling is that processes which cannot be modeled using numerical methods can be investigated. However, a limited but controllable amount of factors of influence can be tested, as every aspect which is varied gives an increase in measurement time. Experiments were carried 39 x 0.8 m wave flume at the Hydraulic Engineering Lab of the Delft University of Technology. A piston-type wave maker is used to generate irregular wave states that travel along the flume. A similar model of a salt marsh cross-section with a homogeneous vegetation field, similar to previous studies, is made.

Waves travel over a wooden structure, consisting of three different parts: a foreshore (mudflat model); a flat horizontal salt marsh meadow made of about 48000 neoprene rubber shoots mimicking *Spartina alterniflora* and a dike with a slope 1:3.6. The model is scaled by 1/10, using the vegetation. The prototype vegetation is scaled down by preserving the Cauchy number, buoyancy number and blade length ratio. Several hydrodynamic states were ran for different combinations of water depth, wave height and wave steepness. These were ran for 6 different setups, which were made by combining the cases of 3 different cliff heights to the cases with and without vegetation applied.

The wave run-up is recorded by a stationary video camera placed above and parallel to the dike. A newly created algorithm, utilizing a moving window of three frames where the variance of pixel intensity is calculated for each pixel along the moving window, effectively isolated water movement from the slope; Where the water can be distinguished from the slope due to high contrast created between the two elements. It is calibrated and validated by comparing the obtained signal from a manually selected reference measurement which is generated from a sample of 470 waves, where the maximum water level across the width is manually selected for each frame. This resulted in an RMSE of 2-5mm. The local maxima obtained from the signal are used to calculate the wave run-up distribution. Wave characteristics are found by the usage of a Guza reflection procedure to split the signal into two parts consisting of an incoming and reflected signal. The incoming wave signal is used in the analysis of the waves and wave run-up.

Using the experiment data, the effect of salt marshes on wave run-up was assessed using water levels higher than the vegetation length. Wave run-up is reduced by the presence of a salt marsh, which is a result of breaking waves on the entire foreshore. The general amount of reduction is strongly dependent on the water level above the salt marsh and the incoming wave height. Similar to what is shown in literature, the influence of vegetation is non-negligible. It was observed that higher water depths for the same wave height without vegetation give almost no reduction, whereas only lower water depths give a reduction. However, when vegetation is included, all tested cases show an (additional) reduction in wave run-up for the same incoming offshore wave height and all water depths. If the results are linearly fitted, a conservative linear extrapolation of the results leads to no influence when water depth on the marsh over vegetation length ratio $d_m/l_s > 6$. Cases with water levels lower than this are affected by vegetation-reducing run-up for where every reduction in water level equal to one vegetation length reduces the run-up by 12.2%. The influence of a cliff on the reduction of wave run-up is dependent on the height of the cliff and the presence of vegetation. The presence of a small cliff (6cm) *without vegetation* has an insignificant influence on the wave run-up, but has influence for the large cliff (12cm). However, when vegetation is applied to cases with and without a cliff, the influence of the cliff becomes noticeable for both heights and becomes dependent on the incoming wave height and water level. This reduction is due to wave breaking at the cliff.

The measured wave run-up height of the dike which 2% of the wave run-up events exceeds $R_{u2\%}$, is compared to the predicted wave run-up using the TAW/EurOtop equation with incoming wave characteristics at the toe of the dike for cases with a water level on the salt marsh of 16mm and higher ($1.78 \leq d_m/l_s \leq 5.78$). Compared to the equation the measurements are mostly lower than predicted (RMSE 24mm for all tests and 27mm for tests with vegetation) and show to be less dependent on the increase in $\xi_{m-1,0}$ than predicted. Waves with an offshore peak wave steepness lower than 0.030 are predicted correctly, however, with an increasing steepness, the predicted values overestimate the wave run-up to 15%. Usage of $H_{1/3}$ instead of the requested H_{m0} in the equation gives results that align more closely with the measurements (RMSE 16mm for all tests and 21mm for tests with vegetation). Still, the influence of offshore peak wave steepness is present. When the Iribarren parameter is calculated using offshore wave characteristics for H_{m0} and $T_{m-1,0}$, and compared with the measured run-up divided by H_{m0} at the dike toe, the results align pretty close with measurements. This shows that the change in wave run-up over the salt marsh is mainly dependent on the change in wave height.

When comparing the measured wave run-up with van Gent's equation in a similar manner, the equation is less accurate. Using van Gent's equation based on $H_{1/3}$, the equation accounts better for the influence of offshore peak wave steepness. However, it under-predicts all tests without vegetation. It over-predicts cases with vegetation and higher Iribarren numbers. Using van Gent's equation based on H_{m0}, it under predicts the wave run-up for tests without vegetation, and shows similar behavior to the TAW/EurOtop equation for tests with vegetation.

The differences between wave run-up predicted using equations found in literature and measurements is most likely due to the influence of wave breaking on the salt marsh. This wave breaking results in a change in the wave spectrum. The vegetation increases wave breaking more than effects only due to the shape of the foreshore. Waves with a higher wave steepness break more than with a lower wave steepness. Hence only assessing wave run-up from the wave height H_{m0} and spectral period $T_{m-1,0}$ from the wave spectra obtained at the toe of the dike describe the current wave run-up behavior not fully accurately. The $R_{u2\%}/H_{m0}$ is lower for tests with higher wave steepnesses. Usage of $H_{1/3}$ gives a better fit, most likely because this parameter is more influenced by shoaling and breaking. The wave run-up exceedance distributions acquired from the measurements are also for tests with vegetation Rayleigh distributed. Hence, the fundamental behavior of the wave run-up is the same.

The wave set-up has not been assessed in this study. However, due to these aformentioned observations it can be deduced that the differences in wave run-up behavior could be mainly dependent on wave set-up. Wave set-up is included in the wave run-up equations, but as these equations are empirical, a significant lowering of wave set-up could give rise to an over-prediction by the equation, which was seen for cases with lower higher steepnesses.

An assessment of the influence of wave set-up and offshore wave steepness with a dataset containing multiple flume configurations is needed to see if this influence is present in general or unique to salt marshes. In this way, these insights can be applied to the specific case to accurately predict $R_{u2\%}$ influenced by a salt marsh. If it is not the case or preferable, three other ideas can be investigated, which show to increase accuracy of the wave run-up equation:

- Calculate $\xi_{m-1,0}$ as if there is no vegetation, even when vegetation is present.
- Adapt the calculation of $T_{m-1,0}$ by way of a lower integration bound, or application of a filtering technique to reduce the influence of certain range of the wave energy spectrum
- Replace H_{m0} with $H_{1/3}$ in the equation

More scenarios using other dike slopes, salt marsh lengths, and vegetation types/heights, can be added to investigate these proposed methods to calculate wave run-up further.

Preface and Acknowledgments

This thesis is the last part of my masters program Hydraulic Engineering (track of Civil Engineering), at the Delft University of Technology. After a request for help in physical modeling experiments, I started supporting Dimitris and Jos with the last preparations of the experiments, as they are quite labor intensive. We started building the whole experimental setup, testing everything and then conducting experiments in the hydraulic laboratory of the university. A small description about this is found in the appendix. This thesis is based on the measurements of these experiments, with a focus on hydraulic processes on the slope of the dike.

The experiments are part of the ‘Living Dikes – Realising resilient and climate-proof coastal protection’ project NWA.1292.19.257, funded by the Dutch Research Council (NWO). The project is led by Bas Borsje, Associate Professor of the University of Twente, which is thanked for the opportunity to delve into this research topic.

The goal of the Living Dikes project is to do research on the effects of salt marshes on flood protection, researching not only the physics, costs and benefits but also legal and governmental aspects of the implementation of salt marshes. If this is understood, these findings can be used to implement in real life cases in collaboration with Dutch water boards and eventually outside of the Netherlands as well. As flood protection with dikes is common in the Netherlands, the effectiveness of salt marshes in the reduction of the physical processes on dikes has direct cost and safety benefits.

The reader of this thesis report is to be expected to be familiar with general concepts, equations and methods related to hydraulic engineering, as commonly used terms in the field are not explained in depth.

The supervision and insightful remarks of Alessandro Antonini and Bas Hofland during the project are greatly appreciated. And the proofreading, help and support of Dimitris Dermentzoglou and Jos Muller during the experiments and the rest of the project are greatly appreciated.

As the experiments were conducted using physical modelling, the support of UTwente student Pieter Faber and the TU Delft technicians Pieter van der Gaag, Chantal Willems, Arno Doorn, Arie van der Vlies, Frank Kalkman and Jennifer Rodrigues Monteiro are appreciated for their help before and during the experiments as well.

To process all the data acquired during the physical experiments Python was used extensively. Jennifer Rodrigues Monteiro and Elmore Vaal are appreciated with their help with video calibration and process optimization in Python.

The staff and students helping during the construction of the salt marsh vegetation plates are thanked for their help. The secretaries of the department of hydraulic engineering at the TU Delft are thanked as well for their assistance during my time working on this project. Otti Kievits is thanked for the care of room 3.95 and interesting conversations during the project.

My fellow master students from room 3.95 (’masterhok’) working on their theses during the project duration are also thanked for bringing motivation, discussion and insights from an outside perspective.

At last my family and friends are thanked for their support during my entire studies.

S.H. Lakerveld
Delft, April 2024

Contents

List of Figures

List of Tables

Nomenclature

Abbreviations

Abbreviation	Definition
BWN	Building with Nature
DS	Displacement sensor
EMF	Electro Magnetic Flow meter
FFT	Fast Fourier Transform
IR	Irregular wave scenario
RMSE	Root mean square error
NAN	Not Any Number
NBS	Nature Based Solutions
SLR	Sea level rise
SU	Wave flume setup (configuration)
SWL	Still water level
WG	Wave gauge

Symbols

Symbol	Definition	Unit
a	coefficient used in equations	
A_w	wave orbital radius	m
b	coefficient used in equations	
B	Bouyancy number	
c	coefficient used in equations	
C	copy of a signal	
Ca	Cauchy number	
d	water depth	m
d_m	water depth on salt marsh	m
D	diagonal run-up signal	m
D_s	diameter of vegetation shoots	mm
$[EI]_s$	Flexural Rigidity	Nm^2
f	frequency	Hz
$f_{s,c}$	sampling frequency camera	fps
f_s, w	sampling frequency instruments	Hz
g	acceleration due to gravity	m/s^2
h_c	height of salt marsh cliff	m
$h_{c,vir}$	virtual height of salt marsh cliff	m
h_n	given height on a dike measured from SWL exceeded by wave run-up	m
H	wave height general use	m
$H_{1/3}$	average wave height of the highest 1/3 of the waves	m
H_{m0}	spectral wave height	m
H_s	significant wave height	m
I_{color}	intensity of a pixel for a given color	
KC	Keuler-Carpenter number	
l_s	length of vegetation shoot	mm

Symbol	**Definition**	**Unit**
L_0	wave length calculated assuming deep water conditions	m
L_B	blade length ratio	
L_c	characteristic length	m
L_{fs}	length of the entire foreshore	m
L_p	peak wave length	m
m	index	
m_n	n^{th}-order moment of wave spectrum	
M	total number of rows in an array / matrix	
n	index	
N	total number of columns in an array / matrix	
N_w	number of waves of a given test	
N_{ot}	number of overtopping eventts of a given test	
q_{fl}	average overtopping rate measured from first to the last overtopping event	mL/s/m
q_{tot}	average overtopping rate measured from first to the last incoming wave	mL/s/m
R_c	crest height of the dike	m
Re	Reynolds number	
R_u	wave run-up height general use	m
$R_{u2\%}$	wave run-up height exceeded by 2% of the incoming waves	m
s	wave steepness general use	
$s_{m-1,0}$	spectral wave steepness, calculated using assuming deep water conditions	
s_p	peak wave steepness	
t	time	s
t_{fl}	time measured from first to the last overtopping event	s
t_{tot}	time measured from first to the last incoming wave	s
T	wave period general use	s
$T_{m-1,0}$	spectral wave period	s
T_p	peak wave period	s
T_w	wave period used in scaling	s
u	velocity general use	m/s
U	Ursell number	
U_w	wave orbital velocity	m/s
V_{pm}	calculated total overtopping volume per meter	m^3/m
V_{tot}	measured total overtopping volume	m^3
w	probability of exceedance of wave run-up for a given dike level	
z	wave run-up signal measured vertically from SWL	m
Z	equivalent pixel index in wave run-up signal	
z_p	local maxima (peaks) of the wave run-up signal	m
$z_{p,corr}$	corrected local maxima (peaks of the wave run-up signal	m
α	Slope of the dike	°
γ_b	coefficient due to berm on a dike	
γ_f	coefficient due to frictional components on a dike	
γ_β	coefficient due to angle of incline of waves on a dike	
ϵ	wave steepness used by Thompson and Vincent (1985)	
ζ	wave run-up signal measured from SWL	m

Symbol	Definition	Unit
η	Median along the transverse direction (width) of the flume	
θ	angle of the (average) foreshore slope	°
ι	general use index	
κ_M	Threshold of run-up detection method in 1D	
κ_V	Threshold of run-up detection method in 2D	
μ	Mean of a given set	
ν	kinematic viscosity of water	Pa s
ξ	Iribarren parameter general use	
$\xi_{m-1,0}$	Iribarren parameter using spectral wave height and period	
ρ	Density water	kg/m^3
ρ_p	Density of the plant	kg/m^3
σ	Standard deviation of a given set	
σ^2	Variance of a given set	
τ	Mean of the variances of every color	
ω	Angular frequency	rad/s
$\square_i$	subscript depicting the numerical time index	
$\square_m$	subscript depicting the numerical row index (y-axis)	
$\square_n$	subscript depicting the numerical column index (x-axis)	
$\square_{nv}$	subscript indicating the variable is only taken no vegetated cases into account	
$\square_o$	subscript indicating that the variable is used at the offshore location	
$\square_t$	subscript depicting the variable at the toe of the dike	
$\square_{veg}$	subscript indicating the variable is taking only vegetation into account	
$\square_{target}$	subscript depicting the input variable at the wave maker, which was set as a target value during the experiment	

Terminology

Term	Meaning
dike crest	top of the dike
dike toe	point where the seaward side of the dike connects with the bottom
exceedance probability	probability that a given event exceeds the according value
foreshore	beginning at the seaward side of the mudflats until the toe of the dike
run-up 2%	used as shorthand for the level on the dike which is exceeded by 2% of the run-up events
mimic	a representation of a single or multiple plants, often scaled down to model size using several dimensionless numbers
salt marsh meadow	area where vegetation can be present on a salt marsh
wave run-up	the height measured from SWL an incoming wave reaches
wave overtopping	the amount of water that surpasses the crest of the dike for a given wave run-up event

1

Introduction

In this chapter, the background of this thesis is described and a general research topic is introduced (section 1.1). Following, the current literature about this topic is analyzed (section 1.2). The lack of information is addressed (section 1.3) and the objective of this thesis is stated (section 1.4). The research question is answered according to the structure given in section 1.5.

1.1. Background

Coasts are under the influence of waves and currents, which can cause flooding and erosion of shorelines. Due to climate change, coasts are subjected to *sea level rise* (SLR) and experience higher occurrence of extreme weather events such as storm surges, which increases the chance of flooding events (IPCC, 2023). Additionally, human activities near the coastline intensify and are expected to rise further in the coming decades, leading to an increase of the financial damages and consequences of flooding events (Neumann et al., 2015). Both increase the total financial risk, and as a result increase the consequences of flooding.

Sea *dikes* or *levees*[1] are structures that are commonly built in the Netherlands to protect lower-lying hinterland from flooding events. Due to the flooding risk rising in the coming decades, the level of safety will diminish if no changes are made. Hence, to keep the same level of safety in this lower-lying hinterland, dikes need to be heightened and reinforced. Recently, the Dutch Minister of Infrastructure and Water Management addressed the need of these measures to the parliament, which are needed to guarantee the same flood safety all around the Netherlands by 2050 (Harbers, 2023). The common way to reinforce these dikes is by heightening and applying a hard surface such as asphalt, blocks, natural stone, or concrete elements, so-called hard solutions. An alternative method in development is called *nature based solutions* (NBS) or *building with nature* (BWN). This method strategically leverages natural processes to effectively meet or sustain the specified sea defense requirements. Simultaneously, it enhances ecosystem services (improving the ecosystem) by improving water quality, promoting carbon sequestration, and fostering habitat creation (Spalding et al., 2014).

In coastal zones, *salt marshes* can be present. These are intertidal habitats consisting of vegetation, such as grasses and salt-tolerant plants, and are typically located in coastal areas such as river mouths, estuaries, deltas, back barrier lagoons, bays, natural embayments and sheltered areas behind islands and coral reefs. The salt marshes are coastal ecosystems that can be found globally in the aforementioned locations, usually outside of the tropics and in moderate climates. In more tropical regions mangrove forest are found in locations with similar conditions (Mcowen et al., 2017).

In the Netherlands salt marshes can be found at the outer side of dikes, and have a long history of use. Before human interventions, the Dutch coast consisted of dunes and salt marshes. In certain locations these marshes were reclaimed for agricultural use and especially for livestock farming, commonly done by the construction of dikes or drainage. Salt marshes were also used in the past for salt or peat extraction, with the latter resulting usually in the altering or drainage of the salt marsh (Knottnerus, 2005). Similar to the Netherlands, salt marshes in other parts of the world, such as the United States

---

[1] Both can be used interchangeably, the term dikes will be used in this thesis

(a) Salt marshes in the Westerschelde (near Rilland) (photo by Edwin Paree). The salt marsh is found outside the dike.

(b) Salt marsh cliff at Saeftinghe (photo by Jos Muller).

Figure 1.1: Characteristic features of salt marshes in the Netherlands.

of America and the United Kingdom, have been reclaimed for the same purposes as they make easy targets for conversion to arable land, coastal development and harbors (Gedan et al., 2009; Seabrook, 2012). Nowadays, many remaining salt marshes have been designated as protected zones or wildlife sanctuaries (UNESCO, 2023). They are valued as such because they serve as important nurseries for various species and provide nutrient cycling and detoxification (Barbier et al., 2011). As they form a transition zone between salt and fresh water, the vegetation and animal life have adapted to varying conditions regarding salinity and flooding.

Salt marshes can be characterized morphologically by a gently sloping vegetated terrain, intersected by a series of tidal channels that broaden and deepen as they move towards the sea (Davidson-Arnott, 2010). The boundary facing the sea can either have a gradual incline, transitioning seamlessly from the plant-covered surface to the adjacent mud or sand flat, or it might have a more distinct *cliff* with an abrupt transition (Brooks et al., 2021). This cliff can range from a few centimeters to a meter tall, over a horizontal distance up to several meters (Callaghan et al., 2010; Vuik et al., 2018). A form of zonation can be observed at the high salt marsh: where the inundation is less frequent and the submergence depths is relatively low, the of occurrence of inundation is less frequent and salinity can be lower in comparison with the pioneering zone which is flooded almost every tide. In front of this vegetated area, intertidal mudflats are present which cannot sustain vegetation. Due to these different conditions each zone is characterized by distinct dominant salt-tolerant species (Brooks et al., 2021). These include varieties of (cord-)grasses, rush and sea lavender. A remarkable species is Common cordgrass (*Spartina angelica*). This species is an unintentionally created hybrid made from *Spartina alterniflora* and *Spartina maritima* which is beneficial for sediment capture and soil stabilization. However, as it is an invasive species, it has displaced some native plant populations.

In Brooks et al. (2021) and Davidson-Arnott (2010) it is explained that coastal salt marshes can develop under a wide range of climatic conditions. The initial stage of salt marsh development starts with the accumulation of sediments. Estuarine and coastal areas accumulate sediments brought in by rivers or tides and tidal action helps transport and deposit these sediments. Over time, as sediment continues to accumulate, mudflats begin to form above the low tide level. These intertidal mud or sand flats are settled by (aforementioned) specific plants. These plants are not only salt-tolerant but can also withstand submergence for several hours at a time. These plants promote the settling of fine sediments and the gathering of organic material when they become established on the salt marsh.

Figure 1.2: De Schorren, Texel. This salt marsh is currently a nature reserve. The dike seperates the salt marsh from the protected hinterland. Several groynes can be seen at the edges (photo from Living Dikes archive).

This process results in the upward expansion of the emerging marshland and the interweaving of the tidal creek systems within the overarching salt marsh creek network. Due to this relationship between plants and sediment deposition, this process can be described as a positive feedback loop. The rate of growth of a salt marsh can vary depending on the supply of sediment and the rate of accumulation of organic matter. In this way it can adjust to hydrodynamic changes, such as SLR (Kirwan et al., 2016). This natural adaptation occurring in salt marshes stabilize shorelines, which could be used as a NBS to maintain the flood risk reducing functions, given that enough sediment supply is present. However, they can be threatened by factors such as SLR, if the rate exceeds sediment deposition, human disturbances (e.g., reclamation, pollution), and invasive species (Gedan et al., 2011).

The morphology and vegetation characteristics of salt marshes contribute to the dissipation of wave energy within the salt marsh environment (Möller et al., 2014). Foreshores always contribute to wave attenuation under regular and extreme design storm conditions. During regular daily conditions, vegetation decreases both wave energy and its variability. During the extreme design storm conditions, foreshores sheltered from prevailing wind directions were more efficient in wave attenuation than exposed shores (Bouma et al., 2014). Moreover, the additional contribution of the vegetated salt marsh appeared to be positively correlated with marsh width. When a dike adjacent to a salt marsh is breached, the morphology and vegetation of a salt marsh have an additional effect. The salt marsh contributes to a decrease in the volume of water flowing through the breach. Consequently, this will reduce the erosion rate of a dike. This reduction in erosion rate, in turn, lowers the inundation rate of the hinterland. The flow through the breach ceases when the water level falls below the salt marsh surface level (Schoutens et al., 2022; Zhu et al., 2020).

The aforementioned literature highlights that salt marshes provide numerous benefits and have the potential to be utilized as a coastal defense. This prompts the question of how to quantify their effectiveness in flood defense, by reducing loads on adjacent dikes, and integrate them into design standards and risk calculations.

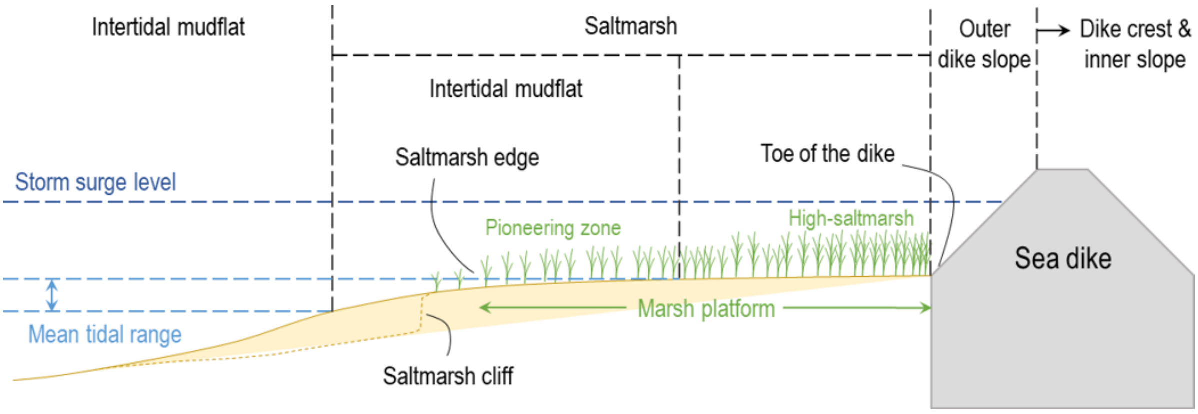

Figure 1.3: Schematic description of a mudflat, salt marsh system with an adjacent dike (by Jos Muller)

1.2. Literature

In recent years, research has been conducted to quantify the effects of wave attenuation, overtopping and run-up, eroding effects of salt marshes.

In Vuik et al. (2016) an overview of wave attenuation studies conducted until the paper's writing date are given. Moreover, their own observations were added to increase the highest range of wave heights and water depths reported in the literature, reducing the gap between measured conditions and design conditions for flood defenses. Using numerical modeling based on these observations, the wave attenuation by vegetation was quantified under severe storm conditions. Vegetated foreshores were found to significantly reduce wave energy during severe storm conditions, with an additional reduction rate of the significant wave height ranging from 25 to 50% compared to the dissipation by only wave breaking and bottom friction on the sloping transects. The presence of vegetation contributed to wave energy dissipation, even for larger inundation depths and when vegetation was in a winter state. In Willemsen et al. (2020), these insights were expanded by including data of a longer time span (65 years, Westerschelde estuary) to model the dynamics of foreshores in an estuary over a decadal time scale. The study investigated various aspects of foreshore width, marsh width, temporal and spatial variability, vegetation effects, and wave attenuation across different conditions. The mean values and temporal variability of the total foreshore (including mudflats) remained relatively constant over time, however the width of the salt marsh did not follow the same dynamics, with temporal variability increasing initially but flattening out over the long term. It was found that wave attenuation was greater per meter of salt marsh at sheltered shores, despite their shorter width, in comparison with exposed shores. Foreshores with smaller widths and steeper profiles demonstrated larger long-term effectiveness of wave attenuation under design conditions. Tidal flats provided a baseline wave attenuation under all circumstances, while a linear relationship was found between wave attenuation and the width of the salt marsh, with longer marshes leading to greater attenuation. In Maza et al. (2022) the hydraulic standing biomass variable was introduced, defined as a function of the mean meadow height, the standing biomass and the incident flow characteristics. This variable was found to have linear relationships with the wave damping coefficient, and can be used for a direct quantification of wave attenuation from field observations.

Dikes have been studied extensively under an assortment of conditions, in order to get a sufficient design and make adequate risk assessments of the adjacent hinterland (summarized in EurOtop (2018)). In comparison with dikes surrounding lakes and rivers, sea dikes are less exposed to large head differences, hence, wave attack[2] and overtopping are the more dominant forces. Wave run-up and overtopping are the most commonly used variables to determine total dike dimensions, where wave attack is used to determine the of armoring layer at the outside of dikes. The rate of overtopping is used as a design parameter, where the quantity of the water volume, in combination with the speed at which the running up wave travels, determines the given load of the overtopping wave on the inner slope, which is often the weakest part of a dike. In the past, wave run-up was used in the same manner, as it can give an indication of the volume of water present above a certain height (TAW, 2002; Van Gent,

---

[2] This means in this case, the interaction of waves with the outside slope of the dike

1999a, 1999b). It is common to use the height which is exceeded by 2% of the incoming waves transformed into wave run-up to design (Dutch) dikes for irregular sea-states, where the equations defined in TAW (2002) are used in calculations [3].

Overtopping equations which can be found in e.g. EurOtop (2018) and TAW (2002), commonly used to determine the dimensions of modern dikes, are expressed in a form of average discharge over time q. An analysis of the way overtopping damages inner slopes shows that large overtopping volumes and velocities lead to higher forces on these inner slopes, leading to more damage and eventually dike failure. The average discharge is therefore used as a *measure* of overtopping, instead of describing the actual volumes that lead to failure. The individual volumes are assumed to follow a two parameter Weibull distribution (TAW, 2002). The probability of overtopping per wave is dependent on the run-up, which has a Rayleigh distribution (Battjes, 1974). A given average discharge can consist of overtopping caused by a large amount of small waves, or a couple large overtopping quantities, the latter of which is substantially more damaging than the former. Damage to grass slopes behave in a way similar to fatigue. So for an accurate description of inner slope damage loads, a description of cumulative load based on larger overtopping quantities is needed (Schiereck & Verhagen, 2012).

Wave run-up and overtopping equations make use of the spectral wave height and wave period. This spectral wave period $T_{m-1,0}$ has been accepted as a characteristic period when describing the interaction between sea waves and coastal structures. It is commonly used to describe many processes like wave run-up, overtopping, reflection, and armor layer stability, especially when the structure has a shallow foreshore. In contrast to the reduction in wave height, such as the aforementioned attenuation studies, Hofland et al. (2017) presented a prediction formula of the change in $T_{m-1,0}$ over mildly sloping shallow foreshores. This study was based on wave flume tests, in combination with numerical modeling. However, the extend of the range of validity of the formulations for e.g. slope irregularities and spectral peak width is not known yet.

As many tests have been conducted on the wave attenuation of salt marshes, there is only a handful of tests which have studied the interaction of a salt marshes and dikes, see table 1.1.

Table 1.1: Overview of wave flume tests conducted on salt marsh and dike interaction. d_m/l_s is inundation depth above the salt marsh meadow bottom over the length of the modeled vegetation shoots

	Keimer et al. (2021)	**Maza et al. (2023)**
model scale	1:10	est. 1:1 - 1:2
mimic material	PVC	PA
varied parameters	vegetation height, meadow length	meadow length
d_m/l_s	1 - 4	0.6 - 1.4
wave type	mostly regular waves	irregular waves
dike slope	1:6	1:2, 1:3, 1:5
$\xi_{m-1,0}$	$0.54 - 3.8$	$2.0 - 6.5$

In Keimer et al. (2021), the experiments focus was to gain a better understanding of wave transformation processes and to determine important parameters. The mechanical properties of the vegetation model, such as elastic forces and the dynamic behavior under wave action, were not considered for a specific plant species and regular waves were used. This was done as the tests were exploratory of nature, so many dimensional parameters of influence were varied. They found a difference of 0.48% in the resulting wave run-up height which was exceeded by 2% of incoming waves, when JONSWAP[4] waves and regular waves were compared. Comparison of wave run-up measurements with the equations found in EurOtop (2018) based on TAW (2002), show substantial differences, as the bulk of their measurements have vastly lower relative wave run-up. These differences were contributed to the considerable foreshore, and shallow water conditions. Measurements show an absolute mean wave run-up reduction due to foreshore vegetation of 9.6%. Where the median values of the run-up reduction varies from 2.3% at high water levels 4 times the vegetation height, up to 16.5% at 1 times the vegetation height. Increasing wave attenuation was observed with larger vegetation heights, but also the decreasing influence of vegetation on wave-related foreshore processes with higher submergence including some scattering due to model and potential scale effects.

---

[3] The usage of the 2% value has historical reasons, which results from limitations in testing methods. See also appendix G

[4] Wave Energy Density spectrum of a not fully developed wave climate, based on the Pierson-Moskowitz spectrum and observations of the North Sea

In Maza et al. (2023), a set of experiments is described, where instead of using wave reflection analyses, the value of incident wave height at the toe of the structure was obtained by the usage of a numerical model. Preliminary analysis shows that obtained results do not agree with EurOtop (2018), similar to Keimer et al. (2021). Cases where water depth was lower than vegetation height were especially different, where non-linear interaction between waves, vegetation and dike is higher than for higher water depths / vegetation height ratios. Relative wave run-up height is lower than expected, when applying currently used equations. This results in an overestimation of wave run-up, causing current methods to be too conservative.

Besides these laboratory tests, some field measurements were conducted of wave run-up by measuring flotsam (Marin-Diaz et al., 2023; Post, 2015), and are still being conducted (Living Dikes WP3).

In conclusion, the literature reviewed provides an understanding of the effects of salt marshes and foreshores on wave attenuation, as well as wave behavior with dikes. However, despite the valuable insights gained from these studies, several gaps and unresolved issues remain. These gaps form the foundation for the problem statement and the scope of the present research.

1.3. Problem statement

Wave attenuation has garnered significant attention in literature (Maza et al., 2022; Vuik et al., 2016; Willemsen et al., 2020), owing to the fact that an accurate description and understanding of wave behavior over the salt marsh can predict interaction at salt marsh interfaces such as a dike. As dikes are crucial in guaranteeing safety of the hinterland, an accurate prediction in wave run-up levels is of importance. The analysis of wave run-up offers a straightforward way to comprehend the interaction between a specific wave climate and a dike, because changes in wave behavior correspond somewhat linearly with changes in run-up behavior (Battjes, 1974). As wave run-up has a large influence on the overtopping behavior, the latter of which is used to assess the safety of modern dikes, the description of wave run-up can provide proper first insights towards a safety assessment of a dike adjacent to a salt marsh.

However, recent studies on wave run-up behavior influenced by a presence of a salt marsh (Keimer et al., 2021; Maza et al., 2023) have challenged conventional understanding by demonstrating that wave run-up does not behave as expected as given in EurOtop (2018) and TAW (2002), even when wave characteristics at the dike toe are known. Moreover, the interpretation of results measuring wave run-up affected by salt marsh vegetation using scaled mimics remains inconclusive, raising questions about whether observed behaviors are test-specific or indicative of broader trends.

While Keimer et al. (2021) pursued a more exploratory approach, encompassing a broader range of water depths, the experiments detailed in Maza et al. (2023) focused solely on lower mean sea levels, reflecting their higher frequency of occurrence. However, it is imperative to consider wave conditions during higher mean water levels in dike design. Extreme storm events can lead to elevated water levels due to wind and wave setup, resulting in linear increases in wave run-up, particularly during high tides. Consequently, there exists a notable knowledge gap regarding wave run-up influenced by salt marshes under higher water levels, crucial in the assessment of the safety of the hinterland protected by these dikes. Furthermore, both studies overlook the influence of cliffs present at the interface of salt marshes and unvegetated flood plains, revealing another gap in understanding.

Models featuring a uniform vegetation field have demonstrated the potential for yielding insightful results. However, incorporating prevalent salt marsh features such as channels and gullies introduces additional complexity, which could hinder understanding of the effects of vegetation and the cliff. Hence, the scope of the this research is limited to the influence of vegetation and a cliff. These complexities and incorporating features like channels and gullies could be considered in future research steps.

1.4. Objective

Given the lack of understanding around these aforementioned wave run-up related aspects, the objective of this thesis is to quantify the effectiveness of a salt marsh on the run-up on a dike during extreme storm surge conditions and to quantify the difference on run-up behavior caused by the wave attenuation of salt marshes. This can be formulated into a research question and subdivided into sub-questions:

> *How does a salt marsh affect the run-up of a dike during extreme storm conditions and how does this compare with the literature?*

- What is the absolute reduction in wave run-up due to the salt marsh?
- Are the equations found in literature valid using tested conditions?
- Is there a change in wave run-up behavior due to the salt marsh?

1.5. Thesis structure

The process to assess these questions is presented in Methodology chapter 2, of which the results of the processes described in the methodology is shown in Results chapter 3. This will be argued and contextualized in the discussion chapter 4. The objective of the thesis will be assessed and sub-questions and research question will be answered in the Conclusion chapter 5, which finishes with recommendations that follow from the performed study section 5.2.

2

Methods

To answer the main objectives of the study, an experimental laboratory test campaign is conducted, described in section 2.1. Physical modeling offers advantages over numerical methods by allowing the investigation of processes that may not be accurately modeled numerically. Despite this advantage, physical modeling imposes constraints on the number of factors that can be varied due to increased measurement time for each aspect altered.

The data acquired by the instruments during the experiments are processed for analysis. In section 2.2, the theory to calculate wave characteristics from the signals is described. The wave run-up is measured by a non-intrusive method, after which the acquired run-up signal is processed, as described in section 2.3. The latter is then converted to several metrics such as the run-up height section 2.3.3.

2.1. Experimental setup

The experiments are carried out at the wave flume of the Laboratory of Hydraulic Engineering of the Delft University of Technology. The flume is 39m long, 79.5cm wide and 105.5cm high. On one side, the flume is equipped with a piston-type wave generator (figure 2.1) which is able to generate regular and irregular wave states. The wave generator is equipped with an active reflection compensation, which is able to absorb 90% of the reflected wave energy.

2.1.1. Physical model

A wooden[1] scaled model representing a cross-section of a salt marsh system is constructed and installed in the wave flume. This is scaled following a Froude similarity and a scaling ratio of 1/10. The model comprises three different parts:

1. a foreshore representing mud-flats with two parts, one with a steep (1:9) slope 1.35m long, and a second with a mild (1:45) slope 4.05m long, which reaches a final height of 0.24m relative to the flume bottom;
2. a horizontal platform representing a salt marsh meadow changing among 6.88m, 7.10m and 7.31m between set-ups[2];
3. a dike with a slope 1:3.6 and a crest height of 1.15m relative to the flume bottom, with an overtopping box equipped at the back.

During these experiments, focus was given to the investigation of the cliff at the salt marsh edge and salt marsh vegetation on local hydrodynamics. For this reason, six different set-ups are used for these experiments. The salt marsh platform is placed 0.24m, 0.30m and 0.36m above the flume bottom. As the sloped foreshore has a 0.24m height at the interface with the salt marsh, this forms a step representing a cliff with a height h_c of 0, 6 and 12cm respectively. These values are decided based on cliff height variability found in the field (see section 1.1). These three set-ups (SU) are tested without (SU1-SU3) and with vegetation (SU4-SU6) (see table 2.1) for several wave scenarios.

---

[1] Shuttering plywood

[2] As a result of the heightening of the salt marsh platform, the marsh platform is also elongated to form a close connection at the dike toe.

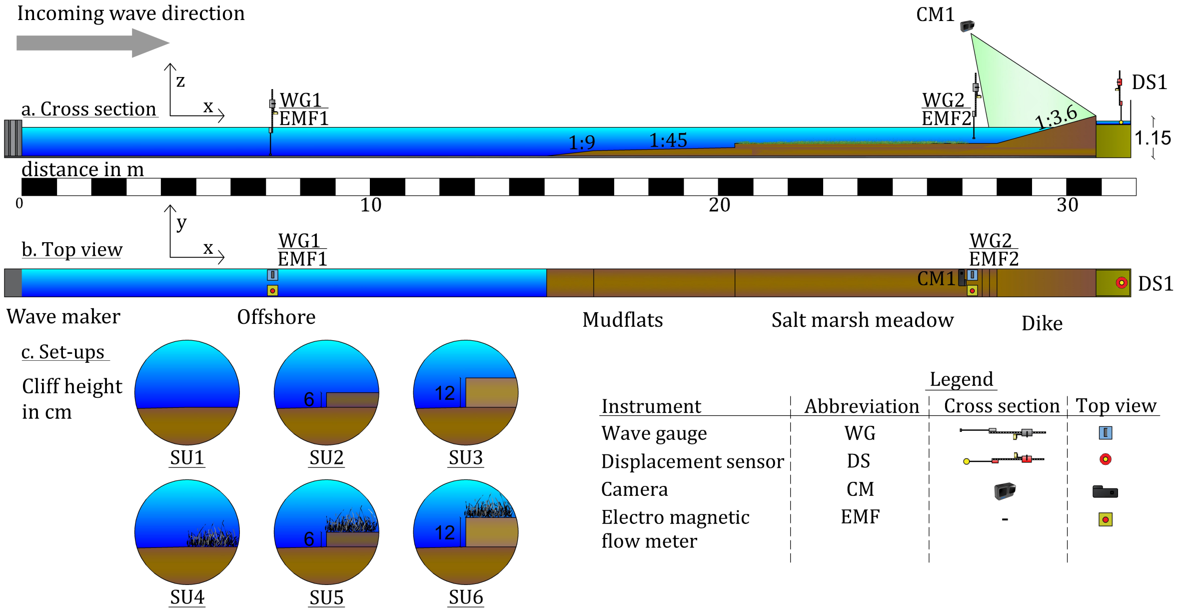

Figure 2.1: Schematic drawing of the physical model used in the wave flume representing a cross-section of a foreshore with mudflats, horizontal salt marsh meadow and a dike, including instruments. Different configurations (SU) are displayed in the bottom left. The incoming waves travel from left to right from the wave maker over the model and reflect at the dike. (Large version: appendix A)

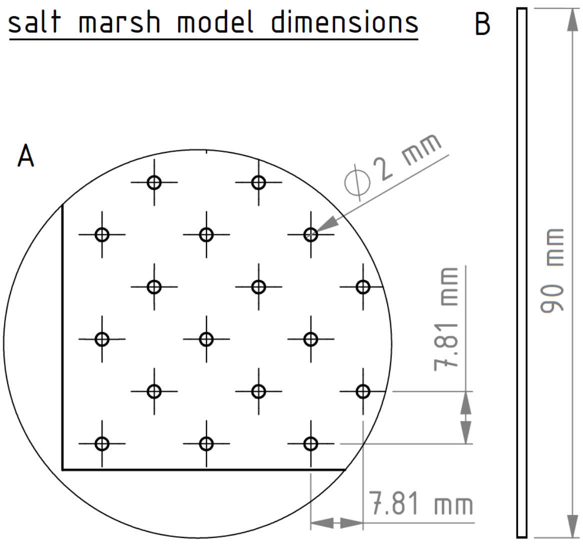

Figure 2.2: Schematic drawing of salt marsh model vegetation plates dimensions. **a.** Pattern of vegetation plates. **b.** Stem length, 2mm diameter. (Large version: appendix A)

Table 2.1: Used variations of flume model configurations. h_c is the height of the cliff at the interface of the foreshore and salt marsh, which is made by heightening the marsh model

ID	h_c[cm]	*vegetation*
SU1	0	no
SU2	6	no
SU3	12	no
SU4	0	yes
SU5	6	yes
SU6	12	yes

Table 2.2: Testmatrix of all wave conditions. The ID depicts the wave conditions which are used as input in the wave maker. IR01 is not used during in this thesis. Depth on the salt marsh meadow d_m is measured from the bottom of the meadow (figure 2.6). e.g. IR02 represents the condition that the water level is just higher than the top of the vegetation. d_o is the water depth at the wave generator (offshore conditions). A corresponding ID for the runs of $h_c = 6$cm and 12cm, performed on the setups with $h_c = 0$cm is given in the 3rd column of their respective wave conditions. IR01 is not used in the wave run-up analysis as $d_m = 0$. A more extensive table is given in table F.2

	shared conditions			$h_c = 0$cm		$h_c = 6$cm		$h_c = 0$cm	$h_c = 12$cm		$h_c = 0$cm
ID	d_m[cm]	H_s[cm]	$s[\%]$	d_0[cm]	T_p[s]	d_o[cm]	T_p[s]	$h_{c,vir} = 6$cm	d_0[cm]	T_p[s]	$h_{c,vir} = 12$cm
IR01	0	8	4	24	1.42	30	1.32	IR10	36	1.26	IR19
IR02	10	12	4	34	1.77	40	1.68	IR11	46	1.61	IR20
IR03	25	14	4	49	1.78	55	1.72	IR12	61	1.68	IR21
IR04	25	14	3	49	2.27	55	2.18	IR13	61	2.10	IR22
IR05	25	14	5	49	1.50	55	1.46	IR14	61	1.43	IR23
IR06	40	10	4	64	1.32	70	1.30	IR15	76	1.29	IR24
IR07	40	12	4	64	1.48	70	1.46	IR16	76	1.44	IR25
IR08	40	14	4	64	1.66	70	1.62	IR17	76	1.60	IR26
IR09	40	16	4	64	1.83	70	1.79	IR18	76	1.76	IR27

Vegetation field

As described in chapter 1, salt marshes consist of a variety of species, meaning that it is quite tough to realize a representative scaled model with mimics. In addition, there is also a high variability in the same species, in terms of mechanical properties (plant elasticity, length, etc). Therefore a single species *Spartina Anglica* has been chosen as the prototype vegetation for this experiment, very common in UK and Dutch coasts. To represent this species, a meadow was constructed made of neoprene shoots with a $D_s = 2$mm diameter and are $l_s = 90$mm long, and have a shoot density of 8100 shoots/m^2. The neoprene shoots are applied in a grid, see figure 2.2. The vegetation is scaled with a Cauchy number, blade length ratio, buoyancy number similarity (Lei & Nepf, 2019; Zhang & Nepf, 2021) and total drag force on the plant. The Reynolds number and Keulegan-Carpenter (KC) change in the scaled model in comparison with *Spartina Anglica* found in reality, which could impose scaling effects. These dimensionless numbers are explained in Box 2.1.

Box 2.1: Dimensionless numbers

Dimensionless numbers are used to describe certain processes, most of the time obtained from differential equations (Buckingham Pi-theorem) or balance equations (Schiereck & Verhagen, 2012). They are used in physical modeling to scale down properly a certain physical process in a scaled physical model, as the behavior of the governing differential equation is the same.

$$\text{Cauchy number} \quad Ca = \frac{\text{hydrodynamic drag force}}{\text{elastic/restoring force}} = \frac{\rho b U_w^2 l_s^3}{[EI]_s/l_s^2} \tag{2.1}$$

$$\text{Buoyancy number} \quad B = \frac{\text{buoyancy}}{\text{elastic/restoring force}} = \frac{\Delta\rho g b d l_s^3}{[EI]_s} \tag{2.2}$$

$$\text{Blade length ratio} \quad L_B = \frac{\text{blade length}}{\text{wave orbital radius}} = \frac{l_s}{A_w} = \frac{l_s \omega}{U_w} \tag{2.3}$$

$$\text{Reynolds number} \quad Re = \frac{\text{inertial force}}{\text{viscous force}} = \frac{u L_c}{\upsilon} \tag{2.4}$$

$$\text{KC number} \quad K_C = \frac{\text{drag force}}{\text{inertial force}} = \frac{U_w T_w}{b} \tag{2.5}$$

Here, $\Delta\rho = \rho{-}\rho_p$ is the density difference between water (ρ) and plant (ρ_p). g is the gravitational acceleration. b, d, and l are the width, thickness, and length of the blade, respectively. U_w is the wave orbital velocity, E is the elastic modulus and $I = bd^3/12$ is the second momentum of inertia, which combine into EI which is the flexural rigidity of the vegetation. $A_w = U_w/\omega$ is the wave excursion (wave orbital radius), and ω is the wave angular frequency.

Experimental scenarios

Each of the model configurations is tested with 9 scenarios, varying the water depth on the salt marsh d_m, wave height H_{m0} and wave steepness s (the last two are defined as the input for the wave generator), all using intermediate wave conditions.

Additionally, setups without a cliff (SU1, SU4 with $h_c = 0$cm) are used as references to compare with the various cliff heights. This approach allows for the isolation of the cliff's effect. Therefore, the hydrodynamic conditions under which setups with a cliff are tested are also applied to the tests without a cliff (SU1 and SU4). In the case of SU1 and SU4, the hydrodynamic conditions of $h_c = 6$cm (SU2 and SU5) and $h_c = 12$cm (SU3 and SU6) are included (referenced as virtual cliff height $h_{c,vir}$), resulting in a total of 27 scenarios for these setups. This leads to a grand total of 90 different tests that need to be conducted (for a full table see table F.2). Due to manual or measurement errors of one of the sensors, some tests were reran. For the tests with multiple runs where all data used in this thesis are correct, are used in the results as well.

(a) Dry salt marsh, a WG (left) and EMF (right) are visible

(b) Inundated salt marsh

Figure 2.3: Photos taken at the salt marsh model looking towards the dike. The wave flume is filled to different water levels.

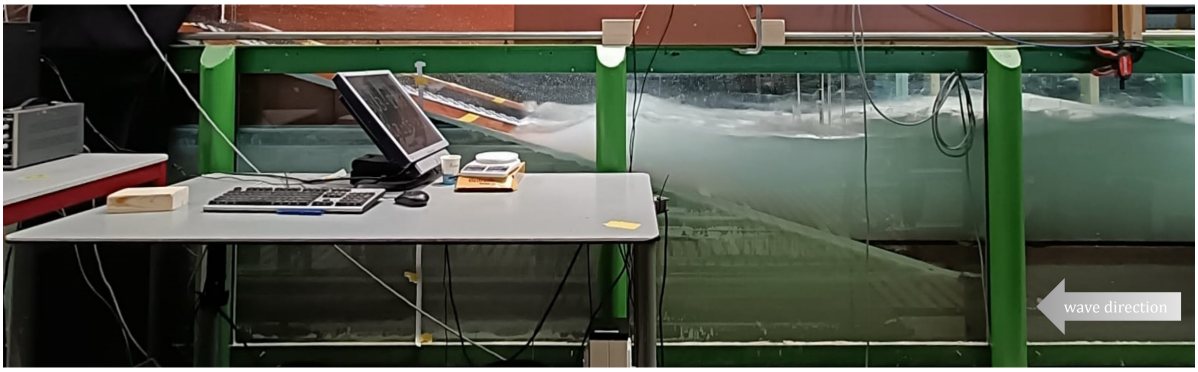

Figure 2.4: View from the side of the dike. The dike slope can be seen in the wave flume with a wave coming in from the right of the picture just before breaking on the dike slope

Figure 2.5: A small plate of modeled vegetation (mimics) used in experiment representing salt marsh vegetation. The vegetation moves with the waves. See also appendix A

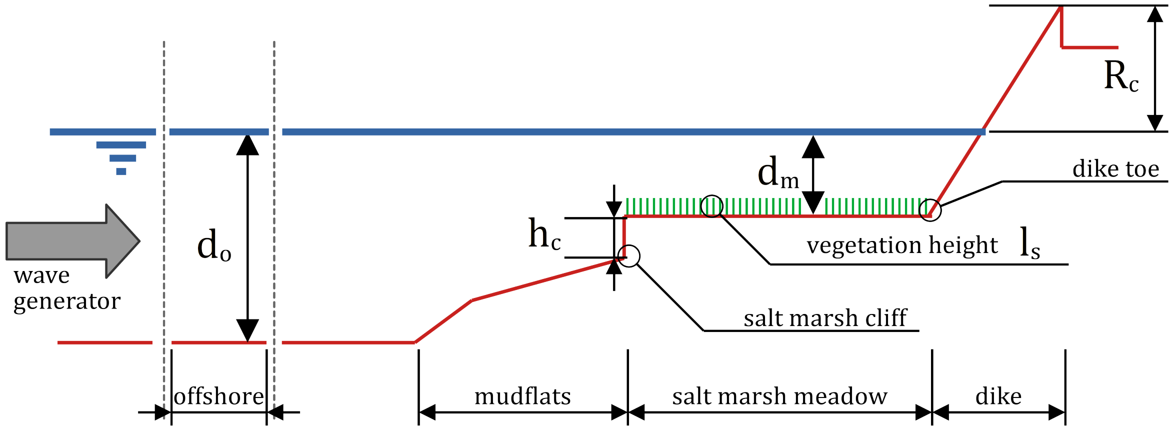

Figure 2.6: Schematic drawing of the construction in the wave flume. Definition of commonly used terms and variables used in this thesis. Furthermore, $d_c = d_m + h_c$ and $d_o - h_c - d_m = 0.24$m

2.1.2. Instruments

A GoPro Hero 10 Black *camera* is used to capture footage of the run-up of the slope of the dike. This camera was chosen because it is lightweight and usable in wet environments. The camera is set to have a frame rate $f_{s,c}$ of 24 fps[3], set in linear lens mode and set to a resolution of 1920x1080 pixels, all together have a high enough time step and pixel density for accurate results in comparison with the storage required. The camera is positioned 2.69m from the bottom of the flume, 28.66m from the reference point (wave generator), angled parallel to the slope of the dike. On the slope of the dike, a reference chessboard pattern of 2.5x2.5cm squares is placed for the calibration of the video data. Besides this a matte black area is placed, which has a low light reflection, see figure 2.3. The Go-Pro cuts the video footage in parts of around 12 minutes (depending on file size), the data obtained from the footage is joined together in the processing.

Nine *Wave gauges* (WG) are positioned along the the flume to measure the water level. The wave gauges are calibrated regularly to take effects such as temperature differences into account.

Eight *Electro Magnetic Flow meters* (EMF) are paired with wave gauges at multiple positions along the flume in order to record the orbital velocity, see figure 2.1. across the salt marsh, pairs of EMFs are placed at three distinct positions. One at 8cm from the salt marsh surface, and the second at half of the water column above the salt marsh platform ($d_m/2$).

A magnetic *displacement sensor* (DS) is used to record the water level in the overtopping box.

The WG, EMF and DS are logged on a central computer with a $f_{s,w} = $ 200Hz sampling frequency. The video footage is synchronized with the data recorded on the computer by a light signal. The video footage is intrinsically calibrated to remove effects due to the curvature of the lens. Furthermore, an extrinsic calibration is applied to correct for minor differences in viewing angle and get a projection that is fully parallel to the dike slope. For this, the chessboard pattern is used to obtain a transformation matrix necessary for the perspective transformation. More information about the calibration process is found in appendix B.

---

[3] The actual frame rate of the camera is 23.976024 fps, which is used in further calculations

2.2. Obtaining wave characteristics

In order to compare wave run-up measurements (described in section 2.3) with each other and with commonly used equations, the incoming wave parameters at the location of the toe of the dike need to be determined. As the recorded wave signal consists of incoming and reflected components, the signal needs to be transformed to split these components. There are many types of reflection analyses, such as the Radon transform (Almar et al., 2014), or reflection analyses using an array of wave gauges (Goda & Suzuki, 1976; Mansard & Funke, 1980; Zelt & Skjelbreia, 1992). The method described in Guza et al. (1984) is chosen, as it was found to be the most reliable method for this setup. As this method is based on shallow water conditions it is more suitable for these flume tests in comparison with other methods. Other methods would alter the wave energy density spectrum by averaging out the wave energy, causing a reduction in obtained wave height and alterations in especially spectral wave period.

The Guza method uses a wave height (WG) signal and a velocity signal (EMF). This is applied to the WG and EMF signals acquired at the toe of the dike (WG2, EMF2), and offshore conditions (WG1, EMF1), which were both placed next to each other [4]. Both EMFs used were positioned at half the water level above the salt marsh platform ($d_m/2$). The obtained incoming wave signal is then used to calculate the needed wave parameters. To account for wave conditions that are not stationary (stationary conditions include both incoming and reflected waves, as well as the development of wave set-up requiring some breaking, all for which a start-up time is needed) the first 10% of the wave signal is cut-off.

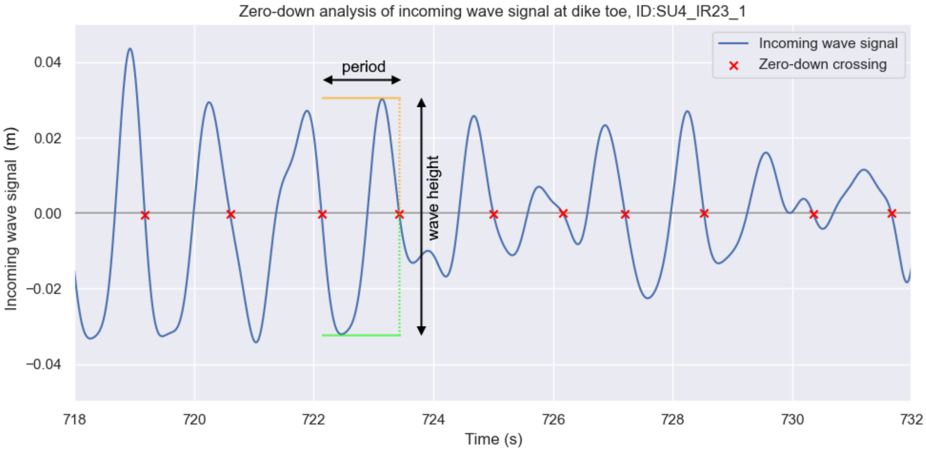

Figure 2.7: Zero-down crossing analysis, at every crossing the period and wave height are determined since the last crossing (see the orange and green markings) The signal used is the incoming wave signal from WG8, which is positioned at the toe of the dike. Test SU4-IR23, run 1

The parameter H_s is the significant wave height, often used in calculations, is not strictly defined. This wave height can refer to $H_{1/3}$ or H_{m0}, which are similar in deep water conditions but differ in more shallow waters (Holthuijsen, 2007). Situations of shallow water can lead to differences of 10-15% (EurOtop, 2018).

A zero-down crossing analysis (Holthuijsen, 2007) (figure 2.7) is performed on the incoming wave signal giving an array of wave heights. to measure the *number of incoming waves* (N_W) and $H_{1/3}$. The latter is calculated as the mean of the highest 1/3 of the wave heights.

$$H_{1/3} = \frac{1}{N_W/3} \sum_{\iota=1}^{N_W/3} H_\iota \qquad (2.6)$$

Where H_ι represents the individual wave heights, sorted into descending order of height, as ι increases from 1 to N_W.

---

[4] The Guza method was applied by D. Dermentzoglou to the signal, where the resulting incoming and reflected wave signals were provided for this thesis

A spectral analysis[5] of the same wave signal is performed to obtain $H_{m0}, T_{m-1,0}$[6], T_p, L_p. With these parameters, the Ursell number U (Ursell, 1953) used to determine the non-linearity of waves and the Iribarren number $\xi_{m-1,0}$ (Battjes, 1974) used to compare the wave steepness and bed slope of the bed are calculated. These are used to compare the measurements with each other and to literature, which are expanded upon further in chapter 3.

$$m_n = \int_0^\infty f^n E(f) df, \quad n \in \mathbb{Z} \qquad n^{th}\text{-order spectral moment} \qquad (2.7)$$

$$H_{m0} = 4\sqrt{m_0} \qquad \text{Spectral wave height} \qquad (2.8)$$

$$T_{m-1,0} = \frac{m_{-1}}{m_0} \qquad \text{Wave energy period} \qquad (2.9)$$

$$L_p = \frac{gT_p^2}{2\pi} \tanh\left(\frac{2\pi d}{L_p}\right) \qquad \text{Peak wave length (linear wave theory)} \qquad (2.10)$$

$$s_p = \frac{H_{m0}}{L_p} \qquad \text{Peak wave steepness} \qquad (2.11)$$

$$s_{m-1,0} = \frac{2\pi H_{m0}}{gT_{m-1,0}^2} \qquad \text{Deep water spectral wave steepness} \qquad (2.12)$$

$$\xi_{m-1,0} = \frac{\tan\alpha}{\sqrt{s_{m-1,0}}} \qquad \text{Spectral surf similarity parameter} \qquad (2.13)$$

$$U = \frac{H_{m0} L_p^2}{d_m^3} \qquad \text{Ursell number} \qquad (2.14)$$

T_p is calculated from the wave spectrum as the frequency bin with the maximum energy (m^2/Hz). m_0 and m_{-1} are calculated by the usage of equation (2.7), which are needed for H_{m0} and $T_{m-1,0}$. The wave energy as shown in the spectrum higher than 5Hz was found to be negligibly small, therefore a numerical upper limit of the integral 5Hz is chosen. The absence of frequencies higher than 5Hz are most likely due to the limits of the frequencies that can be produced by the wave generator.

To decrease the error of the wave spectrum, the analysis is averaged over multiple blocks where the FFT is performed to (Holthuijsen, 2007). For this sensitivity analysis is performed, by calculating H_{m0} and $T_{m-1,0}$ from the acquired incoming wave spectrum (figure 2.8). From the sensitivity analysis it was concluded that H_{m0} did not change significantly for the choice in amount of blocks / length of blocks, as the change is H_m0 between given block lengths is minor. However $T_{m-1,0}$ does change in a way that it could influence the final results, as it shows an logarithmic influence of block length. A block length of 3 minutes ($\equiv 200\text{Hz} \cdot 3\text{min} = 36000\ \text{samples}$) is chosen, as a duration of 3 minutes and longer shows a more constant value for $T_{m-1,0}$[7]. This results in 5-10 blocks containing 100-200 waves (as roughly 1000 waves have been used for each experiment). Using blocks of less than 3 minutes results in a decrease in $T_m - 1, 0$, which is likely due to that low frequencies components are by definition components with a long wave period. As less of these long periods are available in a shorter block size, the response of these low frequencies becomes less. This is due to $m_{-1} = \int_0^\infty E(f)/f df$, which is used in the numerator when calculating $T_{m-1,0}$.

The deep water signal of SU5-IR06-1 has a peak in very low frequencies (0-0.016Hz) which is likely a result of a moving WG during the test. This is not present when a wave spectrum analysis is performed on the other wave gauges. As the calculation of $T_{m-1,0}$ makes use of the m_{-1} spectral moment, this could lead to a higher spectral wavelength. Therefore, for this test data from a wave gauge placed 30 cm towards the wave generator is used (not indicated on the drawing).

---

[5] Spectral analysis uses a Fourier transform to transform the wave signal in energy per frequency. From this obtained spectrum, the n^{th}-order moment m_n can be obtained used to calculate the wave parameters

[6] The usage of $T_{m-1,0}$ is based on Van Gent (1999a, 1999b)

[7] This decision is also made for practical reasons to align the results of this thesis with the findings of the research of D. Dermentzoglou

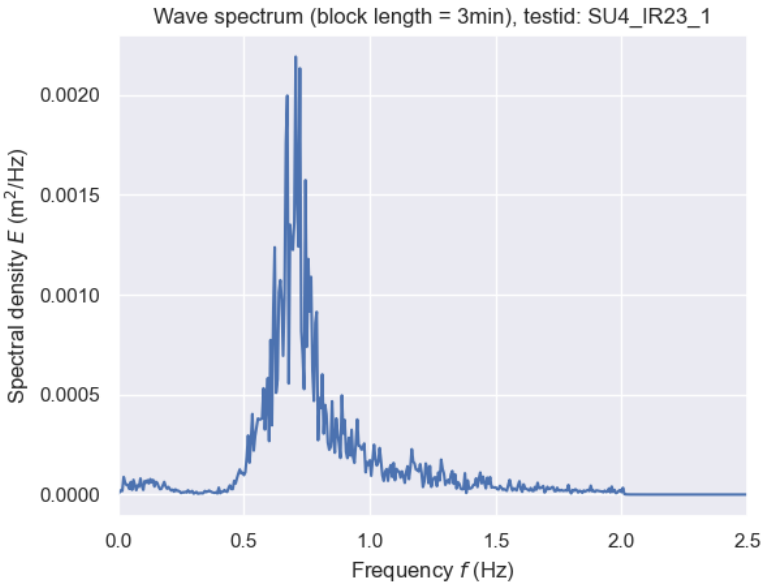

(a) Wave spectrum using a block length of 3 minutes

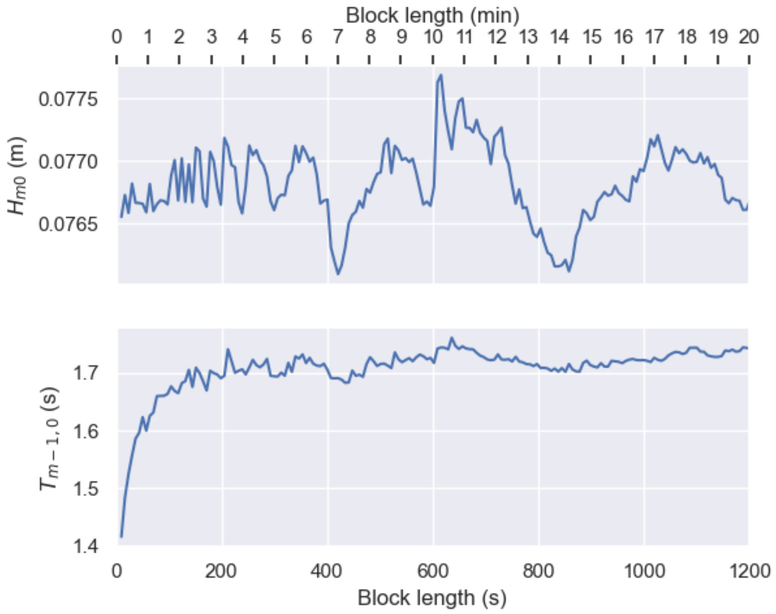

(b) Calculation of H_{m0} and $T_{m-1,0}$ for a given block length

Figure 2.8: Influence of the block length used in determining the spectral wave parameters. Sensitivity analysis performed on incoming waves at dike toe at for testID: SU4-IR23, Run 1. Duration of data is 1360s / 22.66min. f_s, w = 200Hz

2.3. Non-intrusive wave run-up measurements

In order to determine the influence of salt marshes on a dike, wave run-up is measured. The waves interact with the slope of the dike (figure 2.3), where they break and/or run-up the slope. Remaining wave energy is returned towards the seaward side as reflected waves.

A camera films the run-up during the experiment (section 2.1.2). This is chosen because, in principle the detection using visual methods can lead to high accuracy, as the water can be tracked with a very small grid size, in comparison with steplevels. The usage of visual methods has some history, especially in field observations (eg. (Holman & Guza, 1984)). In the past in laboratory conditions this is was done by hand, comparing the water level with measuring markings, in combination with measurements of steplevels.

The camera footage is calibrated intrinsically and extrinsically using a camera calibration procedure described in section 2.1.2 and in further detail in appendix B, in order to have a true one to one agreement with the pixel values and actual height (figure 2.9). This results in an initial resolution of measurement of 2.1mm/pixel along the diagonal (figure 2.10), and consequently 0.562mm/pixel along the vertical distance of the slope of the dike.

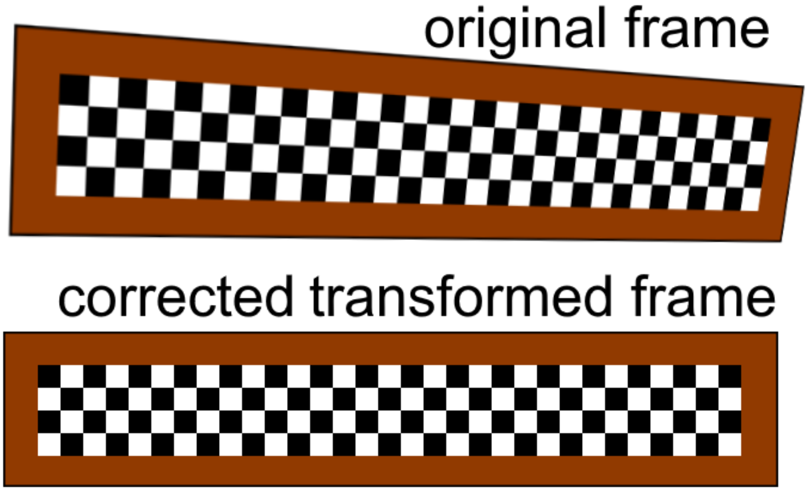

Figure 2.9: Schematic depiction of camera calibration used to align the top view of the slope of the dike. This is done as the slope of the dike is not totally parallel to the camera. By requiring the chessboard to be straight and have right angles, the frame can be corrected by a perspective transform.

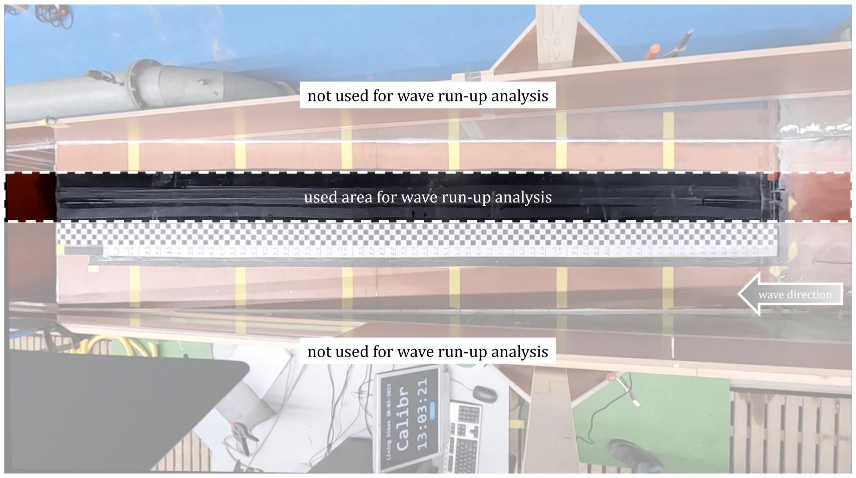

Figure 2.10: Calibrated total frame from top camera pointing downwards at dike slope used in wave run-up analysis. The video footage is cropped to the matte black surface. Left is the top of the dike, toe of the dike at the right, waves are impacting the dike from right

In order to isolate the moving water from the dike surface underneath, a procedure[8] has been developed (figure 2.11). The image contained in each frame of the video is cropped to the black low reflective area figure 2.10. This is done in order to reduce other reflections besides the water reflections, which is needed for the following steps of the procedure to work, as this area was found to have the highest accuracy due to the matte black surface.

As the camera is observing the selected area from a stationary point of view, the only object that moves is the water. A common way to isolate such single object movements in the field of computer vision is Frame Differencing (Migliore et al., 2006; Singla, 2014). Instead of using the absolute difference of intensity of each pixel between consecutive frames (as used in frame differencing); the variance of the intensity of each pixel between consecutive frames is used as a way to quantify the difference. In this way a stark contrast between the moving water and the background can be formed. This contrast forms a clear interface which can be tracked automatically, from which a wave run-up signal can be obtained. This method is chosen in favor of Background Subtraction methods (Migliore et al., 2006) as the top of the water running up the slope of the dike is almost see through, so the difference in pixel intensities between the background and water is very small.

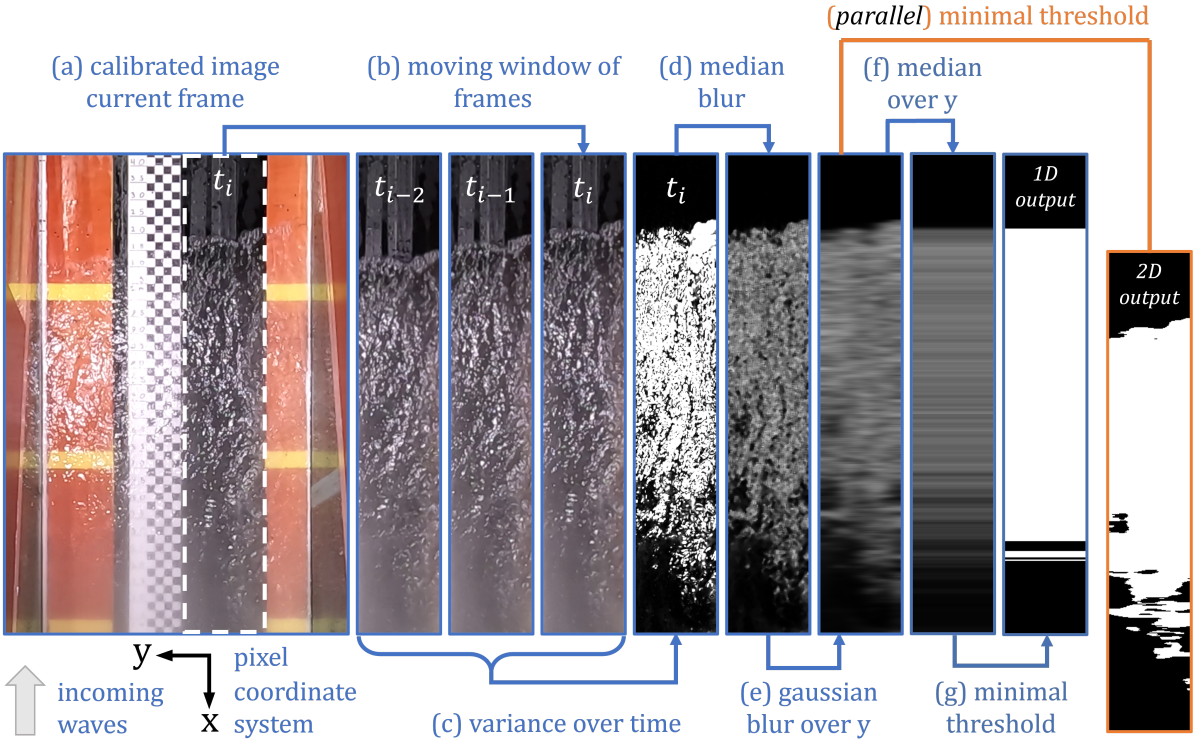

Figure 2.11: Overview of water isolation procedure applied to the run-up video footage, visualized using color and greyscale images. From the calibrated video footage, 3 consecutive frames are placed in a queue of frames. The variance of pixel intensities for every pixel coordinate over the three frames is used to get a difference picture. The difference picture is filtered to obtain 2 outputs of isolated moving water. Steps a to g depict a step-by-step description and visualization of the processing of 3 consecutive frames in a queue to a 1D representation of the isolated water for the last frame in the queue (time = t_i). A parallel step is made to obtain a 2D representation of the isolated water for the last frame in the queue (time = t_i). This is used in appendix E

---

[8] The video data is processed using Python using the OpenCV package, and using filters from the NumPy and SciPy package

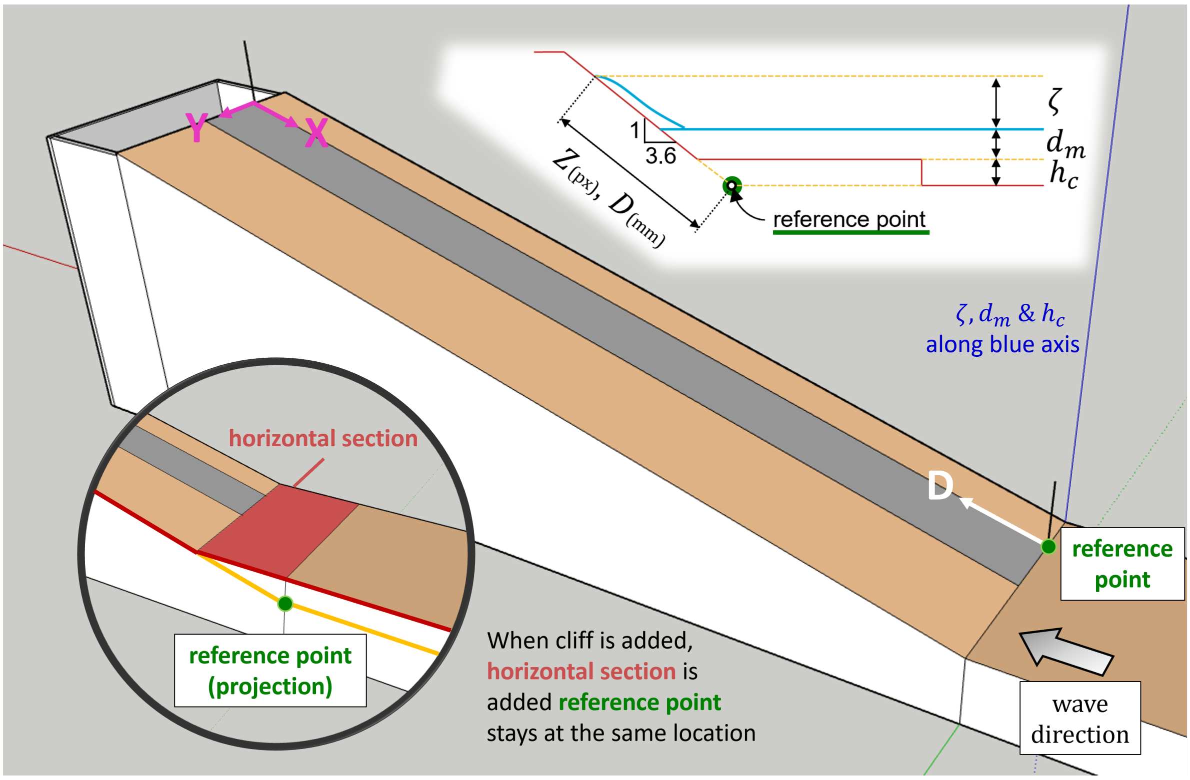

Figure 2.12: Schematic description of definitions of variables and reference points. As a cliff is added to the structure, the reference point stays the same as if no cliff was added. The x-y coordinate system is depicted in pink in the upper left corner, as well as the incoming wave direction and is used in other pictures to represent the viewpoint of the pictures. The grey area depicts the area were wave run-up is recorded. The diagonal distance from the reference point is given as D.

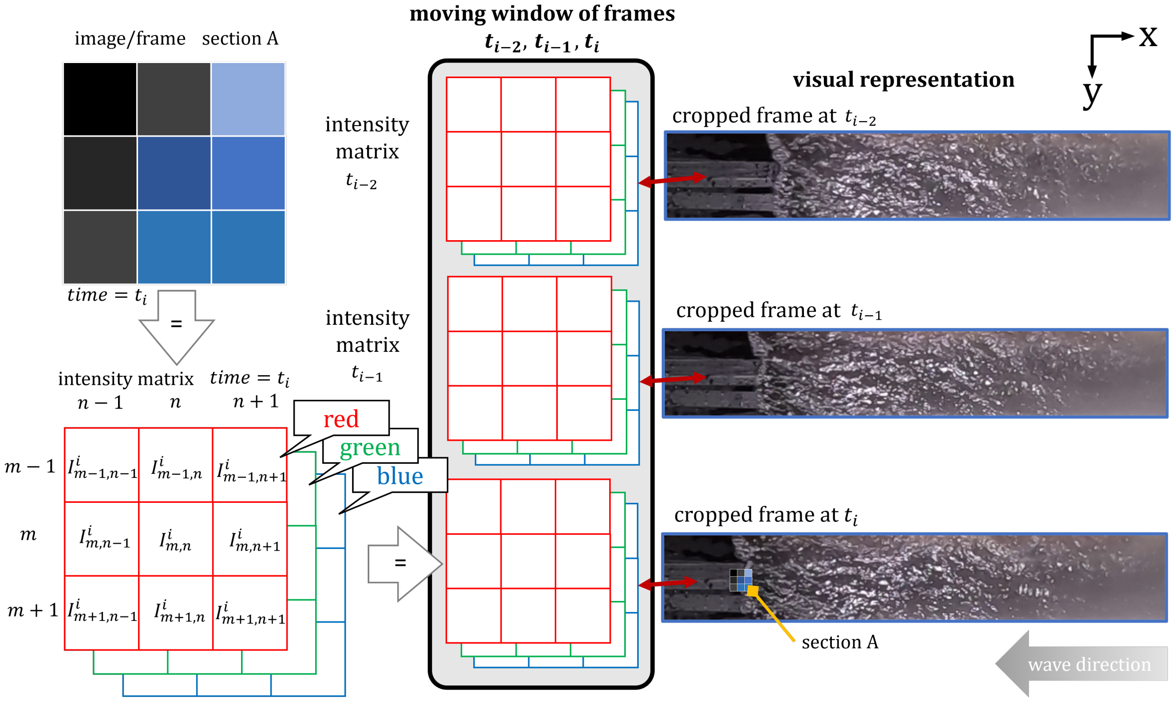

Figure 2.13: Three consecutive frames are placed in a moving window. Section A contains colors, which have RGB pixel intensities. Each frame can be represented as a $M \times N$ intensity matrix, for the red, green and blue channels respectively.

Step-by-step water isolation procedure

The coordinate system which is used in the image processing is shown in the bottom left corner of figure 2.11, other definitions are schematized in figure 2.12.

Each video consists of frames with a certain timestamp or time index (t_i) attached to it. Each pixel of a frame has a certain intensity value ranging from 0 to 255 for the colors red, green and blue (RGB). Combining these two means that each frame can be represented as a 3D-array with a time index, containing the location index[9] for each pixel (m,n) and a certain light intensity (I) of red, green and blue (all ranging from 0 to 255) for time index i[10].

As a first step of the procedure, similar to frame differencing, a 3 (consecutive) frames *moving window*[11] is applied (figure 2.13). This is the smallest moving window which can be used to give accurate results, for the least amount of processing time, which was found by trial-and-error. The usage of a moving window with a larger number of frames did not give a significant improvement in detection, and increased the calculation time significantly.

The *variance*[12] is calculated for the light intensity of each pixel over time t_{i-2}, t_{i-1}, t_i for the color channels red, green, and blue across the frames, to see the difference between these frames in the moving window (figure 2.14, top). The resulting array is set to time t_i, this is the 'newest' time index in the moving window.

$$[\sigma^2_{\text{color}}]^i_{m,n} = \text{var}([I_{\text{color}}]^{i-2}_{m,n}, [I_{\text{color}}]^{i-1}_{m,n}, [I_{\text{color}}]^{i}_{m,n}) \tag{2.15}$$

$$\text{for all} \quad \text{color} \in \{\text{red}, \text{green}, \text{blue}\} \quad \text{and} \quad I_{\text{color}} \in \{0, \ldots, 255\}$$

To obtain a single variance array for t_i, the mean across the colors is calculated of this red, green, blue variance array (figure 2.14, bottom). The obtained 2D-array for each time index i, contains a single intensity variance value for each array index (m,n).

$$\tau^i_{m,n} = [\overline{\sigma^2}]^i_{m,n} = \text{mean}([I_{\text{red}}]^i_{m,n}, [I_{\text{green}}]^i_{m,n}, [I_{\text{blue}}]^i_{m,n}) \tag{2.16}$$

An explanation for the effectiveness of this procedure is that variance is defined as the squared deviation of the mean. Likewise, a large deviation from the mean gives a high variance. As water is highly reflective and a black matte surface is not, the pixels with the highest change in RGB intensity in the moving window, have the highest variance. High turbulence results in a high variance in intensity as well, as reflections are constantly changing from the point of view of the camera. It is important to note that during experimentation regular matte colored surfaces were found to be quite effective as well, and worked in the same manner.

To account for some splashes of water and other small discrepancies two *blurring filters* are used on this 2D-variance intensity array for each time index (figure 2.15). The first filter which is applied is a *median filter* across an 5×5 area of indices (figure 2.15, top). This median filter is used to reduce small noise in the order of several pixels.

$$[\tau_{med}]^i_{m,n} = \text{med}(\tau^i_{m-2,n-2}, \ldots, \tau^i_{m+2,n+2}) \tag{2.17}$$

---

[9] This location is using matrix / array notation, m is the index of the rows, n the index of the columns. These represent the location of a random pixel found in the image/frame. The maximum value which m can be, is denoted as M. Similarly, the maximum value of n is denoted as N

[10] If the specific time in seconds is referenced t_i is used, if the index of the timestamp which is equal to the frame number is referenced, i is used.

[11] A moving window is a selection of a certain amount of items from an array, in this case 3. This window is moved step-by-step along the array one index at the time, for each step observing only at 3 items at once

[12] The variance is defined as the sum of the squared difference between the value and the mean of all values, without any weighing coefficients.

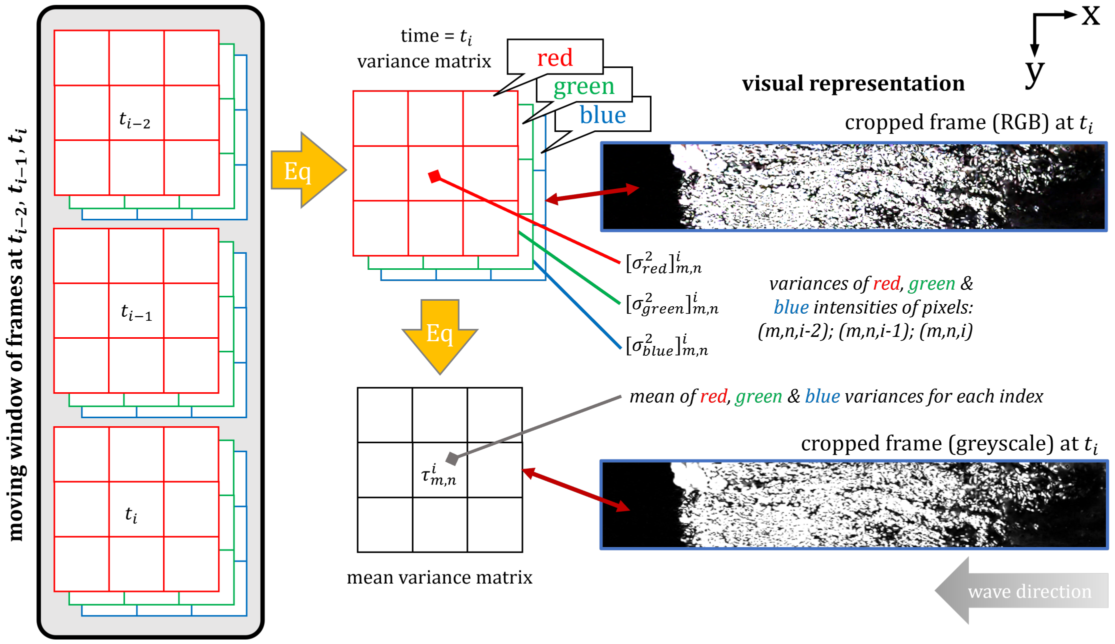

Figure 2.14: The variance between the intensity of index (m, n) for time indices t_{i-2}, t_{i-1} and t_i, for the red, green and blue channels separately is calculated (first Eq: equation (2.15)). The mean of (m, n) of red, green and blue channels of the obtained variance matrix is calculated to obtain a single variance matrix for time index i (second Eq: equation (2.16)). If the resulting matrix is displayed as a greyscale picture, this displays a visualization of the movement of water between the frames in the moving window of frames.

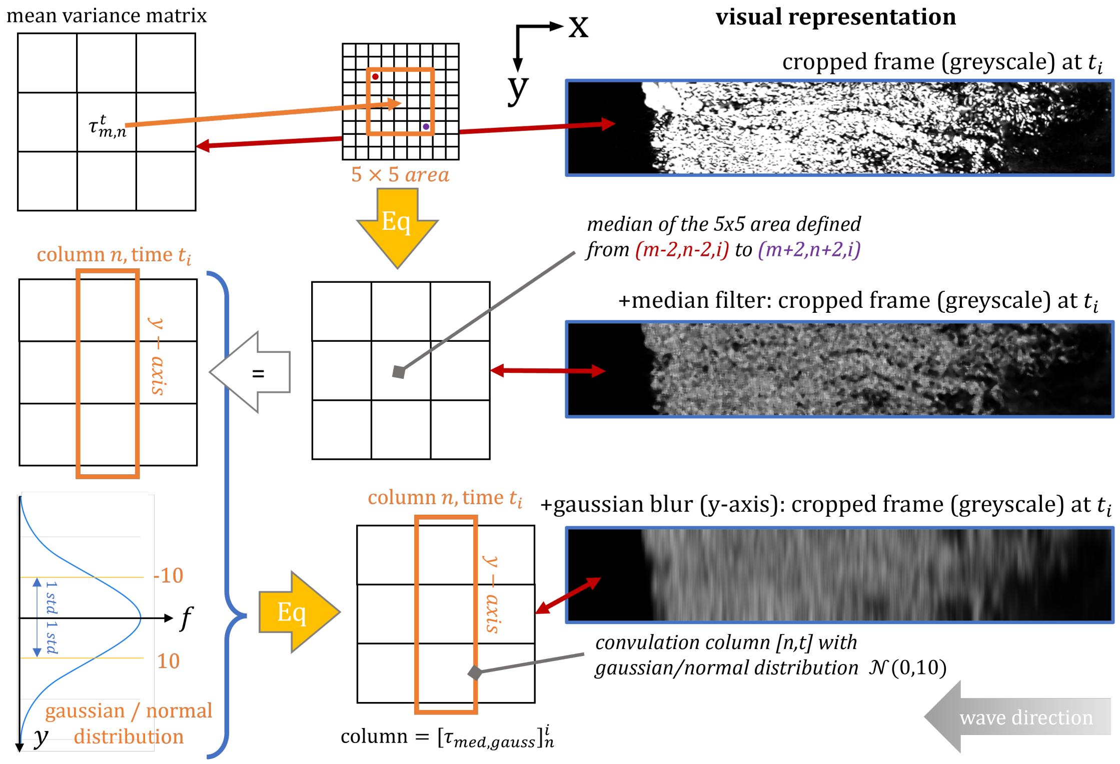

Figure 2.15: The resulting array obtained in figure 2.14, is filtered using two filters: median filter (first Eq: equation (2.17)), and a Gaussian filter (second Eq: equation (2.18)). These filters are consecutively applied to the array, resulting in a representation of water movement at t_i. The visual representation depicts the transformation caused by the filtering of the arrays.

The second filter that is applied is a *Gaussian blurring filter* in the y-direction along the entire column n (in the flume transverse direction) (figure 2.15, bottom). This filter is found to improve detection in the following step, by removing noise along the y-direction. The measurements along the y-direction are otherwise prone to non-realistic jumps, between consecutive points in m. The standard deviation of the Gaussian distribution used in the filter is $\sigma = 10$, found by trial-and-error. This filter is a discrete form of the Weierstrass transform, applied to all columns of the 2D-array (Zayed, 2019). Hence this filter is a convolution of this whole column n with the Gaussian / normal distribution $\mathcal{N}(0, \sigma)$. In this manner, the blurring effect can be indicated and adjusted with standard deviation σ, which is used in this distribution as smoothing metric.

$$[[\tau_{med,gauss}]_n^i] = \text{gaussianFilter}([[\tau_{med}]_n^i], \sigma = 10) \tag{2.18}$$

After the latter filtering step, the resulting array represents the water moving across the dike slope. The resulting array for every time t_i can be represented as a picture, with variance value at index (m, n) depicted as a color intensity, showing the water separated from the total picture (figure 2.15, bottom right visual representation). This can be traced to get out a value to be used in the run-up signal.

Isolated moving water to 'unfiltered' run-up signal

The outside contour at the left hand side of the isolated water frame formed between the black and white areas (see zoomed in: figure 2.16), which is obtained in the last step, can be seen as representative of the water line. This can be compared to methods such as using a run-up gauge, where a single value is used for each time index. It is chosen that the median value along the y-axis is the most representative of the general run-up signal. This is because the n-indices of the contour which is formed in this way, can be seen as readings of a multitude of single run-up gauges placed next to each other in the transverse direction of the flume. This is because each row (n, along x-axis) is displaying an instance of water moving up the slope. Therefore the median is averaging out the readings of the signals, giving the most likely height which would be measured by a single run-up gauge. To contrast this choice, the maximum value along the y-axis is another option. However, this value is by definition prone to outliers, even after filtering. Moreover, as the location in the flume transverse direction of the maximum run-up is not constant, this will lead to results that are higher than tests where a single physical run-up gauge was used.

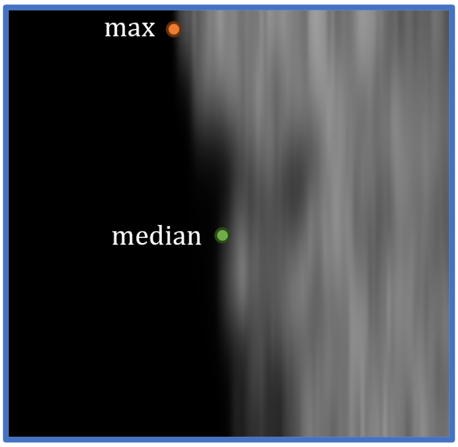

Figure 2.16: Zoom in of the visual representation of the variance matrix. The contrast between the black to white area gives a contour. The contour has a median and maximum value, where the median value is chosen to be representative of the wave run-up signal.

In order to obtain this median value along the transverse direction of the flume, the median of whole isolated moving water frame is calculated along the y-axis (along the columns), giving an 1D representation of the isolated moving water for each time index (figure 2.17).

$$\eta_n^i = \text{med}([\tau_{med,gauss}]_{0,n}^i, \dots, [\tau_{med,gauss}]_{M,n}^i), \quad M = \max(y) \tag{2.19}$$

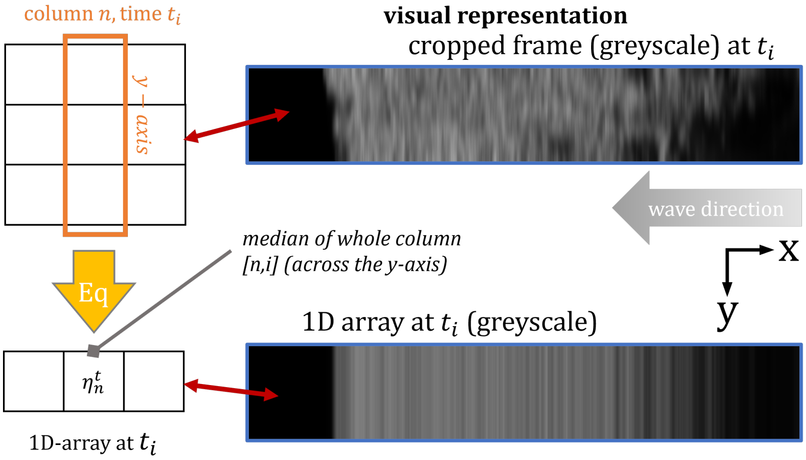

Figure 2.17: Calculation of the median value along the columns (y-axis) of the variance array. Second visual representation is a 2D representation of a 1D array for time = t. The used equation is equation (2.19)

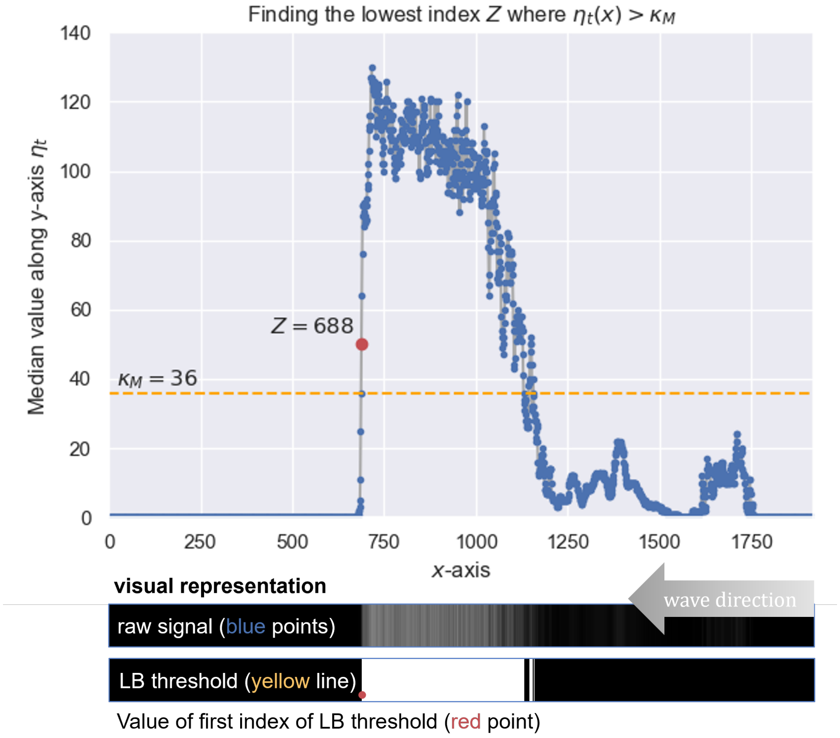

Figure 2.18: Application of a threshold on the variance signal. After this the lowest x-value (argmin (n)) which is greater than this threshold is selected to be representative of the wave run-up signal for time index t_i. As the signal at this time index t_i is 1D, this can be depicted in a graph (top). As well as visual representation as given in the previous images (bottom), representing this 1D signal in a 2D way.

A lower bound threshold $\kappa_M = 36$ in intensity can be assigned to represent the border of the median of this moving water. This is used in order to separate the parts where the variance is greater and smaller than κ_M. In this manner, the border between these parts can be identified by calculating the index of the first value where this lower bound threshold is surpassed. Due this threshold procedure, the obtained index can be seen as equivalent with the run-up signal at t_i.

$$Z_i = \text{argmin}(n) \quad \text{such that} \quad \eta_i(n) > \kappa_M \tag{2.20}$$

With this transformation applied, each time index i has a single pixel index Z representative of the moving water at that time. As each pixel has a corresponding real world measurement, the indices of these pixel values can be converted to diagonal run-up readings measured from the dike toe using the calibration function equation (2.21). These values which are measured on the slope of the dike diagonally can be converted to the vertical run-up signal (equation (2.22)) which is used in the standard practice of measuring wave run-up[13]. This vertical level can be calculated by means of the mean water level in front of the dike (d_m), cliff height (h_c), and the slope of the dike, as shown in Equation 2.21.

$$D(t) = a - bZ(t) \tag{2.21}$$

$$\zeta(t) = \frac{D(t)}{\sqrt{1+3.6^2}} - d_m - h_c \tag{2.22}$$

The wave signal and run-up signal can be aligned with each other, as for both the time relative to a certain starting point is recorded. This is done by recording a LED light in the same video footage as the wave run-up is recorded. This is triggered when the central acquisition system (recording WG and EMF) starts recording, thus providing a visual way to align the two signals (for a detailed description see appendix B).

2.3.1. Filtering run-up signal

As the procedure can be prone to outliers due to random disturbances in the video footage, a selection of filters are applied to the signal. The first filter that is applied is an outlier detection and removal filter[14]. It is set to use a median filter of size 5 (0.21s) and detects outliers where the difference between the input signal and median filtered signal is greater than 1 standard deviation of the median filtered signal (figure 2.19, Box 2.2). The advantage of using such a filter instead of a median filter is that in cases where no outliers are detected, the signal doesn't change from the original measured signal.

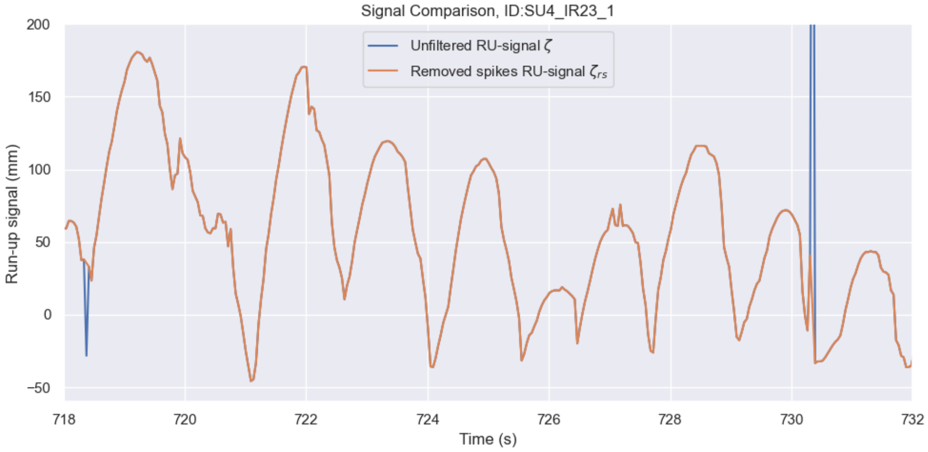

Figure 2.19: The removal of outliers in the signal. These outliers are due to visual artifacts which originates from the procedure.

---

[13] Wave run-up is defined vertically from SWL

[14] such as the function *isoutlier* in MATLAB, however here implemented in Python (Box 2.2)

Box 2.2: Median filter-based outlier detection and removal

1. A median filter with size 5 is applied to a copy of the signal

$$C_i = \mathrm{med}(\zeta_{i-2}, \dots, \zeta_{i+2}) \tag{2.23}$$

2. The absolute difference of the original signal and the filtered signal is calculated
3. All points where this difference is higher than a threshold defined by the standard deviation of the filtered signal are selected

$$|\zeta_i - C_i| > \mathrm{std}(C_0, \dots, C_{i_{end}})$$

4. A new signal is made where the selected positions are replaced with a not-any-number[a] (NAN) value

$$|\zeta_i - C_i| > \mathrm{std}(C_0, \dots, C_{i_{end}}) \rightarrow \zeta_i = \mathrm{nan}, \quad i_{end} = \max(i) \tag{2.24}$$

5. The NAN values are linearily interpolated along the time axis

$$\zeta_i = \mathrm{nan} \rightarrow [\zeta_{rs}]_i = \zeta_{i-1} + \frac{\zeta_{i+1} - \zeta_{i-1}}{2} \quad \textit{(representation)} \tag{2.25}$$

---

[a] A Not Any Number or NAN value is used when no data is recorded for its respective index

After this, a 5 points (0.21s) moving mean is applied to the signal, similar to Van der Meer (2011) (figure 2.20). The application of this filter is chosen as the peak detection algorithm, used in the further processing of the signal, is closer to peak detection which is found during validation. This results that the current peaks of the signal are more 'smeared-out' which causes some inaccuracies in comparison with the actual signal. These inaccuracies can also be a result of the water isolation procedure, which are not known without validation. When comparing the two signals, the difference is quantified with Pearson R=0.9945 and a root mean square error RMSE = 5mm between the filtered and whole signal.

$$z_i = \mathrm{mean}([\zeta_{rs}]_{i-2}, \dots, [\zeta_{rs}]_{i+2}) \tag{2.26}$$

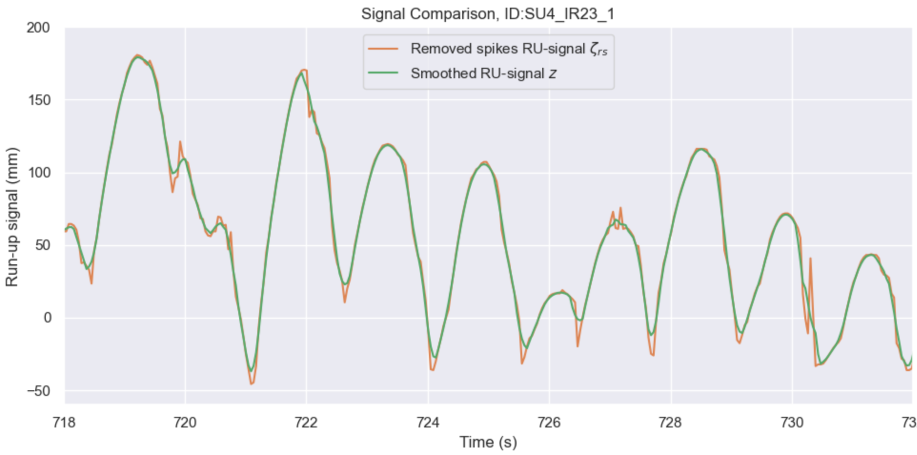

Figure 2.20: Application of moving mean of 5 points (0.21s) to the wave run-up signal. This is done in order to facilitate better peak detection.

This results in a usable wave run-up signal $z(t)$ for each time step t_i, where $z(t)$ is the vertical height from SWL to the top of the median of the run-up along the transverse direction of the flume, running up the slope of the dike in the area of interest. By the use of applying a outlier removal filter and a moving mean, only one 'heavy' filtering step has been applied to the signal, to remain the highest accuracy.

2.3.2. Calibration and validation of procedure

The procedure to isolate the water surface, calculate the run-up signal and filter the wave run-up signal, makes use of filters and thresholds which have set parameters. The ones that are not found in literature (of the moving mean filter) have been determined by calibration with a reference data set. The reference data set is created by manually conducting a frame-by-frame analysis of the maximum run-up level across the width for each frame on a 12-minute video (470 waves). This is done over the same area on the dike used in the aforementioned procedure. The indices of the highest water level in this area are stored for each frame. The highest water level is picked instead of the median, as eye-picking a median is much more prone to bias in comparison to the maximum value. The frame-by-frame analysis is done for two experiments with quite different wave conditions and flume configuration, where the first represents a normal foreshore and the second includes vegetation and a cliff. The specific video footage that is used are SU1-IR12-2, and SU6-IR04-1, both from 12 to 24 minutes after the start of recording. The first is used to calibrate the needed parameters, the latter test is used for validation. A depiction of the resulting eye-picked signal versus the signal obtained from the algorithm is depicted in figure 2.21.

Figure 2.21: Comparison of the hand picked run-up maximum across the width, vs the run-up median across the width. A larger deviation from the median means a wider run-up range along the width. As the reference signal is based on the maximum run-up across the width, a higher deviation could also mean a larger variation along the width of the flume.

Before comparing the reference signal with the signal obtained from the procedure, the indices of the values which could not be determined in the reference signal are selected and removed. This is carried out as these values don't have a direct equivalent of each other when trying to compare the signals. Then, in order to compare the 2 signals, the Pearson Correlation Coefficient (**R**) and Root Mean Square Error (**RMSE**) are used to quantify the error between the two signals. These are shown in table 2.3.

Table 2.3: First validation using Pearson-R and MSE

TestID, Run, Video	**R**	**RMSE(mm)**
SU1-IR12, Run 2, Video 2	0.986	0.4
SU6-IR04, Run 1, Video 2	0.984	0.2

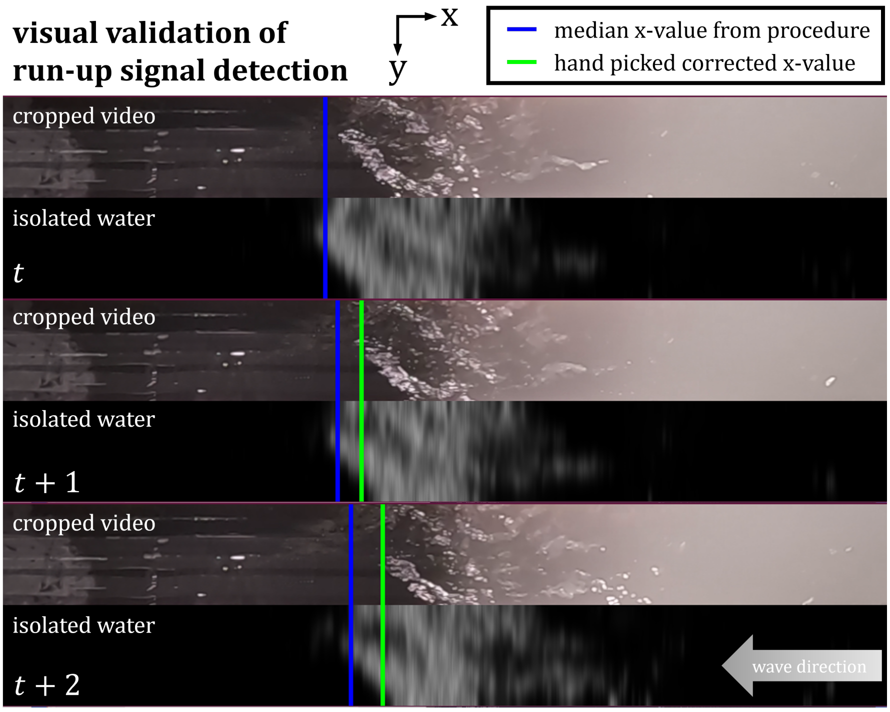

Figure 2.22: Validation of the procedure by comparison of visual estimation (hand picked value) of the median of the wave run-up over width versus the value obtained from the procedure. The test depicted is SU6-IR04, Run 1. The water in the regular cropped frame looks further to the right then the isolated water is showing. The isolated water is positioned more to the left than what is seen in the unaltered image.

However, this validation process does not compare two similar definitions. Within the reference dataset, the *maximum* run-up along the width of the dike is selected and compared with the *median* value. Moreover, this difference is taking the whole signal signal into account for its comparison. All deviations from the reference signal are uniformly accounted for, without assigning additional weight to the signal's upper peaks, which are typically deemed the most crucial. Consequently, a secondary method is necessary to conduct a visual inspection and compare the median of the dataset.

Two measurement data sets are selected which show the largest deviation between the obtained data and determination by eye. Tests SU4-IR05 and SU6-IR04 are selected and are both analyzed from 12 minutes to 24 minutes. The video footage where the signal is acquired from is played alongside a visual representation of the data set (figure 2.22). For the instances where the visual representation from the signal obtained from the algorithm was deviating from what was deemed correct by eye-picking, an estimation of the correct median run-up level at that timestamp was selected. In this way, the obtained signal can be validated in a way that more closely resembles where it is used for.

Table 2.4: Quantification of the signal deviation obtained from run-up tracking algorithm versus an eye-picked correction (figure 2.22. The RMSE is calculated for only the wrong frames and for all frames together. Where the first one depicts the error if the tracing is wrong and the second one depicts the overall error for the given tests. Two videos were used that showed a large visual deviation between the traced position and position which was obtained using visual estimation.

TestID, Run, Video →		SU4-IR05, Run 1, Video 2	SU6-IR04, Run 1, Video 2
Amount of frames	Total	18192	17016
	Wrong	90	75
Percentage of wrong frames		0.495%	0.441%
RMSE of wrong frames	(px)	134	75
	(mm vert.)	75	42
RMSE of all frames	(px)	9	4
	(mm vert.)	5	2

2.3.3. Run-up height parameters

Several metrics can be obtained from the wave run-up signal, such as the distribution of the incoming wave heights, and consequently the 2% exceedance value of this distribution, which can be compared with the state of the art engineering equations.

In order to compare the run-up measurements with each other and literature (Battjes, 1969; Hofland et al., 2015; Van der Meer, 2011; Van Gent, 1999a), a distribution of the maximum reached run-up values for every incoming wave should be made. It is expected that the wave run-up should follow a Rayleigh distribution, as waves are generated using a JONSWAP spectrum resulting Rayleigh distribution of wave heights (Battjes, 1969). If waves break on the dike slope, each single converts into run-up and reaches a certain height according to Hunt's equation:

$$R_u = \sqrt{HL_0}\tan\alpha \quad = \sqrt{H}\cdot T\cdot\sqrt{\frac{g}{2\pi}}\tan\alpha \quad = H\xi \tag{2.27}$$

In the case of a known dike slope $R_u \propto \sqrt{H}\cdot T$. This results in a Rayleigh-like distribution (depending on the dependency of H and T which becomes greater in shallower water) as shown in Battjes (1974).

In order to transform the run-up signal to such a distribution, the probability of maximum run-up heights above a certain level of the dike slope $\mathrm{P}(z_p > h_n)$ is calculated. Where z_p is the local maximum of the run-up signal reached by a single instance of run-up, and h_n is a given height on the dike in comparison with SWL. By the calculation of these probabilities, a distribution can be made describing a certain probability of exceedance for every dike level h_n. As the obtained run-up signal describes the movement of the water over time, the maximum levels reached by the run-up signal for each incoming wave need to be found. These levels correspond with the local peaks Z_p of the run-up signal[15]. In an ideal scenario, when the amount of incoming waves matches exactly with the amount of run-up events, the relation between the probability of exceedance and these peaks is as follows.

$$\begin{aligned} w = F_{z_{p,corr}}(h_n) = \mathrm{P}(z_{p,corr} > h_n) = 1 - \mathrm{P}(z_{p,corr} \leq h_n) \\ \rightarrow F_{z_{p,corr}} = 1 - \mathrm{eCDF}(z_{p,corr}) \end{aligned} \tag{2.28}$$

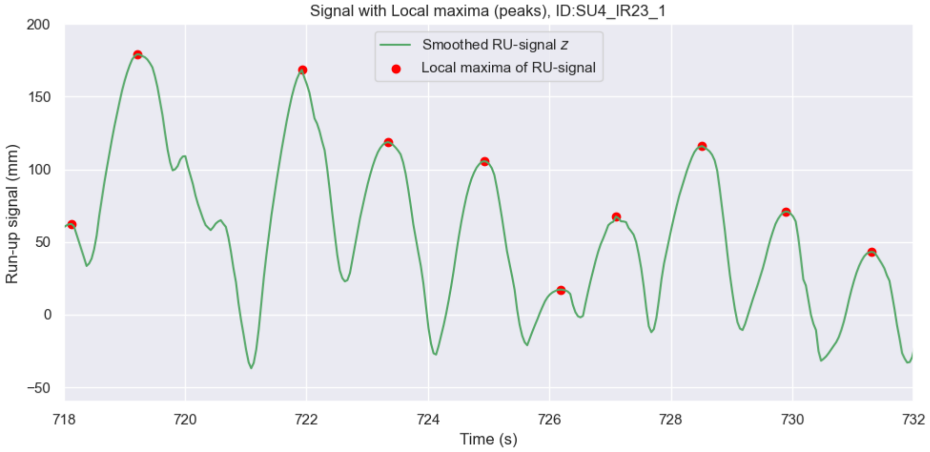

Figure 2.23: The local maxima are found of the wave run-up signal. These local maxima are also known as peaks in the wave run-up signal. These peaks represent the maximum height that an incoming wave has reached. Each of these maxima correspond to a single run-up event. The signal depicted is from test SU4-IR23, Run 1

---

[15] The 'find peaks' function of SciPy Signal is used

Due to the nature of flume tests, the beginning of the tests do not describe stationary wave conditions (see also section 2.2). To account for this, the run-up data from the first 10% of the test duration is cut. This leads to an incoming wave number of around 1000 (ranging from 940 to 1100 waves) waves. Small oscillations in the run-up signal corresponding to a single wave could give rise to double readings, so searching for peaks with a minimum time interval between peaks leads to more accurate results. As there is not a constant wave period in a generated irregular wave spectrum, just using the average wave period could be biased towards higher periods between run-up peaks. Similarly, this would discard some peaks corresponding with waves with smaller periods. Therefore, the 1% percentile of wave periods obtained from the zero down procedure on the incoming wave signal is used as a representative value for the minimum time interval between peaks. This value is deemed low enough that the run-up peaks belonging to smallest periods are taken into account, however the double countings which can occur during the zero-down procedure are ignored. Besides this minimum time interval, a minimum prominence of the peak is also used to reduce double readings, which is set to 10mm, determined by trail-and-error.

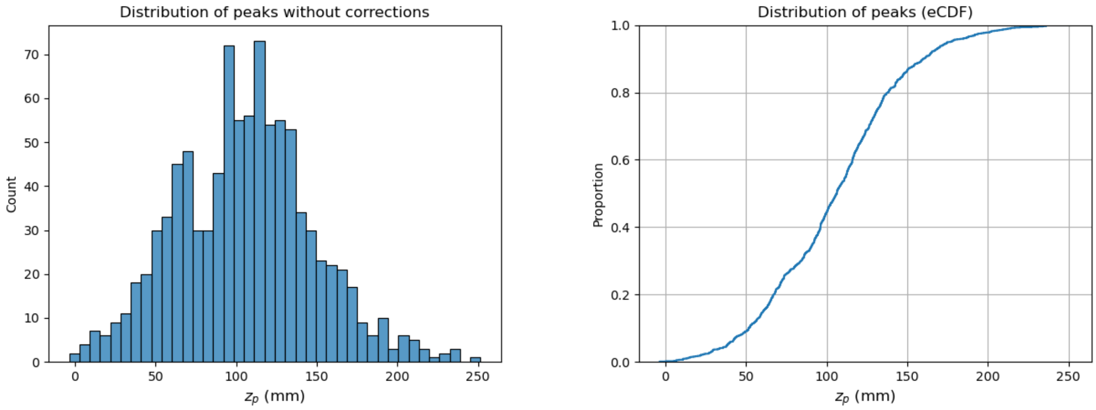

(a) Histogram of run-up peaks

(b) Empirical cumulative distribution plot of run-up peaks

Figure 2.24: Distribution of wave run-up peaks, which correspond with all the heights that incoming waves reach as wave run-up. However, the number of incoming was are not yet taken into account. Test scenario: SU4-IR23, Run 1

As the amount of incoming waves and run-up peaks are not the same, instead of calculating the empirical distribution function (eCDF) of these peaks, the *amount of incoming waves* (N_w) reaching the dike are used in practice (EurOtop, 2018; Hofland et al., 2015; Van Gent & Van der Werf, 2014) to describe the exceedance distribution of the peaks. The wave signal is aligned with the run-up signal, hence the wave signal also is cut by 10% from the start giving an amount of incoming waves of around 1000 (ranging from 940 to 1100 waves). This is done as N_w is more truthful to the actual amount of wave events, and the wave run-up peaks are prone to over counting even with certain measures in place. Moreover, this could also be contributed to multiple waves which combine into a single run-up. The peaks and amount of incoming waves are used to calculate the exceedance probability of run-up for a given level on the dike h_n (Box 2.3). This level for a given probability of exceedance is denoted as $R_{u,w\%}$, where w depicts the probability of exceedance.

The resulting probability distribution needs to be adjusted for the tests with overtopping (10 tests, appendix D). The hypothetical wave run-up measurement during an overtopping event is higher than what is measured. As for these cases of overtopping the hypothetical z_p is actually higher than the freeboard of the dike R_c, which could result in run-up if the dike slope was longer. However, due to the dike crest, the wave run-up reading is (close to) R_c. Hence, these erroneous measurements according to overtopping events are selected from the dataset by finding the closest matching peak with a time index close to the measured overtopping events. To account for this in the resulting run-up distribution, the selected peaks which correspond with an overtopping event are set to the same level as R_c (as smoothing could have potentially have lowered their values), which is the highest run-up level which possible for that experiment. As it is known that the highest peaks should be higher than R_c, the measurements of these peaks are marked erroneous. In order to account for this, the run-up values belonging these highest exceedance probabilities, which are calculated using Box 2.3, have to be set to be undefined. (Example: the 2% exceedance value of a test with 1000 incoming waves needs to be calculated, which corresponds with the 20th highest index ($R_{u,2\%} = z_{p,sorted}(\iota = 20)$). The test has experienced 4 overtopping events, so the wave run-up height for this according index is measured correctly. However, if there were more than 20 overtopping events, the according peak is not measured correctly anymore as it should be higher than R_c, so the according value in the exceedance probability needs to be set to be undefined (NAN))

If the distribution of the run-up is equal to a Rayleigh distribution, it can be described with (equation (2.29), Schiereck and Verhagen (2012)).

$$\frac{R_{u,w}}{R_{u,2\%}} = 0.71\sqrt{-\frac{1}{2}\ln(w)} \tag{2.29}$$

For historic reasons (see appendix G, EurOtop (2018)), the common way to describe the wave run-up behavior of a given combination of factors of influence is given by the 2% exceedance value of the run-up distribution. This value will be used to compare the tests with literature.

Box 2.3: Calculation of $R_{u,w\%}$, where h_n is calculated for a given probability of exceedance w, using incoming waves and corrected for overtopping

1. The peaks are sorted from biggest to smallest $z_{p,corr,sort}$
2. The amount of waves exceeding h_n corresponding to the given probability of exceedance w is calculated. This is equal to the index ι of the peaks in $z_{p,corr,sorted}$

$$\iota = w \cdot N_w \tag{2.30}$$

3. If $\iota \leq N_{ot}$ (n.o. overtopping events) $R_{u,w\%}$ is set to be undefined (NAN), as the corresponding value is incorrect.
4. As the index is likely not a integer, the height h_n according to this intermediate index ι is not present in the dataset. For this the integers below $\lfloor\iota\rfloor$ and above $\lceil\iota\rceil$ are found as they correspond with a value in $z_{p,corr,sorted}$
5. The values in $z_{p,corr,sorted}$ are found according to these indices accordingly $z_{p,corr,sorted}[\lfloor\iota\rfloor]$, $z_{p,corr,sorted}[\lceil\iota\rceil]$
6. Using these calculated variables, the intermediate index is linearly interpolated

$$R_{u,w\%} = h_p = (z_{p,corr,sorted}[\lceil\iota\rceil] - z_{p,corr,sorted}[\lfloor\iota\rfloor]) \cdot (\iota - \lfloor\iota\rfloor) + z_{p,corr,sorted}[\lfloor\iota\rfloor] \tag{2.31}$$

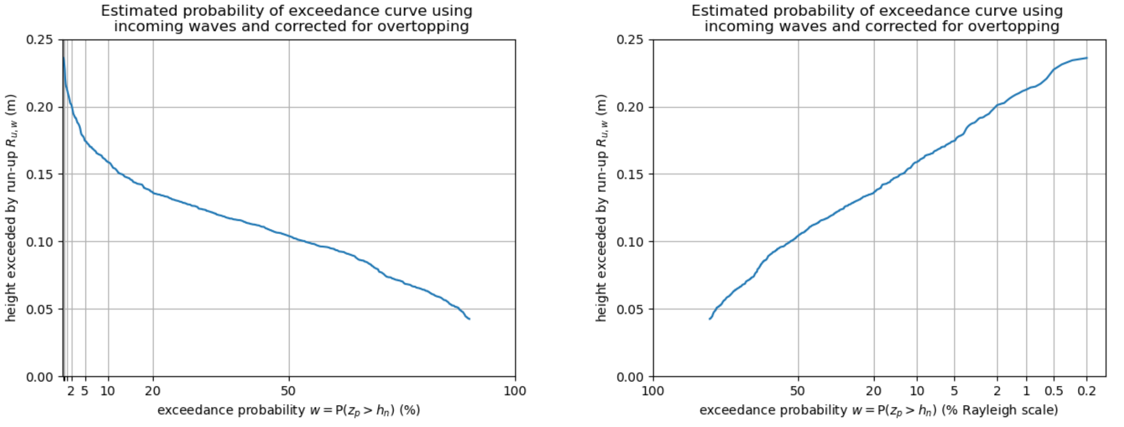

(a) Linear scale, same ticks as used in the Rayleigh scale

(b) Rayleigh scale, similar to a log scale, but the ticks are distributed via $\sqrt{-\ln x}$

Figure 2.25: Empirical probability of exceedance of the run-up peaks. These are calculated with the method described in box 2.3. For every given height on the dike (y-axis), the estimated probability of a given wave run-up event which exceeds this height is given (x-axis)

3

Results

In order to answer the objective of this thesis, the results of the conducted measurements are presented and analyzed. As wave run-up is determined by the wave interaction with the dike, an analysis of the wave characteristics is presented in order to give a better understanding of the wave run-up data. Firstly, the wave characteristics are presented and comparison with literature is depicted in section 3.1. Which will be used to compare the wave run-up in section 3.2, where the distributions are analyzed and the 2% values are compared with literature.

Subscript ***o*** *is used to describe parameters at the offshore location (WG1). Subscript* ***t*** *is used to describe parameters at the toe of the dike (WG2). The wave characteristics of the incoming wave signal are always used in the following analyses unless it is mentioned otherwise.*

3.1. Wave characteristics

The incoming waves offshore (WG1, subscript o) have a target wave height and peak period given in table 2.2. Due to the characteristics of the given conditions in a wave flume, the waves arriving from the wave maker at the offshore location are positioned in intermediate waters. Hence, the measured wave heights offshore are lower than the target values. On average, a 2cm reduction (depending on the relative wave height figure C.1) between the target values and measured wave height can be observed. Moreover, the peak period does not show such an alteration (figure 3.1, figure C.12b).

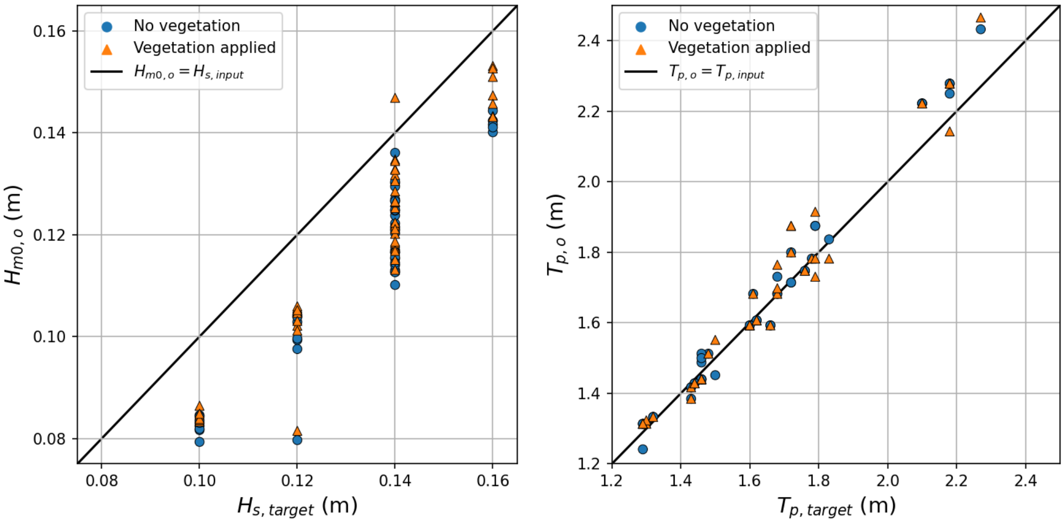

(a) Significant wave height

(b) Peak period

Figure 3.1: Target values which were used as input in the wave maker versus measured values of the incoming waves at the offshore location

The spectral wave period $T_{m-1,0}$ has in deep water conditions a relation with the peak period, where $T_{m-1,0} = 0.9T_p$. When the measured spectral wave periods are compared to the measured peak periods, this relative factor is higher than 0.9 and ranges to 1.2 for offshore conditions (figure 3.2). There is a clear distinction present in the relation between the offshore peak period and the spectral period between tests with and without vegetation (figure 3.2, figure C.13). The tests with vegetation show a lower factor of difference than the tests without vegetation.

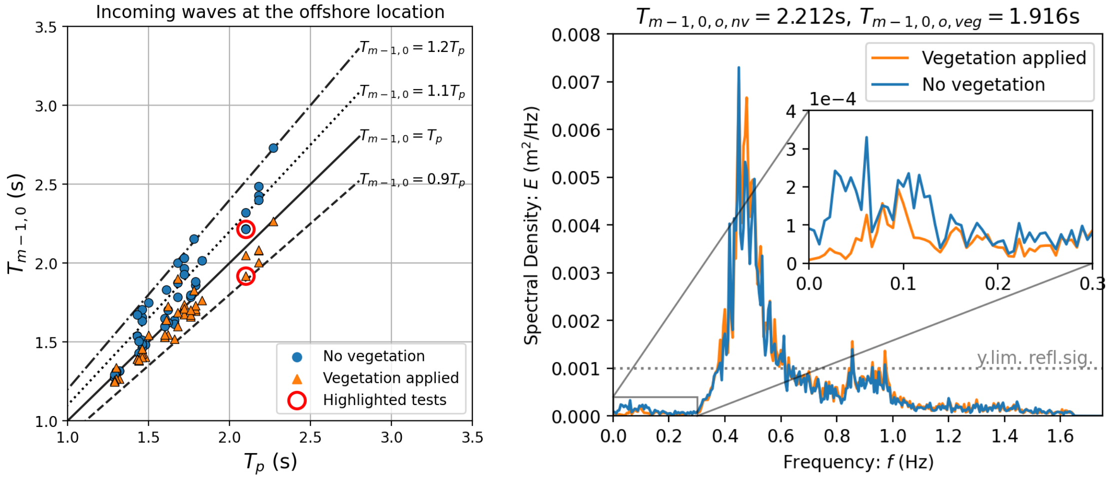

(a) Relation between T_p and $T_{m-1,0}$ of the incoming waves measured at the offshore location. A clear distinction between cases with and without vegetation can be seen, where the factor between $T_{m-1,0}$ and T_p is higher for cases without vegetation

(b) The spectral density of the **incoming** wave signal of the two highlighted tests. In the lower frequency bands, tests without vegetation show a higher value than with vegetation. (IR22)

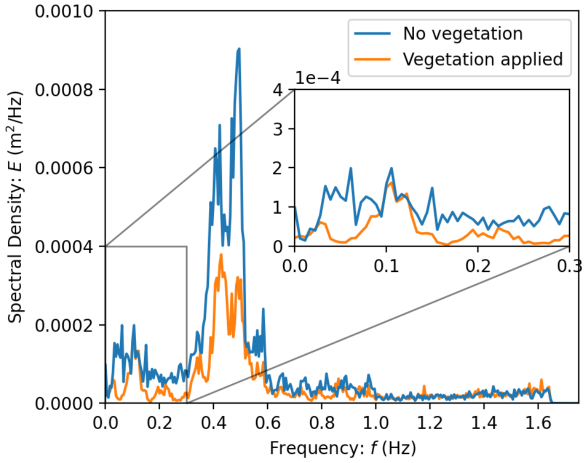

(c) The spectral density of the **reflected** wave signal of the two highlighted tests. Wave reflection is higher for tests without vegetation, in comparison with tests without vegetation (IR22).

Figure 3.2: Wave periods at the offshore location. The relation between T_p and $T_{m-1,0}$ is dependent on especially the low frequency parts of the wave spectrum (zoomed in). The effectiveness of the wave compensation at the wave generator is less for low frequency components than higher frequencies. Hence, these lower frequencies are increased in the offshore signal corresponding with tests without vegetation.

This is most likely a result of the reflection caused by the total foreshore present, where lower frequency components ($f < 0.3$Hz) are reflected from the dike. These are analogous to free infragravity waves which are found in the field. The reflection compensation mechanism implemented in the wave maker exhibits diminished effectiveness at lower frequencies in comparison with higher frequencies. So this frequencies are reflected back from the wave maker towards the dike, which results in an increase in energy density for these lower frequencies in the incoming wave signal. These lower frequencies have a large influence in the resulting value of $T_{m-1,0}$, as $m_{-1} = \int_0^\infty E(f)/f df$, and is therefore increased due to this process. Moreover, vegetation dampens wave reflection (Bouma et al., 2014) (figure 3.2c), which leads to reduced reflected wave energy in the signal. Consecutively, the lesser low frequently energy in this signal leads to a lower value of $T_{m-1,0}$. Hence, the differences which are seen in the relationship between T_p and $T_{m-1,0}$ for the tests with and without vegetation are a direct result of the dampening of the whole foreshore. The presence of a cliff is especially alters $T_{m-1,0}$, for $d_o/H_{m0,o} > 5$, where $T_{m-1,0} : nv/veg$ is increased for h_c = 6cm and decreased for h_c = 12cm in comparison with cases without a cliff (figure C.13).

At the toe of the dike (WG2, subscript t), tests with vegetation show a similar or higher $T_{m-1,0}$ in comparison with tests without vegetation, up to 1.35 times the peak period (figure 3.3a). This is mainly a result of the flattening of the peak of the wave spectrum by wave breaking (figure 3.3b). This flattening can even increase to an extent that a low frequency peak is formed (figure C.2). This is a consequence of lower frequencies which are already present in the incoming signal do not break over the salt marsh, and the generation of low frequency components by the broken waves (Bouma et al., 2014).

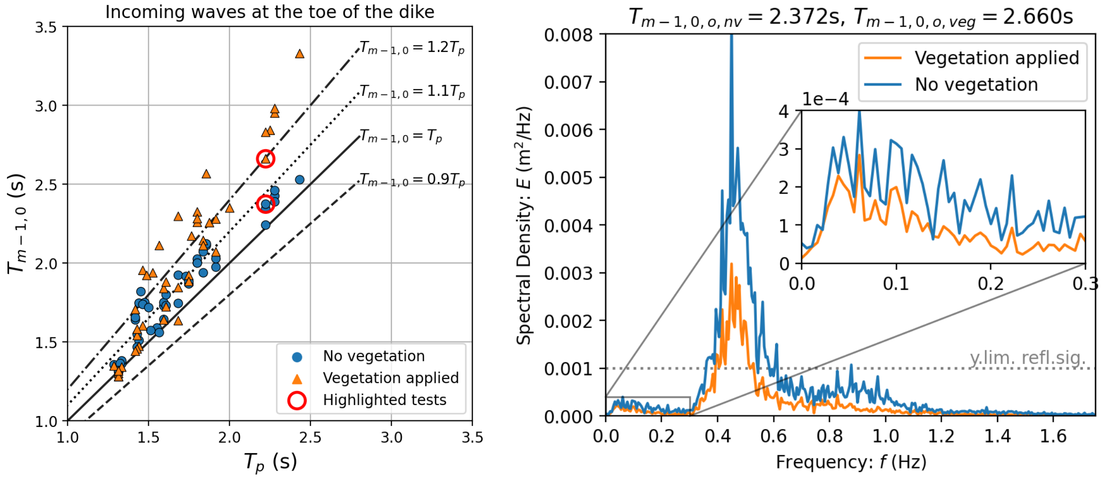

(a) For values of $T_p > 1.7$, the factor between $T_{m-1,0}$ and T_p is higher for cases with vegetation.

(b) Energy density spectrum of incoming waves at the toe of the dike.

Figure 3.3: Shows a spectrum with a relatively high $T_{m-1,0}$, which is due to a low frequency component.

The wave height H_{m0} and local water depth d_o, d_m (depth offshore and salt marsh) are combined with the wave period $T_p, T_{m-1,0}$ to obtain 2 dimensionless parameters $H/gT^2, d/gT^2$ which are based on a Le Méhauté diagram (LeMéhauté, 1976). This is developed and normally used to choose a suitable wave theory for a given singular wave. For the same reasons, this is deemed a suitable way to give an indication of the wave behavior of a given wave spectrum.

At the offshore location, peak period do not differ much between tests with and without vegetation (figure 3.4a). However, a separation can be seen for $d_0/gT^2_{m-1,0,o} > 0.02$ between the tests with and without vegetation, due to the described increase in $T_{m-1,0}$ (figure 3.4b). The distinct branches depict wave heights with similar d/gT^2 (figure 3.4a). These are seen for the tests with vegetation, however not for tests without vegetation when comparing the dimensionless parameters using $T_{m-1,0}$ (figure 3.4b). The outliers in figure 3.4a and b without vegetation (blue dots) are both IR02 with cliff heights 6 and 12cm.

At the toe of the dike, the peak period is well distributed in intermediate waters, which is common for waves which are interacting with dikes (figure C.3c). A distinct reduction can be observed on the H_{m0}/gT_p^2 axis between cases with and without vegetation (figure 3.4c). This reduction is caused primarily by a decrease in wave height, as T_p remains fairly similar in tests with and without vegetation (d_m/gT_p^2 remains the same) (figure C.12a). The two branches showing a difference between H/gT_p^2 of the tests without vegetation are kept. These two branches are not present anymore for the tests with vegetation.

When $T_{m-1,0}$ is used for the dimensionless parameters at the toe of the dike(figure 3.4d, figure C.4d) the distinct reduction in the scatter is visible as well. Moreover, $T_{m-1,0}$ becomes bigger due to the effects described in figure 3.3, which does increase more due to the effects of vegetation. This can be seen by the widening of the scatter along the $d_m/gT_{m-1,0}$ axis (figure C.4d). This results in an even more prominent distinction between the cases with and without vegetation. $H_{m0}/(gT^2)$ depicts value similar to the wave steepness which is used in the Iribarren constant, where $\xi \propto s^{-1/2}$, which is used in wave run-up relations. Hence, it is to be expected that a similar distinction will be observed in the wave run-up.

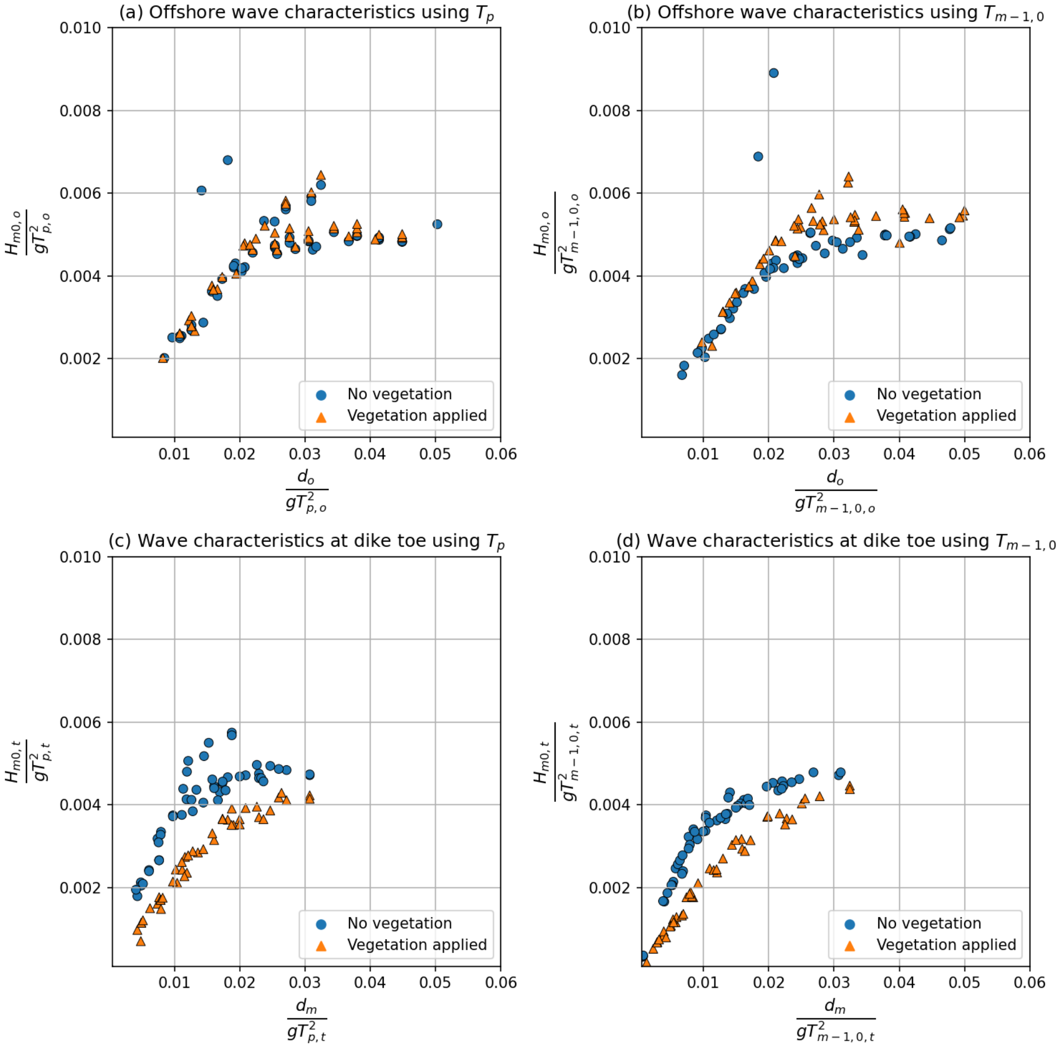

Figure 3.4: The incoming waves offshore and at the toe of the dike are compared using dimensionless parameters d/gT^2 versus H/gT^2 . Waves are separated by tests using vegetated and unvegetated conditions. A clear distinction can be observed between these conditions at the toe of the dike, which is not visible at the offshore location

As both and H_{m0} are $H_{1/3}$ calculated and are used in section 3.2, the difference between the two the values are of interest. In Thompson and Vincent (1985), the difference between H_{m0} and $H_{1/3}$ is shown to be dependent on $d/(gT_p^2)$. Lower water depths give rise to a higher $H_{1/3}$ before breaking as the waves in the wave signal become skewed and asymmetrical.

Offshore the measurements are lower than the average, but are similar for cases with and without vegetation (figure 3.5). This means that some breaking already has occurred, which was also observed in the previous analyses. The measurements do follow the curve which was described in the paper. $H_{1/3}$ is slightly lower than 1 ($H_{1/3}/H_{m0} \approx 0.97$) for $d_o/gT^2_{p,o}$ > 1.5.

At the toe of the dike, more wave breaking has occurred (figure 3.5). The tests without vegetation follow the outermost ends of the wave breaking lines (for which they were given). The relation between $H_{1/3}/H_{m0}$ seems to be mostly constant for all values of $d_m/gT^2_{p,t}$ at on average a factor 0.95. More breaking has occurred for the cases with vegetation, hence $H_{1/3}/H_{m0}$ is lower for these cases. The relation with vegetation shows to be dependent on $d_m/gT_{p,t}^2$ where $H_{1/3}/H_{m0}$ decreases linearly (figure C.5). If $H_{1/3}$ and H_{m0} are compared in absolute sense (figure C.6), $H_{1/3}$ is on average 5mm lower than H_{m0}.

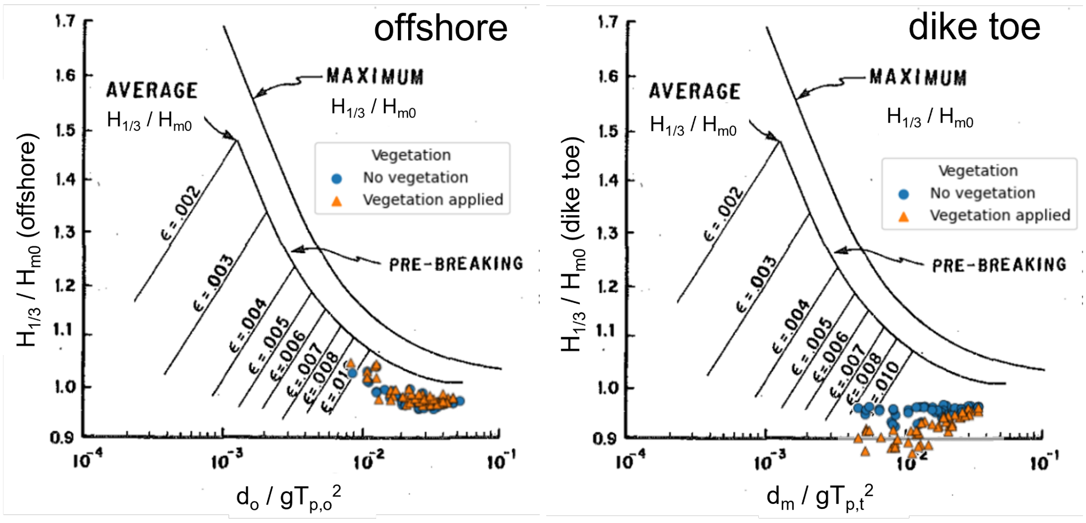

(a) Offshore **(b)** Dike toe

Figure 3.5: $H_{1/3}/H_{m0}$ relationship with $d/(gT_p^2)$ and $\epsilon = 0.25H_{m0}/L_p$, where the depth relationship is used pre-breaking and ϵ is used post breaking. Post breaking higher wave steepnesses lead to significantly lower factors between $H_{1/3}/H_{m0}$. Plotted on modified diagram from Thompson and Vincent (1985). A zoomed in version at the dike toe is found in figure C.5

3.1.1. Changes in wave parameters

Literature, such as described in chapter 1, focuses heavily on the changes wave parameters over the span of the salt marsh due to wave attenuation. As the main focus of this thesis is on wave run-up, the results of wave attenuation will be discussed to a lesser extend. Nevertheless, analysis of wave characteristics could explain differences in behavior shown in the wave run-up.

The difference in wave height between the offshore and at the toe is given as a factor $H_{m0,t}/H_{m0,o}$ (dike toe / offshore). This factor captures wave breaking and wave shoaling on the entire foreshore. For tests *without* vegetation, tests with $d_m \geq 0.30m$ have a minor reduction factor (0.92 to 1) (figure 3.6a). For lower water depths, this factor reduces and the effect of the cliff becomes more prominent, especially for higher waves (higher relative wave height). For tests *with* vegetation, all tests show a reduction in wave height (at least a reduction factor of 0.85). This reduction shows a linear relationship with d_m, where tests with a lower water depths give a lower reduction factor. Every 10cm of reduction in water level shows a decrease of ≈ 0.15 in the reduction factor.

The reduction seems also dependent on the given offshore wave height for that water level, which can be incorporated by dividing the water depth by the offshore wave height (figure 3.6b). Two bands of a hyperbolic tangent like relationship can be observed. The difference between the cases with and without vegetation are easily distinguished, where the tests with vegetation show an increased reduction. For cases *without* vegetation, there is hardly a change in wave height when $d_m/H_{m0} > 2.5$. Lower water depths give a reduction, which is for these more shallow waters likely caused by wave breaking. In contrast with the cases without vegetation, for cases *with* vegetation there is always a reduction in wave height present. Hence, the wave height reduction is reduced more than by only a the reduced water depth on the salt marsh (which would only place the vegetated cases more to the right in figure 3.6b as d_m increases). Additionally, for both cases, there is some dependence on cliff height where values with a larger cliff lead to more reduction in wave height. For cases with vegetation, this effect is minor in comparison with the wave height reduction caused by a decrease in water depth on the salt marsh.

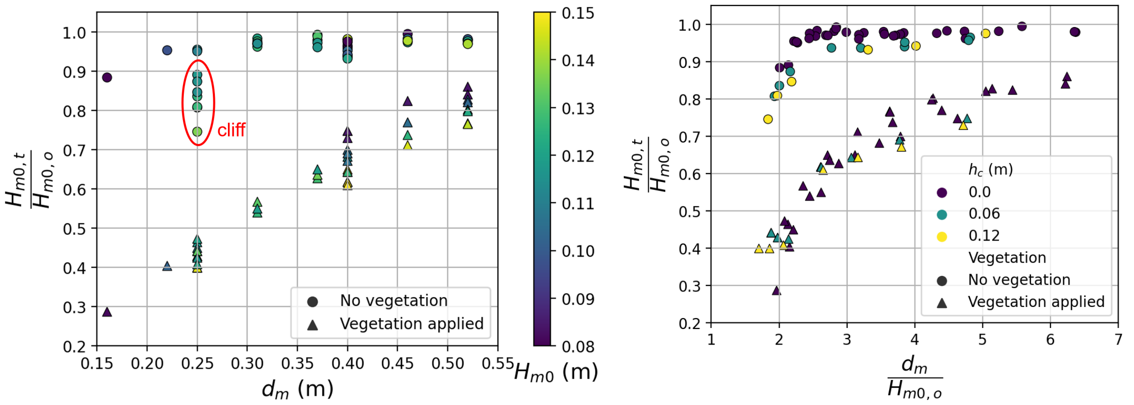

(a) Against d_m. The reduction of the wave height at the toe shows to have a linear dependency with water depth. Measurements with $d_m = 0.25$m show that the wave height reduces more due to the cliff.

(b) Against $d_m/H_{m0,o}$. The cliff reduces the wave height extra by around 4%. For $H_{m0} > 2.5$ the salt marsh without vegetation does not reduce the incoming wave height drastically, but does for lower values. Vegetation has always a reducing factor in the tested cases.

Figure 3.6: Change in $H_{m0,o}$ compared at the dike toe and offshore. Vegetation reduces the incoming wave height more than without vegetation.

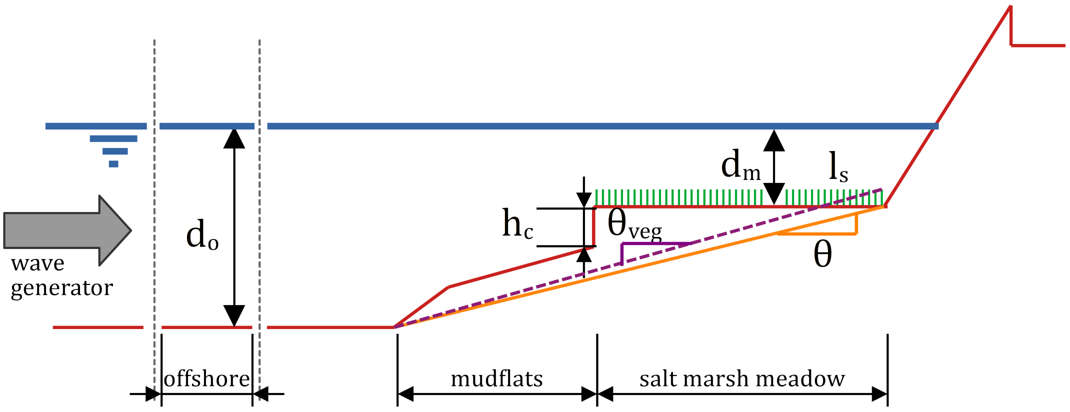

Figure 3.7: Definition of variables used in equations. The foreshore is defined as including the mudflats and salt marsh meadow, which results in a single foreshore length L_{fs}.

The spectral wave period $T_{m-1,0}$ does change over the salt marsh as well. Typically, wave periods exhibit relative stability as they approach the coastline and transition into shallow waters (where the depth-to-wave height ratio h/H is greater than 1). However, the spectral wave period $T_{m-1,0}$ can undergo significant alterations when waves break over an extremely shallow foreshore (where $h/H_{m0,o}$ is less than 1), attributed to the influence of low-frequency / infragravity waves (Hofland et al., 2017). In Hofland et al. (2017) an empirical equation to calculate $T_{m-1,0}$ for a foreshore had been devised (for flume tests):

$$\frac{T_{m-1,0,t}}{T_{m-1,0,o}} = 6\exp(-4\tilde{h}) + \exp(-\tilde{h}) + 1 \tag{3.1}$$

$$\tilde{h} = \frac{d_t}{H_{m0,o}} \tag{3.2}$$

$$\tilde{h} = \frac{d_t}{H_{m0,o}} \left(\frac{\cot\theta}{100}\right)^{0.2} \tag{3.3}$$

Where θ is the slope of the foreshore. Subscript o depicts offshore measurements. The test were conducted on a constant foreshore slope, which is different from this case. The foreshore slopes also did not contain any vegetation. They remark that the influence of the reduction in water depth is the main influence of this reduction (equation (3.2)). The foreshore slope included lead to a slightly better fit (equation (3.3)). For this comparison an average slope is defined as the setup consist of a variable profile. The average slope is defined from the beginning at the foreshore at the 1:9 side closest to the wave generator, until the dike toe (L_{fs}) (mudflats + salt marsh meadow, figure 3.7). The difference in height is defined as $0.24+h_c+al_s$. This results in $\cot\theta = L_{fs}/(0.24+h_c+al_s)$ (figure 3.7). The depth at the toe is given $d_t = d_m - a \cdot l_s$, where a is a influence parameter of the vegetation height. For $T_{m-1,0,o}$, the measured value is used.

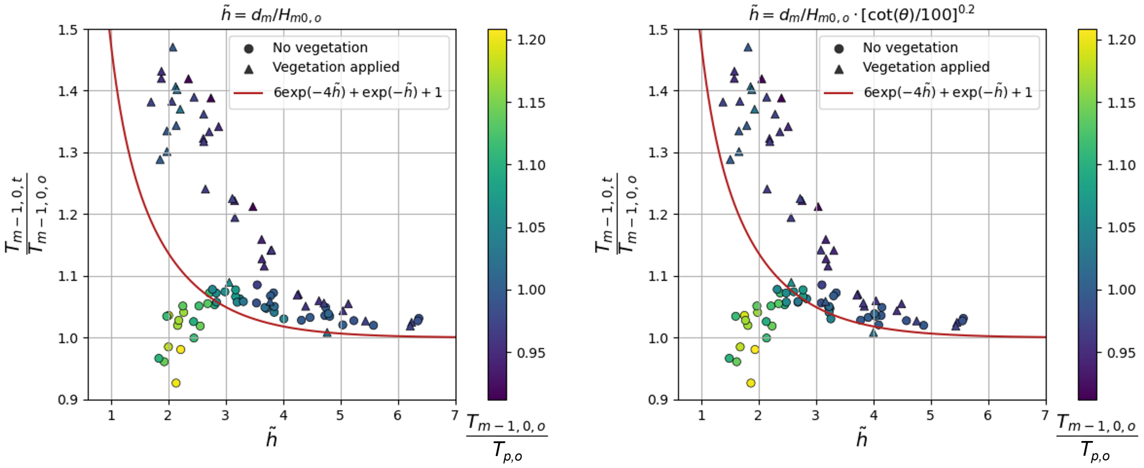

(a) $\tilde{h} = \frac{d_m}{H_{m0,o}}$

(b) $\tilde{h} = \frac{d_m}{H_{m0,o}}\left(\frac{\cot\theta}{100}\right)^{0.2}$, where $\cot\theta = L_{fs}/(0.24+h_c)$

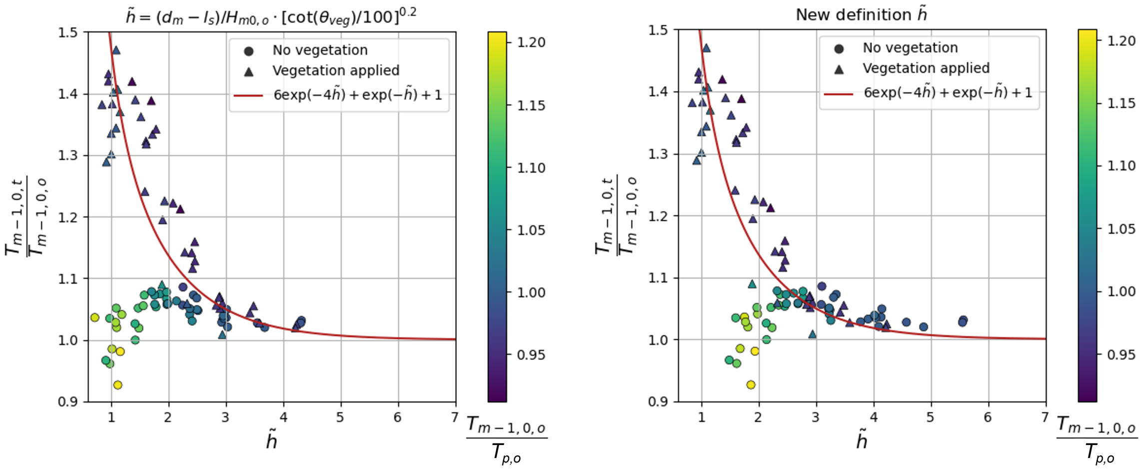

(c) $\tilde{h} = \frac{d_m - l_s}{H_{m0,o}}\left(\frac{\cot\theta}{100}\right)^{0.2}$, where $\cot\theta = L_{fs}/(0.24+h_c+l_s)$

(d) $\tilde{h} = \frac{d_m - a\cdot l_s}{H_{m0,o}}\left(\frac{\cot\theta}{100}\right)^{0.2}$, and $\cot\theta = L_{fs}/(0.24+h_c+a\cdot l_s)$, where $a=1$ for cases vegetation and $a=0$ for cases without vegetation

Figure 3.8: Change in spectral wave period plotted against $\tilde{h}$. By changing this parameter a better fit with equation (3.1) is possible. As mentioned in Hofland et al. (2017) the offshore wave height needs to be (close to/) in deep water conditions. In deep water conditions $T_{m-1,0}/T_p$ is close to 1, hence a large deviation can be attributed to intermediate conditions on which the equation is not based. The resulting fit in **(d)** aligns closely with the equation for all cases which are close to deep water conditions, including vegetation

When applying equation (3.2) with $a = 0$ (no vegetation influence parameter), the increase in $T_{m-1,0}$ is higher than predicted for the cases with vegetation in comparison without vegetation. The lower outliers with are tests with higher $T_{m-1,0}$ values at the toe (a factor higher than $1.05T_p$. These indicate less deep offshore wave conditions. In Hofland et al. (2017) it is mentioned that the formula was calibrated with offshore wave conditions being in deep water, so this can be expected.

If $a = 1$ is chosen, the newly defined definition of $\tilde{h}$ does align better ($R^2 = 0.668$) with the measurements using vegetation (a=1.02 is calculated to be the best fit ($R^2 = 0.669$) with the data). This suggest that the behavior of the change in $T_{m-1,0}$ is largely dependent on the overall water height *above* vegetation. In this way, for the change in spectral wave period, the vegetation acts like a new bottom.

When using $a = 1$ for cases with vegetation and $a = 0$ for cases without vegetation, the predicted values resemble the measured values quite well. However, the cases without vegetation for $\tilde{h} < 2$ are lower than expected.

Both the $T_{m-1,0}$ and wave height are used in $s_{m-1,0}$, which is used to calculate $\xi_{m-1,0}$. For the offshore Iribarren number, the slope of the dike is used for $\tan\alpha$. Similar to before, the factor between the conditions at the dike toe and offshore is calculated. In this way, the transformation of the wave can be combined in a single parameter (figure 3.9). For the tests *without* vegetation, the wave steepness and consequently the Iribarren parameter remain pretty similar and show a slight deviation for relative water depths around $d_m/H_{m0,o} = 2.5$. For the tests *with* vegetation the difference is vastly higher. Lower $d_m/H_{m0,o}$ values show an almost exponential decrease in the wave steepness, which leads to a similar (square root) increase in Iribarren number. As the Iribarren number is used to calculate the wave run-up, such similar behavior is to be expected to be seen in the wave run-up.

The change in peak period stays generally constant, with some scatter which seems to be present for the cases with and without vegetation (figure C.11a). This results in a transformation which is similar for cases with and without vegetation of the peak wave length over the salt marsh. However, the peak wave steepness shows a similar separation as what could be seen in figure 3.9 due to the distinct change in wave height. For lower relative water depths (around $d_m/H_{m0,o} = 2$), the presence of a cliff reduces the wave steepness further.

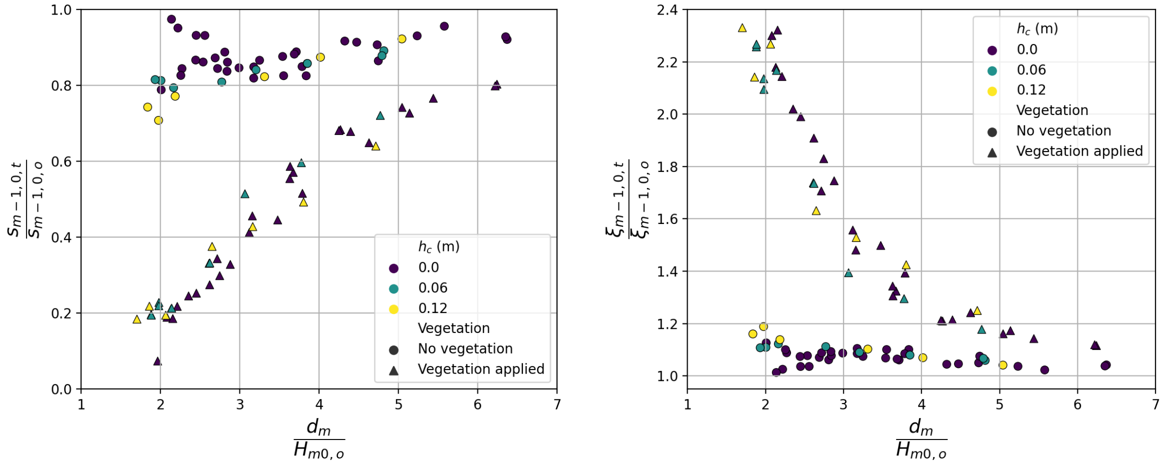

(a) Change in spectral wave steepness, compared with $d_m/H_{m0,o}$

(b) Change in Iribarren number using $\tan\alpha = 1/3.6$, compared with $d_m/H_{m0,o}$

Figure 3.9: The change between incoming waves at the dike toe and offshore show of the spectral wave steepness and Iribarren number show a combined influence of wave height and spectral wave length. Lower water depths over wave height ratios give a reduction in spectral wave steepness which causes an increase in Iribarren parameter. The influence of the cliff is shown primarily in cases without vegetation.

3.2. Wave run-up

The wave run-up is expressed as a distribution (section 2.3.3), which gives for a certain height of a dike the probability of wave run-up exceeding this height. This distribution is often used vice versa, where for a given exceedance probability the according height is found. In many equations found in literature such as described in Box 3.1, the 2% exceedance values ($R_{u,2\%}$) are used. Hence, these values are used to compare the 2% exceedance values obtained from measurements with those calculated using the same wave characteristics used by the equations.

Box 3.1: EurOtop / TAW wave run-up formula

The currently most used formula used to calculate the 2% exceedance value for the wave run-up for gentle dike slopes is given in EurOtop (2018) and TAW (2002):

$$\frac{R_{u2\%}}{H_{m0,t}} = \min \begin{cases} 1.65\gamma_b\gamma_f\gamma_\beta\xi_{m-1,0} \\ \gamma_f\gamma_\beta\left(4 - \frac{1.5}{\sqrt{\gamma_b\xi_{m-1,0}}}\right) \end{cases} \tag{3.4}$$

Where $H_{m0,t}$ is the spectral wave height of the incoming waves at the toe of the dike. This is equation is based on the mean values of the conducted experiments. γ_b, γ_fandγ_β are all equal to 1 in the case of these experiments, as there is no berm, there are no additional elements which cause friction placed on the dike slope, the angle of incidence is parallel to the dike slope.
A coefficient of variation ($CV = \sigma/\mu$) is used to depict the variation of the tests. A CV = 7% is given in TAW (2002). 95% of the tests where the equation is based on have deviation less than $2CV$ from the mean. (See also appendix G)

3.2.1. Wave run-up exceedance probability distributions

The exceedance probability distribution of the wave height and the wave run-up are combined in a double axis plot, using Rayleigh scaling on the x-axis (figure 3.10). Both distributions are similar to Rayleigh distributions, as the function resembles (graphically) a straight line. Wave run-up does more closely align a Rayleigh distribution than the wave heights, as the wave heights are positioned in intermediate water. The wave run-up distribution between tests using vegetation versus no vegetation is analyzed, using IR24 ($d_o = 76cm$, $H_{s,target} = 10$cm, $s = 0.04$, see figure 3.11). Even for this relative high water depth for the given wave height, there is a reduction visible. When the incoming wave height is used to make the run-up dimensionless, the run-up distribution shows a similar distribution. This suggests that the behavior of the run-up does not change.

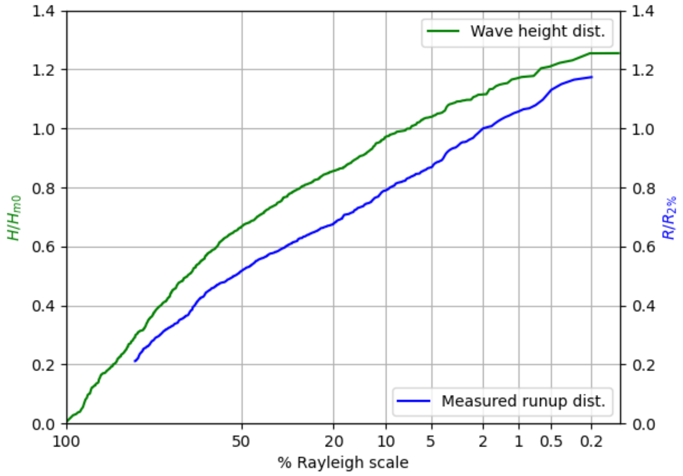

Figure 3.10: Comparison of dimensionless wave height distribution vs dimensionless run-up distribution. Test SU4-IR23-1 is shown. Everything is plotted on a Rayleigh scale, where a Rayleigh distribution corresponds with a linear line

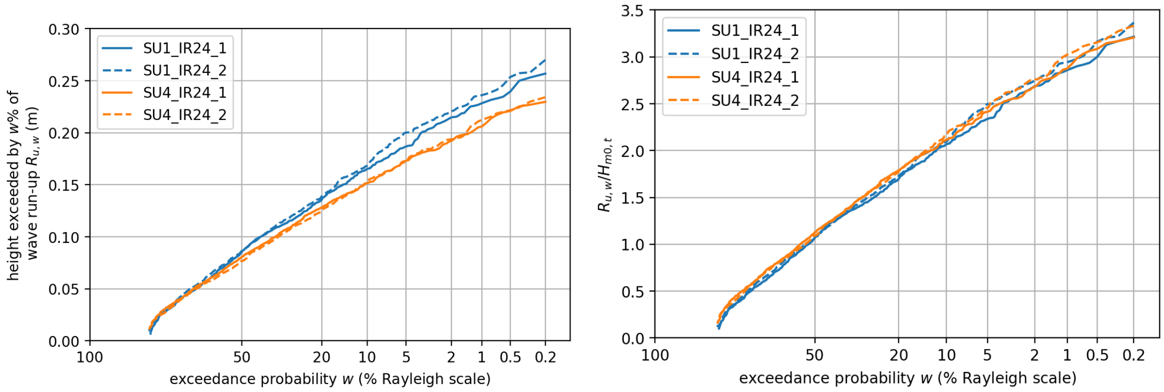

(a) Run-up distribution, for a given level on the dike

(b) Dimensionless run-up distribution: A given level on a dike divided by the incoming wave height $R_{u,w}/H_{m0,t}$

Figure 3.11: Estimated probability for wave run-up to exceed a given dike height ($w = \mathrm{P}(z_p > h_n)$) for tests IR24 ($d_o = 0.76$m, $H_{s,target} = 10$cm, $s_{target} = 4$ and $h_c = 0$m), without vegetation (SU1) and with vegetation (SU4) compared. The shape wave run-up distributions is primarily dependent on the wave height at the dike toe.

For a first analysis of wave run-up behavior to observe general behavior, plots showing the probability of exceedance distribution of wave run-up are made of wave conditions IR03 - IR09 (section 3.2.1). These are all water depths are higher than the vegetation height l_s, as these tests represent the extreme scenarios which are of interest for this thesis. The conditions of these tests are based on the water depth on top of the salt marsh, hence for an increase of cliff height h_c, d_m stays the same and d_o increases. For both cases with and without vegetation (Veg: Y and N) the distributions are examined.

The distributions of the unvegetated and vegetated salt marsh show a grouping of their distributions. In all cases the presence of vegetation reduces the height exceeded by run-up for a given exceedance probability. The influence of the cliff on the change in distribution, seems to be minor but is present. When analyzing IR03-IR05, which vary the wave steepness for the same water level and wave height, for unvegetated cases, having no cliff gives highest values for a given exceedance probability, where the cases with the largest cliff of 12cm give the lowest values.

Tests which have no cliff and no vegetation (light blue) show a slightly different behavior for exceedance probabilities higher than 50% in especially IR04, however which can also be seen in IR07. This could be either due to very shallow conditions or due to an error in the procedure for this test.

As all these wave run-up distributions results of the experiments all show a Rayleigh like shape, the 2% exceedance value of the distributions is suitable for the following comparisons.

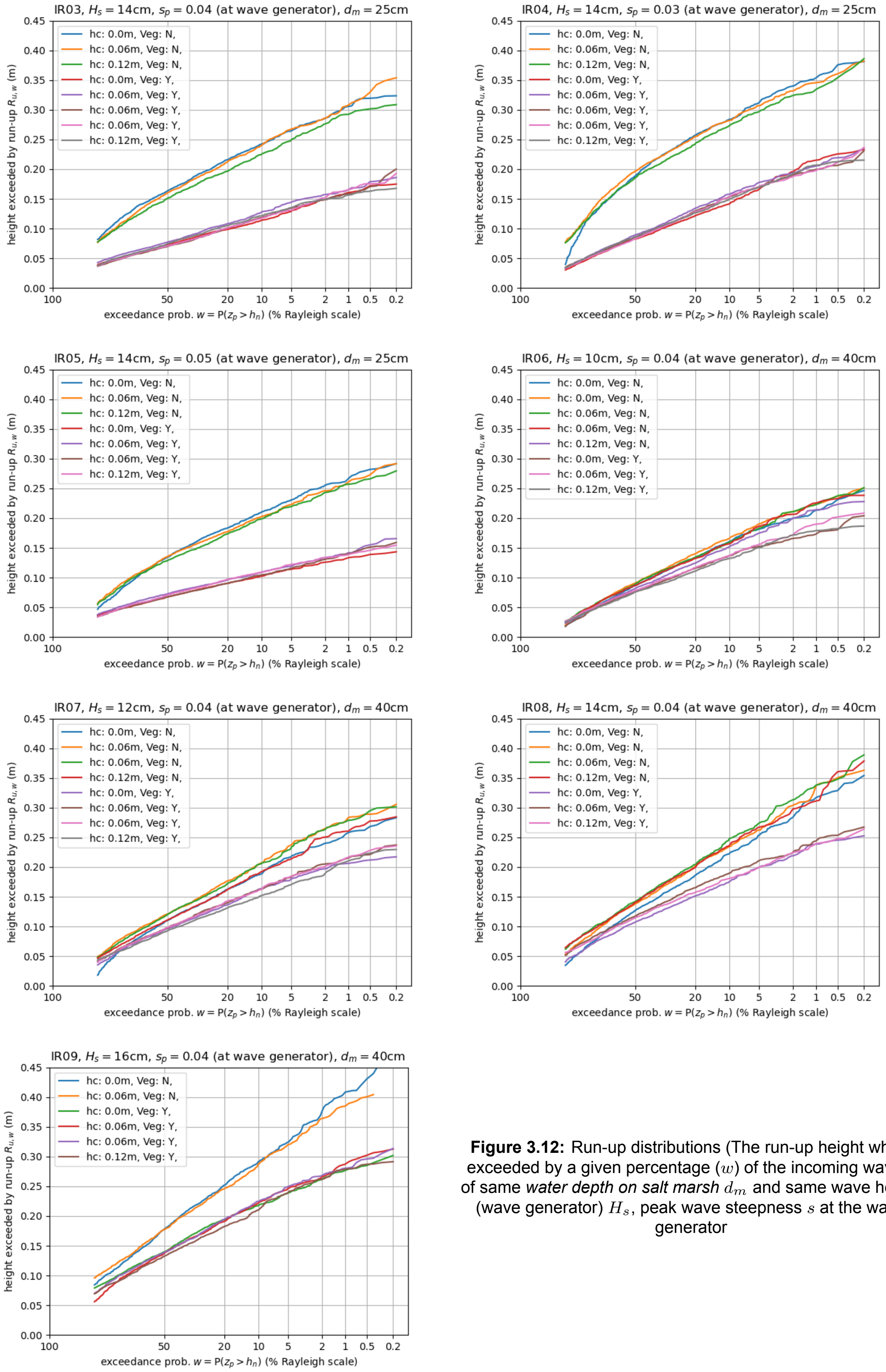

Figure 3.12: Run-up distributions (The run-up height which exceeded by a given percentage (w) of the incoming waves) of same *water depth on salt marsh* d_m and same wave height (wave generator) H_s, peak wave steepness s at the wave generator

3.2.2. Influence of wave height and wave steepness

A more detailed analysis can be made of how wave height and wave steepness is influencing wave run-up. The wave height is plotted versus $R_{u2\%}$ comparing the influence of vegetation and a cliff using the same offshore water depth (figure 3.13). As expected from equation (3.4), the increase in wave height leads to an increase in wave run-up. Vegetation shows a reduction in $R_{u2\%}$ where the reduction increases for a higher offshore wave height.

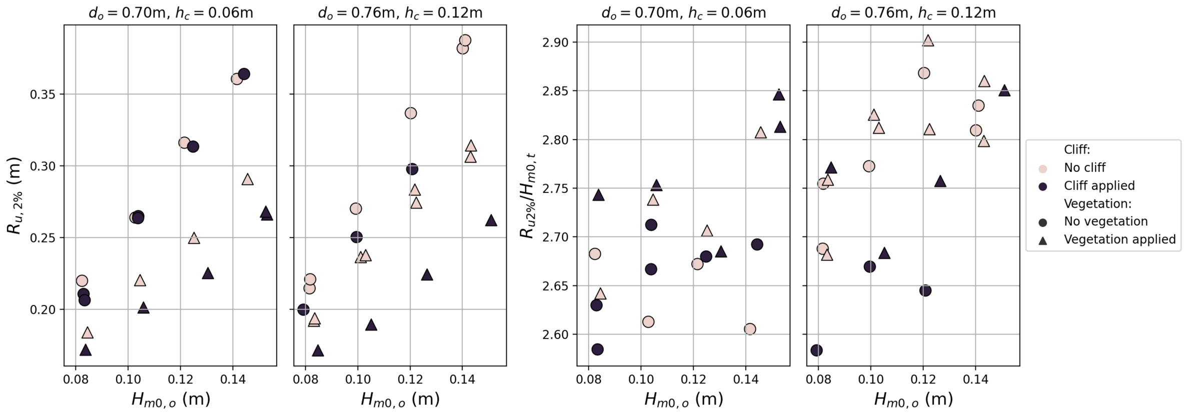

Figure 3.13: 2% exceedance values for different $H_{1/3}$ in deep water and different offshore water level (d_o), $s_p = 0.04$ at wave generator. If a cliff is present d_m = 0.40m. Wave run-up dependent on wave height, there is little influence of the cliff for $h_c = 0.06$m without vegetation, but with vegetation the presence of the cliff influences the wave run-up more. The cliff of $h_c = 0.12$m has for all cases influence.

The influence of the cliff is minor for a cliff height of 6cm ($d_o/h_c = 11.67$, and $d_c/h_c = 7.67$) (left), however becomes more prevalent at 12cm ($d_o/h_c = 6.33$, and $d_c/h_c = 4.33$) (right), where d_c is the water depth just before the cliff. Moreover, for a cliff height of 6cm the influence of the cliff is negligible for the cases without vegetation. This difference is mainly be due to wave breaking at the cliff, as observations during the experiment also show more breaking at the cliff and on the marsh for this larger height. This can also be seen in the wave height reduction analysis (figure C.10a), where waves with a higher reduction in wave height for the same water depth on the salt marsh correspond with a higher cliff height. Furthermore, this can't be due to breaking by the reduction in water level as the depth on the salt marsh is the same for both ($h_c = 0.06$ and 0.12) cases (0.40 m). This difference between cliff and no cliff becomes even more apparent when vegetation is present. In section 3.1.1 it is suggested that the presence of vegetation increases the 'perceived' bottom level, thus reducing the water level which affects the incoming wave. This same behavior could also explain this increased difference in run-up, which is influenced by an increased cliff step due to vegetation.

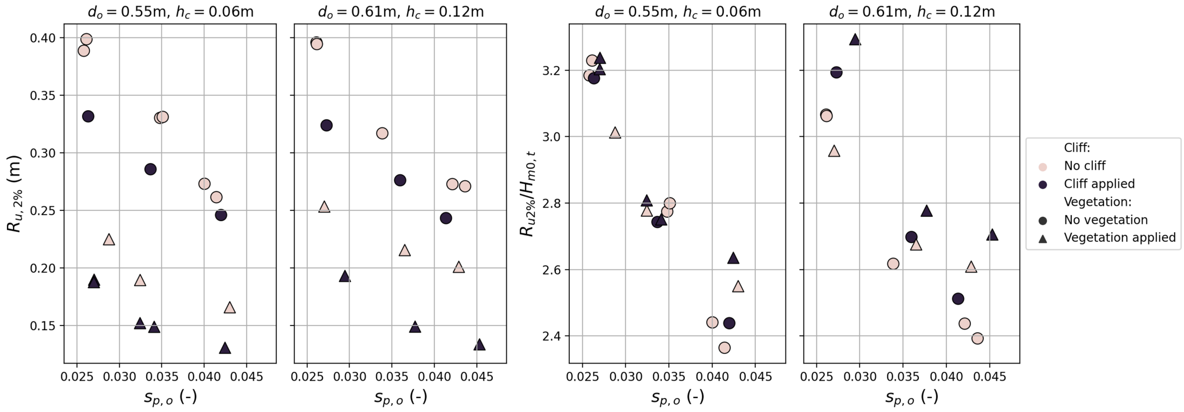

Figure 3.14: 2% exceedance values for different s_p in deep water and different deep water level, $H_s = 0.12$ at wave generator. If a cliff is present d_m = 0.25cm.

The offshore peak wave steepness $s_{p,o}$ vs $R_{u2\%}$ is plotted comparing the influence of vegetation and a cliff using the same offshore water depth (figure 3.14). As expected from equation (3.4) an increase in wave steepness leads to a decrease in $R_{u2\%}$. The contrast between the differences when a cliff is applied versus no cliff for cases with and without vegetation, which is seen when the wave height is varied, is not as strong when the wave steepness is varied.

3.2.3. Influence of water depth

To see how the water depth has influence on wave run-up, the water depth d_m versus $R_{u2\%}$ is plotted (figure 3.15). The selection is based on waves of $H_s = 12$cm and 14cm with $s = 0.04$ at the wave generator, for cases without a cliff. The influence of vegetation on the reduction of wave run-up can be seen to be increasing for lower water depths. For the largest water depths ($d_m = 0.64$) the influence is minimal and is in the order of a couple cm. The difference shows similar behavior to the difference in water height (figure C.9).

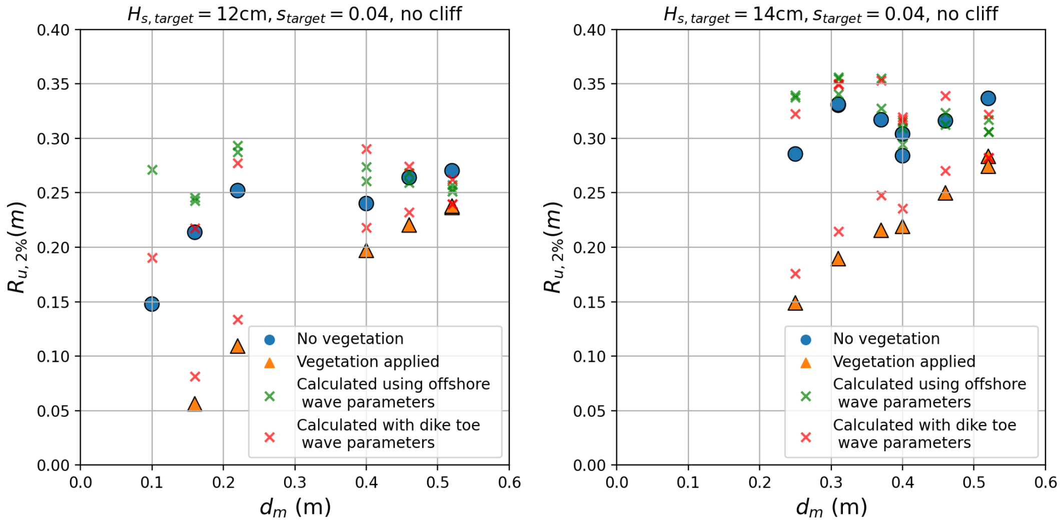

(a) Tests with $H_{s,target} = 12$cm

(b) Tests with $H_{s,target} = 14$cm

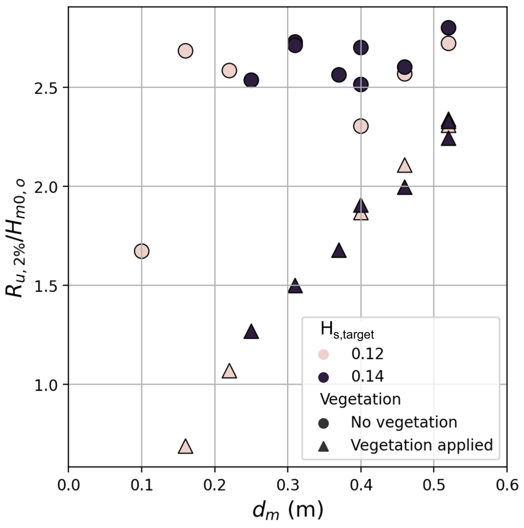

(c) Dimensionless run-up, combining a and b

Figure 3.15: Influence of water depth on $R_{u2\%}$ for cases with and without vegetation applied. For the calculated run-up value, the parameters $T_{m-1,0}$ and H_{m0} (offshore) are used to calculate $\xi_{m-1,0}$. The reduction in (dimensionless) wave run-up is strongly correlated with the water depth for cases with vegetation. Without vegetation, this relation is not as clear. Using $R_{rot} = 8H_s \tan\alpha$ (see appendix G) gives $R_{rot}(H_s = 0.12) = 0.27$m and $R_{rot}(H_s = 0.14) = 0.31$m

The EurOtop / TAW equation to calculate $R_{u2\%}$ (equation (3.4)) is applied to the cases described in figure 3.15, and displayed with red crosses in the figure. The run-up using red crosses is calculated using the wave conditions at the toe of the dike, the green crosses depict the run-up which is calculated using offshore wave parameters. As can be seen in figure 3.8, $T_{m-1,0}$ does not change significantly for most cases without vegetation when compared at the offshore location and at the toe of the dike.

Also, the wave height does not change much between the incoming waves and the figure C.9 for cases without vegetation (for higher water depths). Hence, the measurements without vegetation, for water levels greater than 0.1m are similar to the calculated values. A dimensionless run-up using the offshore wave height $R_{u2\%}/H_{m0,o}$ for these aforementioned cases is plotted for each water depth on the salt marsh d_m. For both cases, a similar reduction of this dimensionless run-up is observed.

The same plot is made including all tests, to see if this behavior is still present. Using a colormap of $\xi_{m-1,0}$ calculated using the measured offshore wave parameters (subscript o) (figure 3.16a) and a colormap of the cliff height (figure 3.16b), the dependence of these two variables on the dimensionless run-up can be shown (see also figure 3.16d). From equation (3.4) it is known that a higher Iribarren number leads to a higher relative run-up. If the Iribarren number is already high due to a lower wave steepness at offshore conditions, this results in a higher dimensionless run-up as well. The value of the dimensionless run-up is relatively constant, where the mean of $R_{u2\%}/H_{1/3,o} = 2.645$ (this will be explored further in section 3.2.4). The dimensionless run-up is affected by tests using a vegetated salt marsh, where a lower depth on the marsh leads to a lower dimensionless run-up, which seems to have a linear-like relation. For lower water levels (d_m =0.25m), the influence of the cliff also seems to play a role in the reduction of this dimensionless run-up. The higher water levels (d_m=40m) show less of an influence of the cliff. This influence is the same as described in section 3.2.2.

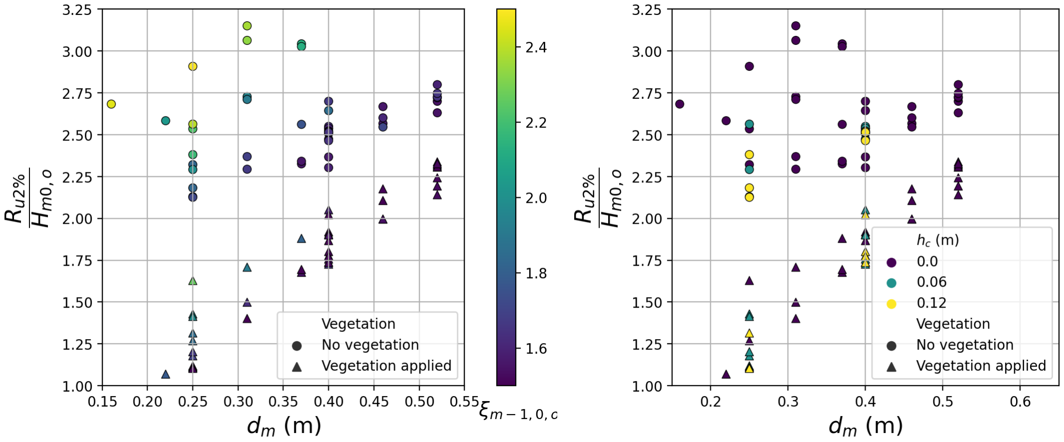

(a) Colormap of $\xi_{m-1,0,o}$ (offshore). High values of this offshore Iribarren parameter correlate with higher wave run-up.

(b) Colormap of h_c. Cases with a cliff are lower for $d_m = 0.25$m for unvegetated cases, but do differ less for others.

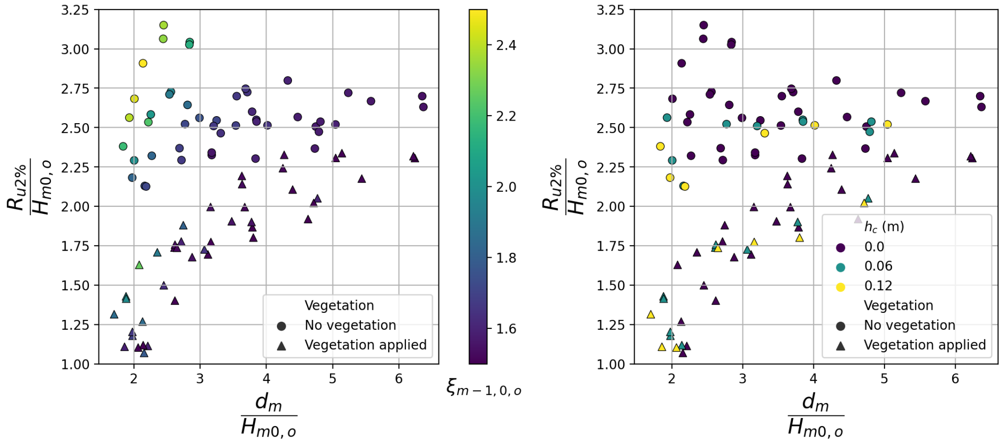

(c) $\xi_{m-1,0,o}$, using $d_m/H_{m0,o}$

(d) h_c, using $d_m/H_{m0,o}$

Figure 3.16: Influence of water depth on the wave run-up on all tests, with two colormaps. Similar behavior can be seen as in figure 3.15.

All tests which have equivalent input wave conditions are matched with each other (For example: SU1 IR05 is combined with SU4 IR05, both having $Hs_{target} = 14$, $s_{target} = 0.03$ and $d_m = 25$). In this way, the reduction of wave run-up can be estimated. This is expressed using a reduction factor due to vegetation present (veg) versus no vegetation (nv) $R_{u2\%,veg}/R_{u2\%,nv}$. As the measured offshore wave height of tests with vegetation in comparison without vegetation is 1-5% higher, the difference is taken into account in the comparative parameter by dividing each $R_{u2\%}$ by its respective $H_{m0,o}$. This run-up reduction factor is plotted versus the water depth (figure 3.17a). To make the water depth dimensionless, the water depth is divided by the length of the shoots of the vegetation model. As only 1 vegetation length is tested, this is done with the purpose to give a sense of dimension (see upper axis). The reduction in $R_{u2\%}$ is mainly affected by the depth of the water column on the salt marsh, where a lower depth gives a larger reduction and a higher depth a lower reduction. This is expected as wave breaking and wave shoaling is highly affected by water depth. The wave steepness is also of importance for these processes, which can also be seen in the figure (coloring of the points). The wave steepness has an influence which seems to determine the speed in which a certain water depth reduces the wave run-up. If the tests with and without vegetation including a cliff are compared to each other, the presence of the cliff reduces the relative effect of the vegetation, as a larger part of wave breaking is happening around the cliff. However, this effect is more clear for $d_m = 0.25$m than 0.40m. Another way to make the relation dimensionless is by dividing d_m by $H_{m0,o,veg}$ or $L_{p,o,veg}$ as the presence of vegetation dampens the additional reflections at the wave maker (figure 3.2). A slightly more curved but still linear like relation is observed between the run-up reduction factor and this parameter (figure 3.17b). The scatter which was seen for $d_m = 0.40$m is reduced by the usage of the wave height.

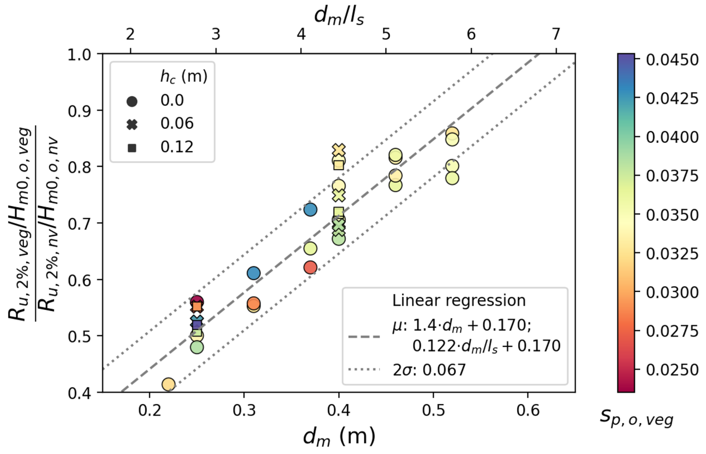

(a) Reduction versus salt marsh depth d_m. A linear fit is made with 2σ bands

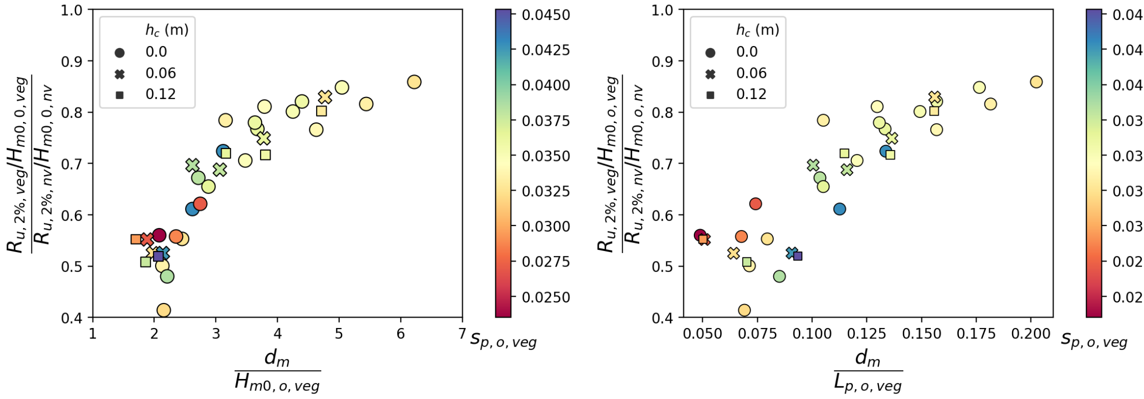

(b) Reduction versus $d_m/H_{m0,o,veg}$

(c) Reduction versus $d_m/L_{p,o,veg}$

Figure 3.17: Reduction factor in run-up 2% due to vegetation. For every wave condition, with similar flume configuration except the presence of vegetation is compared with each other. The wave run-up is made dimensionless by using the offshore wave height. The reduction of wave run-up has a linear correlation with primarily the water depth on the salt marsh. If wave height or wave length are added to make the relation dimensionless, the relation becomes slightly curved. See also figure 3.16d

The reduction of wave run-up shows to be mainly affected by the water level on the salt marsh, with also an influence of the offshore wave height and wave steepness. This is similar to the reduction of wave height and spectral period (which can be combined into an increase in Iribarren number) over the salt marsh shown in section 3.1.1. A conservative linear extrapolation of the results lead to no influence when $d_m > 0.55 \approx d_m/l_s > 6$. Cases with water levels lower than this are affected by vegetation reducing run-up for where every reduction in water level equal to one vegetation length reduces the run-up by 12.2%.

3.2.4. Comparison with literature and changes in behavior

The wave measurements at the toe of the dike are calculated, hence they can be used to compare the wave run-up measurements with equation (3.4).

EurOtop / TAW wave run-up equation

The Iribarren parameter $\xi_{m-1,0}$ vs dimensionless run-up R_u/H are plotted in figure 3.18 (for all tests with wave conditions IR03 - IR09, IR11-IR18, and IR20 - IR27, which represent intermediate wave conditions, see table F.1). The equation is designed to be used using H_{m0} and $T_{m-1,0}$ obtained at the toe of the dike (section 3.1.1). The measurements are in general lower than predicted using the equation (table 3.1), especially for the tests with vegetation for $\xi_{m-1,0}$ between 2 and 4. This cannot be solely due to errors in the calculation of $T_{m-1,0}$, as this is also observed if T_p is used to compare the measurements versus calculated values (figure 3.18b). For T_p is directly obtained from the wave spectrum without any calculations. The presence of the cliff does not seem to be of significant influence when the parameters of the toe are used (figure 3.18d). This means that the wave parameters at the toe do already capture this change, and the wave breaking in the cliff does not lead to an alteration in the physical way the wave interacts with the dike.

$H_{1/3}$ is slightly lower than H_{m0} at the toe of the dike, due to heavy breaking on the foreshore. Hence, an alteration to the equation can be proposed were $H_{1/3}$ is used in the calculation of all variables instead of H_{m0}. The influence of this altered wave height moves the positions up on the graph, as the reduction of the $H_{1/3}$ in comparison with H_{m0} gives an increase in R_u/H. In this way, the equation aligns closer to the measurements than by using $H_{m0,t}$ as given in equation (3.4) (table 3.1). This relatively small increase in value for wave height, increases the fit between the formula and measurements quite substantially, hinting at the sensitivity of the formula on the wave height.

The Iribarren parameter $\xi_{m-1,0}$ is situated at 1.6 and higher, which is already close to the beginning of the higher part in the equation. This means that the wave run-up in these measurements are mostly dependent on the incoming wave height, as the relation between $R_{u2\%}/H_{m0}$ flattens out from around $\xi_{m-1,0} = 1.7$ and onward. As the change in $H_{m0,nv}$ (cases without vegetation) over the salt marsh remains fairly constant for $d_m/H_{m0,nv,o} > 2.5$ (figure 3.6b), the wave run-up behavior is not strongly affected by the presence of the foreshore alone. For cases with vegetation, there is always influence on the decrease in wave height. Therefore the behavior shown in figure 3.16 and figure 3.17a can be explained, where the main difference between the wave run-up with and without vegetation is related to the water depth on the salt marsh.

Replacing H_{m0} with $H_{1/3}$ in equation (3.4), seems to account for the largest differences with the measurements and the equation. In figure 3.5, a relation between $H_{1/3}/H_{m0}$ and d_m/gT_p^2 was described, which was dependent on d_m/gT_p^2. Therefore, if $R_{u2\%}/H_{m0}$ is compared against d_m/gT_p^2, the influence on wave run-up can be analyzed further. There is a general reduction for both tests with and without vegetation for $0.007 > d_m/gT_p^2 > 0.024$ (figure 3.19). It can be derived that there are more parameters of influence than the wave height, water depth and spectral period at the toe for the tested cases (see also figure C.14).

Table 3.1: Errors between measured and calculated run-up 2% for tests with intermediate wave conditions, obtained with H_{m0} and $H_{1/3}$ at the toe of the dike of incoming waves

R^2	H_{m0}	$H_{1/3}$
All	0.885	0.950
No vegetation	0.852	0.976
Vegetation applied	0.786	0.878

$RMSE(mm)$	H_{m0}	$H_{1/3}$
All	24	16
No vegetation	19	8
Vegetation applied	27	21

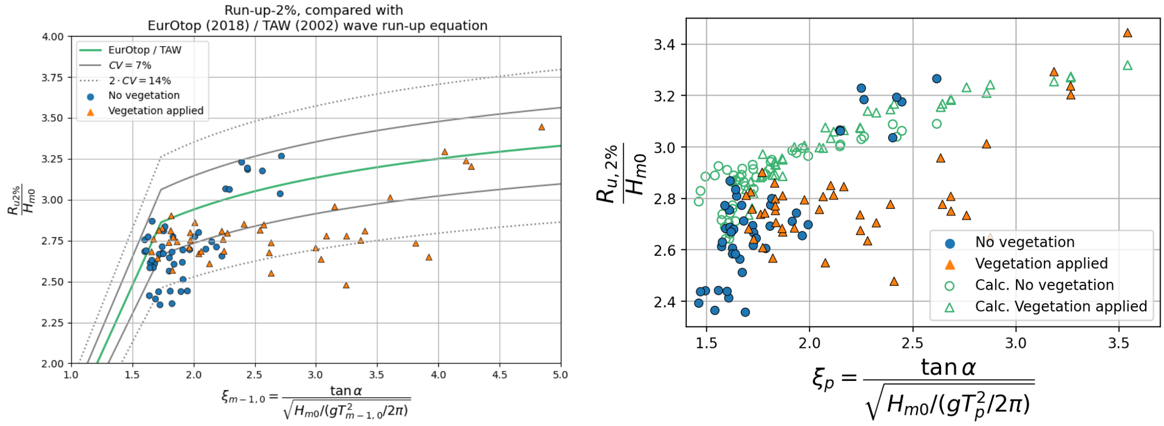

(a) Using H_{m0}. Most measurements are lower than predicted, this includes the measurements without vegetation.

(b) Iribarren parameter calculated using T_p, versus $R_{u,2\%}/H_{m0}$. The calculated values are calculated using the EurOtop / TAW equation, using H_{m0} and $T_{m-1,0}$.

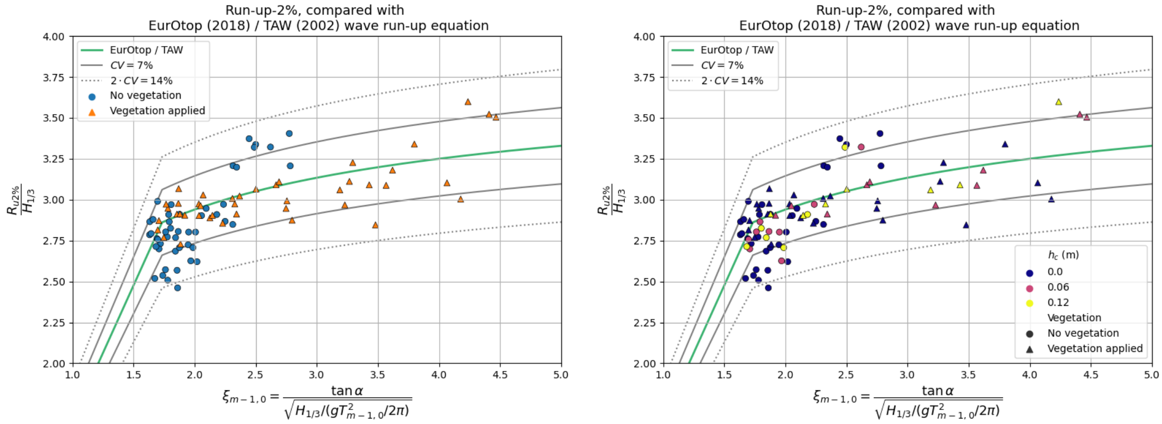

(c) Using $H_{1/3}$. Most measurements are around the predicted value using the equation where H_{m0} is replaced with $H_{1/3}$.

(d) Influence of cliff, using $H_{1/3}$. The cliff shows to be not of major influence as the spread is similar to cases without a cliff

Figure 3.18: Comparison wave run-up vs Iribarren parameter at the toe of the dike. The EurOtop (2018) and TAW (2002) formula is calculated using the displayed definitions, and plotted to compare the measurements. A coefficient of variation $CV = 7\%$ (TAW, 2002) is used to depict the exceedance. $2 \cdot CV$ corresponds with the $2\sigma = 95.45\%$ confidence bands

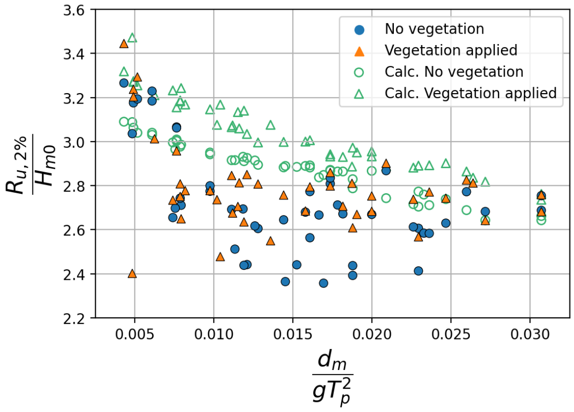

Figure 3.19: Influence of $d_m/gT_{p,t}^2$ at the toe of the dike. The calculated values are calculated using the EurOtop / TAW equation, using H_{m0} and $T_{m-1,0}$.

The change between the wave run-up with and without vegetation is visually depicted using vectors (figure 3.20). The increase in $\xi_{m-1,0}$ due to vegetation leads to a slightly upwards rightwards movement when $H_{1/3}$ is used, following equation (3.4). This increase in Iribarren number is caused by the change in wave height and spectral wave period over the salt marsh. However, increase in $\xi_{m-1,0}$ due to vegetation leads to a only a mostly rightwards movement when H_{m0} is used. This means that this dimensionless wave run-up (using H_{m0}) is largely unaffected by the change in $\xi_{m-1,0}$.

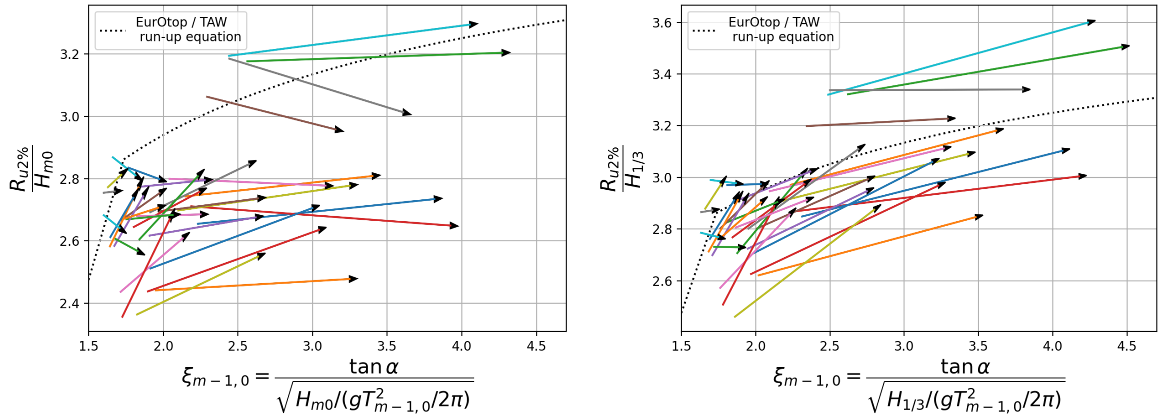

(a) H_{m0}. The change in dimensionless wave run-up is mostly horizontal, showing a lower dependency of the Iribarren parameter.

(b) $H_{1/3}$. The change in dimensionless wave run-up follows the equation, where a higher Iribarren parameter increases this dimensionless wave run-up as well.

Figure 3.20: Change in run-up 2% from cases without vegetation to cases with vegetation. To give a sense of the amount of change on the plot, equation (3.4) is plotted.

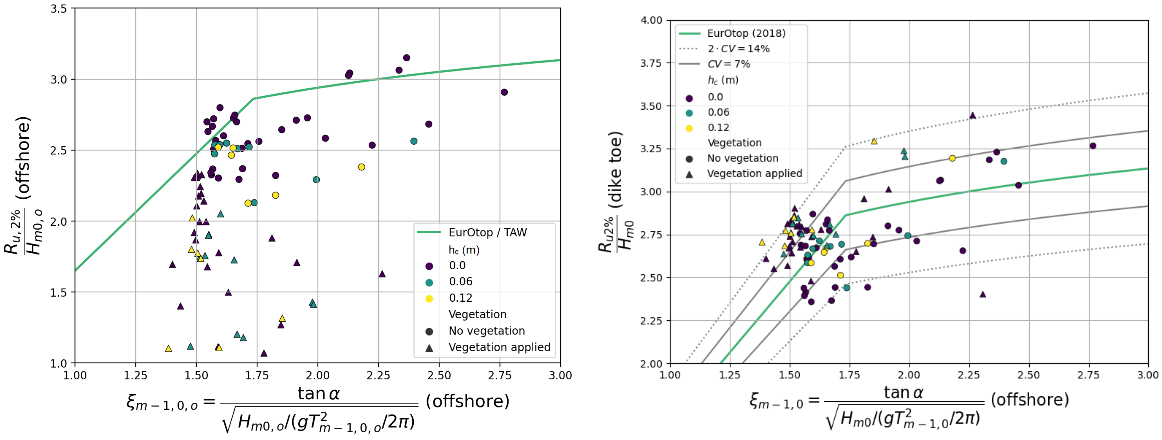

(a) $\xi_{m-1,0}$ calculated using dike slope (1./3.6) and offshore wave characteristics.

(b) An 'engineering' fit can be made with equation (3.4) using H_{m0}, in the left-hand side of the equation. This is accomplished by using the Iribarren parameter which is calculated using offshore wave characteristics and the run-up is divided by the wave height at the dike toe.

Figure 3.21: Usage of the wave run-up equation (EurOtop, 2018; TAW, 2002) with wave characteristics measured offshore.

Table 3.2: Errors between measured and calculated $R_{u2\%}$, of figure 3.21b. Using the Iribarren parameter which is calculated using offshore wave characteristics and the run-up is divided by the wave height at the dike toe

	R^2	$RMSE(\mathrm{mm})$
All	0.911	21
No vegetation	0.872	21
Vegetation applied	0.847	20

Using color mapping of the wave characteristics described in section 3.1.1 on the wave run-up plot, an visual understanding on the affected change is displayed (figure C.16, using $H_{1/3}$). As $\Delta\xi \propto \Delta T/(\Delta H)^{1/2}$, the change in $T_{m-1,0}$ is more dominant than the change in $H_{1/3}$. Therefore, the wave height decrease over the salt marsh is overruled by the increase in spectral wave period. As the resulting relative run-up needs to be multiplied by the incoming wave height, which is significantly reduced, the resulting non dimensionless run-up becomes less.

In figure 3.21a the run-up is estimated using offshore wave characteristics. Most measured values, especially using vegetation are lower than predicted. This is to be expected as the significant wave height reduces along the salt marsh. If instead of using all parameters at offshore location in equation (3.4), the wave height H_{m0} at the toe of the dike is used in the left-hand side of the equation, the change in wave height is taken into account without changing the Iribarren number. In this way, a better prediction can be made than using all parameters at offshore location (figure 3.21, table 3.2). The scatter is reduced by the inclusion of the wave height at the toe. Such a relation could be used in the developing in an engineering method to predict wave run-up for salt marshes.

Influence of s_p in deep water and shallow water is plotted using color mapping on the measured data versus equation (3.4) (figure 3.22, figure C.17), which is depicted as well by calculation of the factor between measured versus the predicted wave run-up (using equation (3.4)). A negative correlation between the offshore peak wave steepness $s_{p,o}$ and the difference in the measured run-up value versus the predicted value can be seen (see also figure C.17a). Lower offshore peak wave steepnesses (0.025 - 0.030) correlate with correctly predicted wave run-up values. The higher wave steepnesses (0.040 - 0.045) correspond with lower than predicted values. This is present in especially the non linear part of the wave run-up equation (equation (3.4)). Hence, if the relation using H_{m0} is deemed correct, this means that the influence of the wave breaking occurring leads to an altered wave spectrum. This leads to a lowered wave run-up versus the predicted parameter. This is way less visible seen for the peak wave steepness at the toe of the dike (figure C.18). This is for both cases with and without vegetation. This relation is also less present when $s_{m-1,0,o}$ is used (figure C.19).

This is likely due to the influence of wave steepness and wave breaking. As wave steepness is defined as H/L, a lower wave steepness means a longer wavelength for the same wave height. Less steep waves do not break as much as steeper waves. Wave breaking results in a redistribution of the wave spectrum, where the peak flattens out and the generation of lower frequency components give rise to a double peaked wave spectrum. From section 3.1.1 it is known that the change in peak wave steepness between the vegetated and unvegetated cases is mostly dependent on the change in wave height. However, plotting the water depth over wave height ratio does not give as clear as an distinction as peak wave steepness (figure C.20)

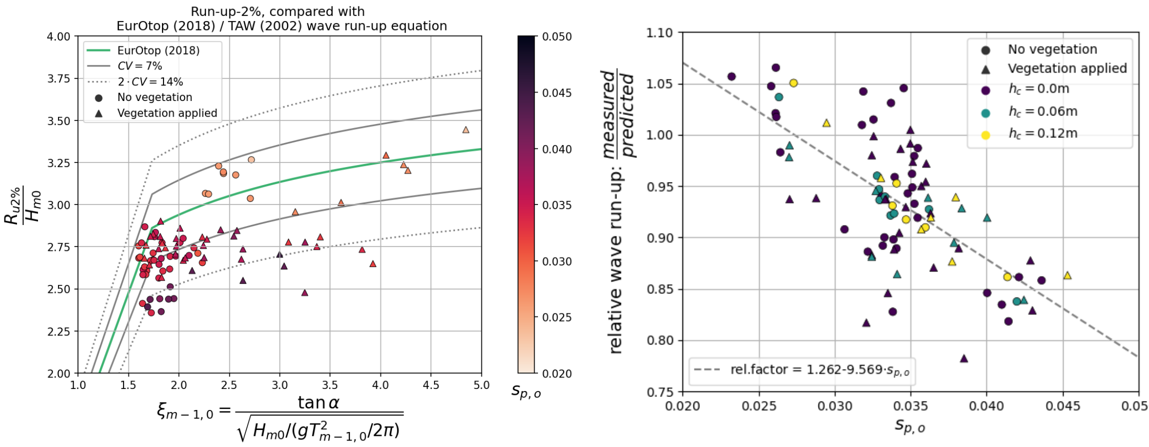

(a) Comparison wave run-up vs Iribarren parameter at the toe of the dike. The peak wave steepness is plotted using a colormap.

(b) Correlation between $s_{p,o}$ and the difference factor between measured and predicted relative wave run-up ($R_{u2\%}/H_{m0}$)

Figure 3.22: Influence of offshore peak wave steepness on measured wave run-up compared with EurOtop (2018) and TAW (2002). A correlation can be found between the reduction in (dimensionless) wave run-up and offshore wave steepness.

Van Gent wave run-up equations

Experiments were carried out by Van Gent (1999a), using double peaked wave spectra which occur in shallow water depths. This resulted in a different wave run-up relation than equation (3.4). In the report the following empirical relationship was devised:

$$\frac{R_{u2\%}}{H_{s,t}} = \begin{cases} c_0 \cdot \xi_{m-1,0} & \text{for } \xi_{m-1,0} \le \frac{1}{2}c_1/c_0 \\ c_1 - c_2/\xi_{m-1,0} & \text{for } \xi_{m-1,0} > \frac{1}{2}c_1/c_0 \end{cases} \quad , c_2 = \frac{1}{4}\frac{c_1^2}{c_0} \tag{3.5}$$

Where H_s could be chosen as H_{m0} or $H_{1/3}$. The values of the coefficients change depending on the choice. For $H_{m0} : c_0 = 1.45, c_1 = 3.8$ (**VG0**) and for $H_{1/3} : c_0 = 1.35, c_1 = 4.7$ (**VG3**).

From the comparison with the EurOtop (2018) and TAW (2002) equation, it can be seen that interchanging H_{m0} and $H_{1/3}$ could lead to additional alternative equations with potentially better fit. Hence, **VG0** and **VG3** are compared with using both equations with H_{m0} and $H_{1/3}$.

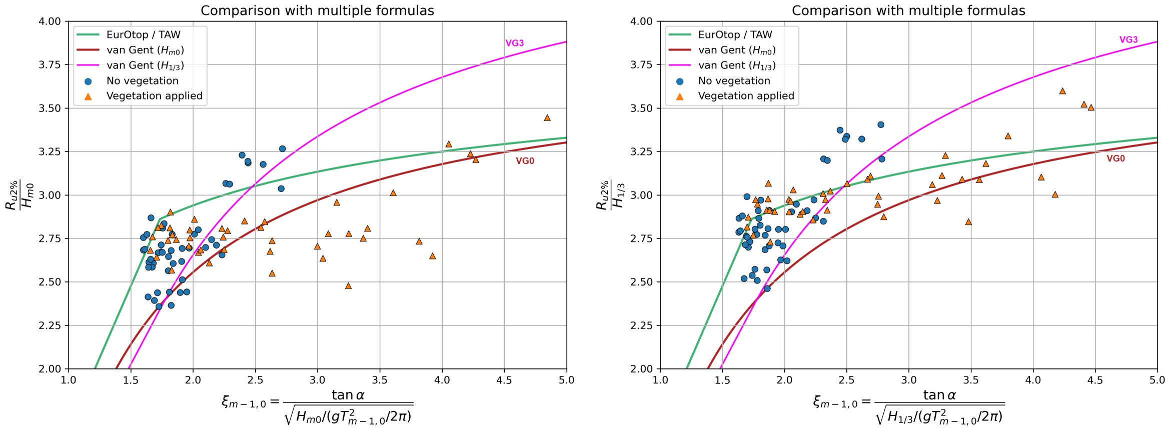

(a) Using H_{m0}, **VG0**

(b) Using $H_{1/3}$, **VG3**

Figure 3.23: Comparison wave run-up vs Iribarren parameter at the toe of the dike. Comparing the measurements with formulas derived in TAW (2002) and Van Gent (1999a).

Table 3.3: Errors between measured and calculated run-up for tests with intermediate wave conditions, obtained with H_{m0} and $H_{1/3}$ at the toe of the dike of incoming waves. VG0 depicts the van Gent formula derived using H_{m0} in the his results, VG3 depicts the van Gent formula derived using $H_{1/3}$ in his test results

(a) R^2

R^2	**VG0**		**VG3**	
	$\boldsymbol{H_{m0}}$	$H_{1/3}$	H_{m0}	$\boldsymbol{H_{1/3}}$
All	0.85	0.768	0.818	0.819
No vegetation	0.715	0.557	0.763	0.679
Vegetation applied	0.845	0.765	0.646	0.778

(b) $RMSE$

$RMSE$ (mm)	**VG0**		**VG3**	
	$\boldsymbol{H_{m0}}$	$H_{1/3}$	H_{m0}	$\boldsymbol{H_{1/3}}$
All	27	33	29	29
No vegetation	32	39	29	34
Vegetation applied	20	25	30	24

The van Gent formula using $H_{1/3}$ (magenta curve, **VG3**) shows a visually better alignment with the cases without vegetation which were deviating from the EurOtop / TAW formula (figure 3.23, table 3.3). This is most likely due to the similar conditions tested in van Gent and this experiment. However, the test using vegetation do align better with the van Gent formula using H_{m0} (**VG0**). But in general the EurOtop / TAW formula using $H_{1/3}$ aligns the best.

To summarize, comparing the measurements to the EurOtop (2018) and TAW (2002) wave run-up equation, shows that more than half of the measured $R_{u2\%}/H_{m0,t}$ values are lower than what is predicted by the equation, if the equation is used without alterations. The following observations relevant to this for wave run-up were made:

- Substituting H_{m0} with $H_{1/3}$ in the equation resulted in an increase in the fit of the equation. This while on average $H_{1/3}$ is measured 5mm / 5% lower than H_{m0} (up to 10% for cases with vegetation), which depicts the large influence of H_s on the equation.
- The offshore peak wave steepness $s_{p,o}$ has influence on the fit with the equation for all experiments. $s_{p,o}$ has a negative correlation with the difference factor between measured and predicted relative wave run-up. This influence is only half as strong when the peak wave steepness is calculated at the toe of the dike.
- The change between $R_{u2\%}/H_{m0,t}$ for cases without vegetation to with vegetation is less dependent on the change in $\xi_{m-1,0,t}$ than predicted by the equation, for $\xi_{m-1,0,t,nv} > 1.8$.
- The change between $R_{u2\%}/H_{1/3,t}$ for cases without vegetation to with vegetation does follow the equation more closely
- Substituting $\xi_{m-1,0,t}$ (dike toe) with $\xi_{m-1,0,o}$ (offshore) in the equation does show a good fit with the considered cases.

From this it can be argued that the reduction in wave height plays a more important role in the wave run-up behavior changes due to vegetation than the increase in Iribarren number. This is relation is present for both cases with and without vegetation, but is especially present for cases with vegetation for $\xi_{m-1,0,t} > 2.4$. The fit using the Van Gent (1999a) wave run-up equation, is less in general than EurOtop (2018) and TAW (2002).

4

Discussion

The wave characteristics and wave run-up are analyzed in a detailed manner in the Results. A more comprehensive discussion about the implications of these results is discussed. After this the intricacies of the methodology are discussed.

4.1. Wave characteristics

At the wave maker, a portion of the incoming waves are not compensated and are reflected back onto the wave flume, which influence is visible in the incoming wave signal (figure 3.2). This is especially prevalent for frequencies between 0-0.3 Hz. This shows as an increase in $T_{m-1,0,o}$ as these lower frequency components have a large influence on this parameter. This increase is especially apparent for the tests without vegetation, because vegetation dampens the reflected wave energy. These additional long waves added to the incoming wave spectrum are not bound to the generated wave spectrum and can have an influence on the spectrum at the toe of the dike (as they act as unbound infra-gravity waves), which was used for example in the comparison in the wave run-up.

Wave measurements were obtained at the dike toe from WG and EMF readings during the same experiments as when the wave run-up was obtained. Common analysis procedures for wave run-up require the wave height of the incident waves at the toe of the dike as input (Van Gent, 1999a). The usage of the Guza et al. (1984) reflection analysis can be too inaccurate, especially for tests in more shallow water, since some wave breaking and other non-linear phenomena are present at the toe of the structure. In Van Gent (1999a), this was accounted for by repeating the tests without the dike in position to obtain the incident waves at the toe of the structure. Besides doubling the experiment duration, this procedure also introduces undesirable effects since waves reflected by the dike interact with incident waves, which cannot be modeled in this way. 'Surfbeat-phenomena (the propagation of wave groups and their associated long wave motion) for which wave reflection is important, play a role in shallow water with breaking waves' (Van Gent, 1999a). Hence, these effects need to be modeled including the effects of vegetation.

To account for the unwanted reflections at the wave maker and the inaccuracies of the wave reflection analysis, an accompanying computational model (digital twin) can be made to validate the wave measurements, and assess the influence of the wave reflection at the wave generator (e.g. (Maza et al., 2023)). This can give further validity to the experiments, which is needed to assess if the given observations are caused by physical phenomena or effects of physical modeling / processing.

The measured wave conditions at the offshore location (WG4) experience intermediate water conditions, which is a result of the chosen test conditions. As a result, the wave transformation, over the distance from the wave generator to the measured wave, is lower than the input wave height. Hence, the wave height H_{m0} and $H_{1/3}$ show already difference at this offshore location. Similarly, $T_{m-1,0}$ is already bigger than $0.9T_p$ at this location. However, this has some effects on the analyses. The fact that the offshore conditions are already in intermediate waters, means that relations that are described, are comparing these already intermediate water conditions with other intermediate water conditions. This can be influencing for instance the transformation of wave height and wave length. For example in the comparison of the change in $T_{m-1,0}$ between offshore and the toe of the dike (figure 3.8), the measurements without vegetation with $d_m/H_{m0,o} < 3$ deviated from the predicted equation, due to the offshore conditions not being in deep waters and the presence of the unbound long waves. The vegetated salt marsh tests use the same wave conditions for their relative cases, which could mean that the compared equation under predicts the same cases. This same influence is for the same reasons also present in other results where the difference between offshore and at the toe of the dike conditions is shown.

4.2. Wave run-up

All described differences between the wave run-up measurements and literature could be explained by an alteration in the wave set-up during the experiments versus what is used in the equations. Wave set-up is not taken into consideration separately when calculating wave run-up, as the effects of wave set-up are included by the empirical fit of the wave run-up equation, as wave run-up is calculated from SWL (TAW, 2002). Wave set-up is altered by wave breaking, which occurs more on salt marshes. Significant wave breaking was also observed in the measurements (section 3.1). A significant reduction in wave height, and alteration of the relationship between $H_{1/3}$ and H_{m0} was seen for the experiments with and without vegetation. Hence, a major alteration in wave breaking behavior, leads to a change in wave set-up behavior, which is unaccounted for in the empirical fit of the wave run-up equation. Hence, the major deviations of the wave run-up results could be explained by the increase or reduction in wave set-up in comparison with the fitted experiments.

Morover, offshore peak wave steepness is shown to have a correlation with the deviation of the measured wave run-up in comparison of what is predicted by the wave run-up equation (EurOtop, 2018; TAW, 2002) (figure 3.22). Lower wave steepnesses correlate with a higher wave set-up for the same shoreline (Battjes, 1974; Goda, 2008). The influence of wave steepness on the wave run-up is captured generally by the Iribarren number which divides the bottom slope (in this case the dike slope) by a form of wave steepness equation (2.14). However, this takes the wave set-up only indirectly into account. The increased fit where H_{m0} is replaced by $H_{1/3}$ in equation (3.4), also alludes to the influence of wave set-up, as the relation between $H_{1/3}/H_{m0}$ and wave set-up are both dependent on the amount of wave breaking and shoaling (Holthuijsen, 2007; Thompson & Vincent, 1985). H_{m0} at the dike toe can be up to 14% higher than $H_{1/3}$, depending on the water depth. This difference is the highest for the tests using a vegetated salt marsh. The reduction in $R_{u2\%}/H_{m0}$ in comparison with the equation could be a result of a reduction in wave set-up, which was also observed in Keimer et al. (2021).

In Keimer et al. (2021) and Maza et al. (2023) a similar reduction of the $R_{u2\%}/H_{m0}$ between the measurements and (EurOtop, 2018; TAW, 2002) equation was seen. However, the correlation with offshore wave steepness or similar correlations were not described yet, as well as the comparison with $R_{u2\%}/H_{1/3}$.

Using the van Gent equations, a closer alignment with tests with an offshore steepness away from 0.035 can be seen. This could be due to the definition of the formula being made with a foreshore present, where more wave transformation has occurred. Moreover, this dependency of offshore wave steepness on wave run-up could also be increased as a result of scaling effects. Hence, this different behavior which is affected by wave breaking is not described fully. A comparison with a dataset using multiple flume configurations is needed to see if this influence is present in general or unique to salt marshes.

In figure 3.21, the Iribarren parameter is calculated using wave parameters from the offshore location, and $R_{u2\%}$ is divided by the wave height in the dike toe. The fit using this method is mostly accurate as the scatter is situated in the 2σ area. This fit does work as the change between $R_{u2\%}/H_{m0,t}$ for vegetated and unvegetated cases is mostly independent of the Iribarren parameter measured at the toe of the dike (figure 3.20). The Iribarren parameter does not change substantially for cases without vegetation when calculated offshore or at the toe of the dike, but does for the cases with vegetation (figure 3.9b). The Iribarren parameter changes much under the influence of vegetation due to the exponential increase in $T_{m-1,0}$ depending on the water depth (by the increasing presence of a low frequency peak) and the more linear decrease in H_{m0}. As $\Delta\xi \propto \Delta T/\Delta\sqrt{H}$, the exponential increase in $T_{m-1,0}$ is dominant in determining the Iribarren parameter. However, this increase due to these low frequencies is not seen in the wave run-up results (figure 3.20). Two methods can be suggested to account for this phenomenon, if the influence of the change wave set-up is not accounted for:

- In Holterman (1998), the usage of $T_{m-1,0}$ was found to have the best fit with wave run-up. However, a lower integration bound of 0.03Hz (33s) in the calculation of the spectral moments was proposed, to account for the lowest frequencies in the wave spectrum, which have a large influence on $T_{m-1,0}$. Such an integration bound, or application of a filtering technique where the response to certain lower frequencies are reduced, could increase the fit.
- The Iribarren parameter could be based on the predicted change as if there is no vegetation present (figure 4.2). However, this needs to be validated, as the incoming wave height offshore is slightly higher for tests with vegetation than tests without vegetation. The wave run-up can be calculated by calculating the Iribarren parameter as if there is no vegetation. The dimensionless wave run-up can be calculated with the wave run-up equation in EurOtop (2018) and TAW (2002). However, instead of multiplying this dimensionless wave run-up by the wave height without the influence vegetation at the toe, it should be multiplied by the wave height with vegetation taken into account.

If these relations hold true for different vegetation heights, dike slopes and salt marsh lengths, it could be a basis for a relatively straightforward prediction of wave run-up influenced by a salt marsh, without altering the equation.

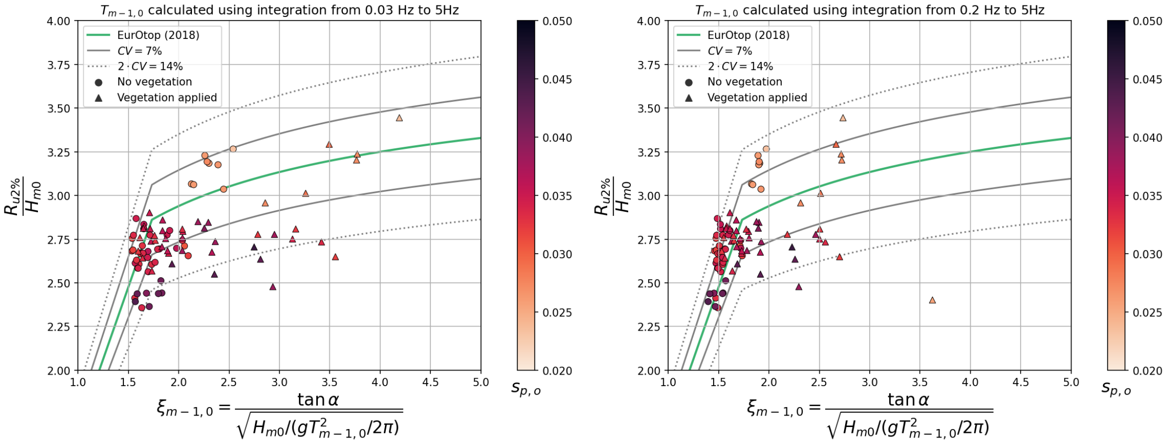

(a) m_{-1}, m_0 obtained from an integration from 0.03Hz to 5Hz **(b)** m_{-1}, m_0 obtained from an integration from 0.2Hz to 5Hz

Figure 4.1: Wave run-up compared with EurOtop (2018) and TAW (2002), using different integration bounds for the spectral moments used in the calculation of $T_{m-1,0}$.

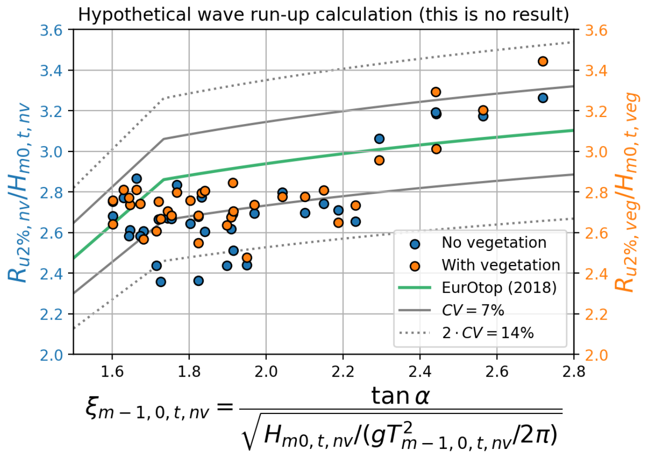

Figure 4.2: Wave run-up compared with EurOtop (2018) and TAW (2002). Unchanged for tests without vegetation. The Iribarren number for tests with vegetation is replaced by the Iribarren number of the same test-id without vegetation. $R_{u2\%}$ is divided by the measured wave height of the original vegetated test (right side, orange)

To summarize, the following adaptations can be considered when assessing wave run-up influenced by a salt marsh:

- Implement the influence of wave set-up into the calculation of wave run-up.
- Calculate $\xi_{m-1,0}$ as if there is no vegetation, even when vegetation is present.
- Adapt the calculation of $T_{m-1,0}$ by way of a lower integration bound, or application of a filtering technique to reduce the influence of certain range of the wave energy spectrum
- Implement another term which captures the influence of the offshore wave steepness
- Replace H_{m0} with $H_{1/3}$ in the equation

If these adaptations does not solve the issue, a new fit for the right-hand side of the wave run-up equation may be necessary.

4.3. Methodology

The methodology makes use of a video tracking procedure to track wave run-up, which is used in a physical scale model. The intricacies of both are discussed.

Video tracking procedure

A computer vision method is chosen to measure wave run-up, which has some disadvantages compared with the usage of wave run-up gauges. Any visual disturbances, to the area of the field of view that is being processed, are captured as well, because it is a visual method. These can range from light flickering and splashes to people moving in range of the area. It takes also a considerable amount of time to process (the video files belonging to a single test take about 30-40 minutes of processing time). However, this processing time could be significantly improved by implementing the process using a graphics card, which is optimized for these kinds of calculations. Further verification of this method is necessary since a conventional run-up gauge was not available during these experiments. Video cameras could be positioned in other run-up measurement scenarios where resistance-type gauges are present, facilitating a thorough comparison with the method and potential enhancements. Since only the maximum run-up over a restricted area was verified, a full-width verification is essential. Additionally, since the method has only been tested in a controlled laboratory setting, more research is needed to determine its suitability for less controlled settings and field measurements.

The advantages of this method are the non-intrusive nature of the measurements, as well as the potential for measurements with high detail, and the ability to capture wave run-up over the whole width of the dike (transverse direction of the flume) (appendix E). If by comparison an array of pressure sensors is used, a more coarse grid is needed due to practical considerations, giving a more staggered wave run-up signal. A pressure sensor array has also a given minimal water depth when it is activated in the order of 2.5mm (Holterman, 1998; Van Gent, 1999a), which can be significant in model tests. If a resistance-type gauge is used, there needs to be a distance between the surface of the dike and the gauge, which alters the measurements in a similar manner. Moreover, as wave run-up varies quite substantially along the alongshore direction of a dike, the spatial differences can give a deeper understanding of this wave run-up behavior. Furthermore, visual methods could be used to detect breaker types using for example the variance used in the procedure. Wave-breaking types are determined by the wave-dike interaction, which determines the type of force that is exercised on the dike slope.

The algorithm that is being used in the procedure needs to be calibrated on the conditions present during the measurements. The hand-picking of the reference datasets amounted to significant effort and time (a video with a duration of 12 minutes takes about 10 hours to pick accurately). Hence, the effort to automate this process gives a significant reduction in processing time.

Physical modeling

In the results, the water depth on top of the salt marsh is a dominant metric to display the changes caused by the addition of vegetation. The vegetation has a double influence as it reduces the unaffected water depth, and influences bottom friction due to the drag caused by the vegetation. The salt marsh model is modeled after real-life vegetation *Spartina Angelica*. Cauchy number, blade length ratio, and buoyancy number are similar, while Reynolds and KC-number change, due to the nature of a scale model test. In the field, breakage of vegetation is common during heavy storms, thereby lowering the vegetation depth. This breaking was not modeled in this physical model, however, heavy movement of the vegetation was observed, especially for lower water depths. Higher water depths should therefore be less prone to vegetation breakage. As the wave run-up reducing effect is highly dependent on the water depth on the salt marsh in combination with the vegetation height (which can be seen calculating the change in $T_{m-1,0}$ over the salt marsh), a breakage of vegetation could diminish the effects of this vegetation on the reduction in wave run-up.

When the change of $T_{m-1,0}$ along the salt marsh was fitted with Hofland et al. (2017), the vegetation seemed to behave like a solid mass. This could be a result of scaling effects, as a result of which the effectiveness of vegetation is over-represented. For tests using real vegetation, this should be assessed as well. This was not the case for analysis of the change in wave height, which showed additional dependencies. These dependencies could be represented as the unit of standing biomass of the vegetation (Bouma et al., 2010; Maza et al., 2022), but are only tested for lower water depths/vegetation ratios, which is out of the scope of this thesis. In the field, vegetation varies along the cross-section of the salt marsh. Additionally, in the field there are gullies present, which need to be accounted for in later studies, for instance using computational modeling.

5

Conclusion

The objective of this thesis is to quantify the effectiveness of a salt marsh system on the wave run-up on a dike during extreme storm surge conditions and to quantify the difference on run-up behavior caused by the wave attenuation of salt marshes. This will be concluded and recommendations for further research are given.

5.1. Conclusions

To answer the objective, wave flume tests using a scale model of a salt marsh cross-section are conducted. The wave run-up is measured using image processing, using a newly created algorithm. The following conclusions can be made from the results of these tests.

General amount of wave run-up reduction by a salt marsh

Wave run-up is reduced by the presence of a salt marsh, resulting in breaking waves on the entire foreshore. The general amount of reduction is strongly dependent on the water level above the salt marsh. The influence of vegetation is non-negligible: higher water depths for the same wave height without vegetation give almost no reduction, whereas only lower water depths give a reduction. However, when vegetation is included, all tested cases show an (additional) reduction in wave run-up for the same incoming offshore wave height. The spectral wave period $T_{m-1,0}$ increases due to vegetation, which seems mainly dependent on the decrease in water depth due to the increase in bottom level by the vegetation height. The wave height reduces over the salt marsh, which is dependent on the decrease in water depth, however, more factors are in play.

A general estimation of the reduction due to vegetation can be given, as the general amount of wave run-up reduction by the **vegetation** is strongly dependent on the water level above the salt marsh. In all tested cases, for every water depth on the salt marsh, measurements were altered due to the influence of vegetation. If the results are linearly fitted with the water depth, a conservative linear extrapolation of the results leads to no influence when water depth on the salt marsh $d_m > 0.55 \approx d_m/l_s > 6$, where l_s is the vegetation length. Cases with water levels lower than this are affected by vegetation-reducing run-up for where every reduction in water level equal to one vegetation length reduces the run-up by 12.2%. When comparing the reduction in wave run-up to $d_m/H_{m0,o}$ (offshore wave height), a less linear but an even stronger relation is visible.

The influence of a **cliff** is dependent on the height of the cliff and the presence of vegetation. The presence of a small cliff without vegetation ($d_c/h_c = 7.67$, depth seaward side of the cliff over cliff height) has an insignificant influence on the wave run-up. However, when vegetation is applied to cases with and without a cliff the influence of the cliff becomes noticeable and becomes dependent on the incoming wave height. The presence of the higher cliff without vegetation ($d_c/h_c = 4.33$) shows a reduction in run-up level also dependent on wave height. Including vegetation increases the reduction even further. The wave height is also reduced (by on average 4%) by the presence of the cliff, where the difference is bigger for cases without vegetation. Hence, the reduction in wave height is due to wave breaking at the cliff, which reduces the wave run-up level.

Comparison of wave run-up measurements with literature

The measured wave run-up $R_{u2\%}$ (height of the dike which 2% of the wave run-up events exceeds) is compared to the predicted wave run-up, using EurOtop (2018) and TAW (2002) with incoming wave characteristics at the toe of the dike, for cases with a water level on the salt marsh of 16mm and higher ($1.78 \leq d_m/l_s \leq 5.78$). Compared to the equation the measurements are mostly lower than predicted (RMSE 24mm for all tests and 27mm for tests with vegetation) and show to be less dependent on the increase in $\xi_{m-1,0}$ than predicted. Waves with an offshore peak wave steepness lower than 0.030 are predicted correctly, however, with an increasing steepness, the predicted values overestimate the wave run-up to 15%. Usage of $H_{1/3}$ instead of the requested H_{m0} in the equation gives results that align more closely with the measurements (RMSE 16mm for all tests and 21mm for tests with vegetation). Still, the influence of offshore peak wave steepness is present. When the Iribarren parameter is calculated using offshore wave characteristics for H_{m0} and $T_{m-1,0}$, and compared with the measured run-up divided by H_{m0} at the dike toe, the results align pretty close with measurements. This shows that the change in wave run-up over the salt marsh is mainly dependent on the change in wave height.

When comparing the measured wave run-up with Van Gent (1999a) in a similar manner, the equation is less accurate. Using van Gent's equation based on $H_{1/3}$, the equation accounts better for the influence of offshore peak wave steepness. However, it under-predicts all tests without vegetation. It over-predicts cases with vegetation and higher Iribarren numbers. Using van Gent's equation based on H_{m0}, it under predicts the wave run-up for tests without vegetation, and shows similar behavior to TAW (2002) for tests with vegetation.

Differences in wave run-up behavior due to a salt marsh

The differences between wave run-up predicted using equations found in literature and measurements is most likely due to the influence of wave breaking on the salt marsh. This wave breaking results in a change in the wave spectrum. The vegetation increases wave breaking more than effects only due to the shape of the foreshore. Waves with a higher wave steepness break more than with a lower wave steepness. Hence only assessing wave run-up from the wave height H_{m0} and spectral period $T_{m-1,0}$ from the wave spectra obtained at the toe of the dike describe the current wave run-up behavior not fully accurately. The $R_{u2\%}/H_{m0}$ is lower for tests with higher wave steepnesses. Usage of $H_{1/3}$ gives a better fit, most likely because this parameter is more influenced by shoaling and breaking. The wave run-up exceedance distributions acquired from the measurements are also for tests with vegetation Rayleigh distributed. Hence, the fundamental behavior of the wave run-up is the same.

The wave set-up has not been assessed in this study. However, due to these aformentioned observations it can be deduced that the differences in wave run-up behavior could be mainly dependent on wave set-up. Wave set-up is included in the wave run-up equations, but as these equations are empirical, a significant lowering of wave set-up could give rise to an over-prediction by the equation, which was seen for cases with lower higher steepnesses. An assessment of the wave set-up and comparison with a dataset using multiple flume configurations is needed to see if this influence is present in general or unique to salt marshes.

5.2. Recommendations

The breaking of waves over a salt marsh alters the response of wave run-up, which is not fully described using the current formulations. As mentioned, the offshore wave steepness plays an important role in determining wave run-up behavior. As well as the more dominant role of wave height in comparison to Iribarren number. A better understanding of change in wave behavior can give a way in which the wave run-up be predicted better. More scenarios using other dike slopes, salt marsh lengths, and vegetation types/heights, can be added to expand the influence of the dike slope on wave run-up. However, the main recommendation for further study is to assess the influence of wave set-up and offshore wave steepness on wave run-up in general.

From this set of experiments, the following options using current formulas to predict wave run-up of a dike adjacent to a salt marsh without alteration of the wave run-up equation are recommended to be investigated:

- Calculate $\xi_{m-1,0}$ as if there is no vegetation, even when vegetation is present.
- Adapt the calculation of $T_{m-1,0}$ by way of a lower integration bound, or application of a filtering technique to reduce the influence of certain range of the wave energy spectrum
- Replace H_{m0} with $H_{1/3}$ in the equation

The change in spectral wave period is predicted quite accurately using Hofland et al. (2017), which seems to be mainly affected by the decrease in water level caused by the increase in vegetation. Experiments using real-life vegetation are needed to verify this behavior in non-modeled cases.

The methodology using visual run-up detection is tested in controlled lab conditions using a small-scale model. The method was limited to selection along the width of the dike due to the calibration board. If the extrinsic calibration could be accomplished by a removable calibration plate, the visual run-up detection method could be applied along a whole dike slope in the lab. The effectiveness of the application of the described procedure in environments such as outside lab conditions and field applications is still unknown. Furthermore, as the method calculates the variance between several frames, breaker types could possibly be detected by the variance number as the breaking wave has high turbulence. This could lead to more insight into the types of wave-dike interaction for a given wave climate.

As overtopping is currently the standard method to design dikes, it is important to measure. This can be done with Hofland et al. (2015), using virtual overtopping. Overtopping can also be measured with video. This was attempted during the experiments as well. The overtopping width can be obtained from the footage of the run-up camera as the position of the water line is known and the seaward edge of the dike crest. The thickness of the overtopping event can be calculated by the usage of a side-facing camera at the crest. From the top video camera footage the position of the overtopping event from the side is known. The side-facing camera can then be calibrated externally for each position in depth along the dike slope on the plane parallel to the dike slope. The position of the edge of the dike crest needs to be selected in the external calibration. For each given frame in an overtopping event, the footage can be calibrated by using the external calibration transformation which corresponds with the farthest position from the side-facing camera. With this, the coordinates of the width of this farthest end can be selected and can be subtracted from the position of the edge of the dike. As the distance in pixels can be converted to a distance in reality by the external calibration, the depth of the overtopping for that frame is known. This can be automated by using for example the water isolation procedure. However, the end of an overtopping event is hard to identify as little water flows for a long time after the initial overtopping front over the dike crest. Another possibility is by using a telecentric lens at the side.

References

Almar, R., Michallet, H., Cienfuegos, R., Bonneton, P., Tissier, M., & Ruessink, G. (2014). On the use of the radon transform in studying nearshore wave dynamics. *Coastal Engineering*, *92*, 24–30. https://doi.org/10.1016/j.coastaleng.2014.06.008

Barbier, E. B., Hacker, S. D., Kennedy, C., Koch, E. W., Stier, A. C., & Silliman, B. R. (2011). The value of estuarine and coastal ecosystem services. *Ecological Monographs*, *81*(2), 169–193. https://doi.org/10.1890/10-1510.1

Battjes, J. A. (1969). Run-up distributions of waves breaking on sloping walls [Publisher: TU Delft, Section Hydraulic Engineering]. Retrieved January 19, 2024, from https://repository.tudelft.nl/islandora/object/uuid%3A819f9c36-1241-4996-a266-6b91972dc168

Battjes, J. A. (1974). *Computation of set-up, longshore currents, run-up and overtopping due to wind-generated waves* (Doctoral dissertation). Retrieved January 4, 2024, from https://repository.tudelft.nl/islandora/object/uuid%3Ae126e043-a858-4e58-b4c7-8a7bc5be1a44

Bouma, T. J., Vries, M. B. D., & Herman, P. M. J. (2010). Comparing ecosystem engineering efficiency of two plant species with contrasting growth strategies. *Ecology*, *91*(9), 2696–2704. https://doi.org/10.1890/09-0690.1

Bouma, T. J., van Belzen, J., Balke, T., Zhu, Z., Airoldi, L., Blight, A. J., Davies, A. J., Galvan, C., Hawkins, S. J., Hoggart, S. P., Lara, J. L., Losada, I. J., Maza, M., Ondiviela, B., Skov, M. W., Strain, E. M., Thompson, R. C., Yang, S., Zanuttigh, B., … Herman, P. M. (2014). Identifying knowledge gaps hampering application of intertidal habitats in coastal protection: Opportunities & steps to take. *Coastal Engineering*, *87*, 147–157. https://doi.org/10.1016/j.coastaleng.2013.11.014

Brooks, H., Möller, I., Carr, S., Chirol, C., Christie, E., Evans, B., Spencer, K. L., Spencer, T., & Royse, K. (2021). Resistance of salt marsh substrates to near instantaneous hydrodynamic forcing. *Earth Surface Processes and Landforms*, *46*(1), 67–88. https://doi.org/10.1002/esp.4912

Callaghan, D. P., Bouma, T. J., Klaassen, P., van der Wal, D., Stive, M. J. F., & Herman, P. M. J. (2010). Hydrodynamic forcing on salt-marsh development: Distinguishing the relative importance of waves and tidal flows. *Estuarine, Coastal and Shelf Science*, *89*(1), 73–88. https://doi.org/10.1016/j.ecss.2010.05.013

Davidson-Arnott, R. (2010). *Introduction to coastal processes and geomorphology* [OCLC: 650349557]. Cambridge University Press.

EurOtop. (2018). Manual on wave overtopping of sea defences and related structures. An overtopping manual largely based on european research, but for worldwide application. Van der Meer, J.W., Allsop, N.W.H., Bruce, T., De Rouck, J., Kortenhaus, A., Pullen, T., Schüttrumpf, H., Troch, P. and Zanuttigh, B. www.overtopping-manual.com

Gedan, K. B., Silliman, B., & Bertness, M. (2009). Centuries of human-driven change in salt marsh ecosystems. *Annual Review of Marine Science*, *1*(1), 117–141. https://doi.org/10.1146/annurev.marine.010908.163930

Gedan, K. B., Kirwan, M. L., Wolanski, E., Barbier, E. B., & Silliman, B. R. (2011). The present and future role of coastal wetland vegetation in protecting shorelines: Answering recent challenges to the paradigm. *Climatic Change*, *106*(1), 7–29. https://doi.org/10.1007/s10584-010-0003-7

Goda, Y. (2008). *Random seas and design of maritime structures* (2. ed., Reprint). World Scientific.

Goda, Y., & Suzuki, T. (1976). Estimation of incident and reflected waves in random wave experiments [Number: 15]. *Coastal Engineering Proceedings*, (15), 47–47. https://doi.org/10.9753/icce.v15.47

Guza, R. T., Thornton, E. B., & Holman, R. A. (1984). Swash on steep and shallow beaches [Number: 19]. *Coastal Engineering Proceedings*, (19), 48–48. https://doi.org/10.9753/icce.v19.48

Harbers, M. (2023, November 8). Kamerbrief over landelijk veiligheidsbeeld primaire waterkeringen. Retrieved November 15, 2023, from https://www.rijksoverheid.nl/documenten/kamerstukken/2023/11/08/kamerbrief-landelijk-veiligheidsbeeld-primaire-waterkeringen

Hofland, B., Chen, X., Altomare, C., & Oosterlo, P. (2017). Prediction formula for the spectral wave period Tm-1,0 on mildly sloping shallow foreshores. *Coastal Engineering*, *123*, 21–28. https://doi.org/10.1016/j.coastaleng.2017.02.005

Hofland, B., Diamantidou, E., van Steeg, P., & Meys, P. (2015). Wave runup and wave overtopping measurements using a laser scanner. *Coastal Engineering*, *106*, 20–29. https://doi.org/10.1016/j.coastaleng.2015.09.003

Holman, R., & Guza, R. (1984). Measuring run-up on a natural beach. *Coastal Engineering*, *8*, 129–140. https://doi.org/10.1016/0378-3839(84)90008-5

Holterman, S. R. (1998). *Golfoploop op dijken met ondiep voorland* (Master's thesis). Retrieved May 7, 2024, from https://repository.tudelft.nl/islandora/object/uuid%3Ae1794634-9a66-4624-ba1f-b7e4e301a035

Holthuijsen, L. H. (2007). *Waves in oceanic and coastal waters* [OCLC: 663973262]. Cambridge University Press.

IPCC. (2023). *Climate change 2023: Synthesis report. contribution of working groups i, II and III to the sixth assessment report of the intergovernmental panel on climate change [core writing team, h. lee and j. romero (eds.)]. IPCC, Geneva, Switzerland.* [Edition: First]. Intergovernmental Panel on Climate Change (IPCC). https://doi.org/10.59327/IPCC/AR6-9789291691647

Keimer, K., Schürenkamp, D., Miescke, F., Kosmalla, V., Lojek, O., & Goseberg, N. (2021). Ecohydraulics of surrogate salt marshes for coastal protection: Wave–vegetation interaction and related hydrodynamics on vegetated foreshores at sea dikes. *Journal of Waterway, Port, Coastal, and Ocean Engineering*, *147*(6), 14. https://doi.org/10.1061/(ASCE)WW.1943-5460.0000667

Kirwan, M. L., Temmerman, S., Skeehan, E. E., Guntenspergen, G. R., & Fagherazzi, S. (2016). Overestimation of marsh vulnerability to sea level rise [Number: 3 Publisher: Nature Publishing Group]. *Nature Climate Change*, *6*(3), 253–260. https://doi.org/10.1038/nclimate2909

Knottnerus, O. S. (2005). History of human settlement, cultural change and interference with the marine environment [Number: 1 Publisher: BioMed Central]. *Helgoland Marine Research*, *59*(1), 2–8. https://doi.org/10.1007/s10152-004-0201-7

Lei, J., & Nepf, H. (2019). Wave damping by flexible vegetation: Connecting individual blade dynamics to the meadow scale. *Coastal Engineering*, *147*, 138–148. https://doi.org/10.1016/j.coastaleng.2019.01.008

LeMéhauté, B. (1976). *An introduction to hydrodynamics and water waves*. Springer. https://doi.org/10.1007/978-3-642-85567-2

Mansard, E. P. D., & Funke, E. R. (1980). The measurement of incident and reflected spectra using a least squares method [Number: 17]. *Coastal Engineering Proceedings*, (17), 8–8. https://doi.org/10.9753/icce.v17.8

Marin-Diaz, B., van der Wal, D., Kaptein, L., Martinez-Garcia, P., Lashley, C. H., de Jong, K., Nieuwenhuis, J. W., Govers, L. L., Olff, H., & Bouma, T. J. (2023). Using salt marshes for coastal protection: Effective but hard to get where needed most. *Journal of Applied Ecology*, *60*(7), 1286–1301. https://doi.org/10.1111/1365-2664.14413

Maza, M., Lara, J. L., & Losada, I. J. (2022). A paradigm shift in the quantification of wave energy attenuation due to saltmarshes based on their standing biomass [Number: 1 Publisher: Nature Publishing Group]. *Scientific Reports*, *12*(1), 13883. https://doi.org/10.1038/s41598-022-18143-6

Maza, M., Roldán, M., Lara, J. L., & Losada, I. J. (2023). EXPERIMENTAL ANALYSIS OF HYBRID SOLUTIONS FOR COASTAL PROTECTION. *Coastal Engineering Proceedings*, (37), 71. https://doi.org/10.9753/icce.v37.management.71

Mcowen, C. J., Weatherdon, L. V., Bochove, J.-W. V., Sullivan, E., Blyth, S., Zockler, C., Stanwell-Smith, D., Kingston, N., Martin, C. S., Spalding, M., & Fletcher, S. (2017). A global map of saltmarshes. *Biodiversity Data Journal*, (5), e11764. https://doi.org/10.3897/BDJ.5.e11764

Migliore, D. A., Matteucci, M., & Naccari, M. (2006). A revaluation of frame difference in fast and robust motion detection. *Proceedings of the 4th ACM international workshop on Video surveillance and sensor networks*, 215–218. https://doi.org/10.1145/1178782.1178815

Möller, I., Kudella, M., Rupprecht, F., Spencer, T., Paul, M., van Wesenbeeck, B. K., Wolters, G., Jensen, K., Bouma, T. J., Miranda-Lange, M., & Schimmels, S. (2014). Wave attenuation over coastal salt marshes under storm surge conditions. *Nature Geoscience*, *7*(10), 727–731. https://doi.org/10.1038/ngeo2251

Neumann, B., Vafeidis, A. T., Zimmermann, J., & Nicholls, R. J. (2015). Future coastal population growth and exposure to sea-level rise and coastal flooding - a global assessment (L. Kumar, Ed.). *PLOS ONE*, *10*(3), e0118571. https://doi.org/10.1371/journal.pone.0118571

Oosterlo, P., Hofland, B., van der Meer, J. W., Overduin, M., & Steendam, G. J. (2021). Calibration and preparation of field measurements of oblique wave run-up and overtopping on dikes using laser scanners. *Coastal Engineering*, *167*, 103915. https://doi.org/10.1016/j.coastaleng.2021.103915

Post, T. M. I. (2015, October 8). *Assessment of wave run-up reduction by salt marshes* (Master's thesis) [Publisher: University of Twente]. Retrieved January 25, 2023, from https://essay.utwente.nl/68775/

Schiereck, G. J., & Verhagen, J. G. (2012). *Introduction to bed, bank and shore protection (2nd edition)* [Publisher: VSSD]. Retrieved November 16, 2023, from https://repository.tudelft.nl/islandora/object/uuid%3A7e6e6425-8304-4992-96be-aa277811f616

Schoutens, K., Stoorvogel, M., van den Berg, M., van den Hoven, K., Bouma, T. J., Aarninkhof, S., Herman, P. M. J., van Loon-Steensma, J. M., Meire, P., Schoelynck, J., Peeters, P., & Temmerman, S. (2022). Stability of a tidal marsh under very high flow velocities and implications for nature-based flood defense. *Frontiers in Marine Science*, *9*. Retrieved November 20, 2023, from https://www.frontiersin.org/articles/10.3389/fmars.2022.920480

Seabrook, C. (2012). *The world of the salt marsh: Appreciating and protecting the tidal marshes of the southeastern atlantic coast* [OCLC: 757935630]. University of Georgia Press. Retrieved September 25, 2023, from http://site.ebrary.com/id/10556468

Singla, N. (2014). Motion detection based on frame difference method. *International Journal of Information & Computation Technology*, *4*(15), 1559–1565.

Spalding, M. D., McIvor, A. L., Beck, M. W., Koch, E. W., Möller, I., Reed, D. J., Rubinoff, P., Spencer, T., Tolhurst, T. J., Wamsley, T. V., van Wesenbeeck, B. K., Wolanski, E., & Woodroffe, C. D. (2014). Coastal ecosystems: A critical element of risk reduction. *Conservation Letters*, *7*(3), 293–301. https://doi.org/10.1111/conl.12074

TAW. (2002, May). *Technisch Rapport Golfoploop en Golfoverslag bij Dijken*. Technische Adviescommissie voor de Waterkeringen.

Thompson, E. F., & Vincent, C. L. (1985). Significant wave height for shallow water design [Publisher: American Society of Civil Engineers]. *Journal of Waterway, Port, Coastal, and Ocean Engineering*, *111*(5), 828–842. https://doi.org/10.1061/(ASCE)0733-950X(1985)111:5(828)

UNESCO, W. H. C. (2023). *Wadden sea* [UNESCO world heritage centre]. Retrieved November 16, 2023, from https://whc.unesco.org/en/list/1314/

Ursell, F. (1953). The long-wave paradox in the theory of gravity waves [Publisher: Cambridge University Press]. *Mathematical Proceedings of the Cambridge Philosophical Society*, *49*(4), 685–694. https://doi.org/10.1017/S0305004100028887

Van der Meer, J. W. (2011). The wave run-up simulator: Idea, necessity, theoretical background and design [Publisher: Van der Meer Consulting]. *project vdm11355*. Retrieved September 19, 2023, from https://repository.tudelft.nl/islandora/object/uuid%3Aeb4d5eca-10d8-4b5e-bf4b-9bda52958c46

Van Gent, M. R. A. (1999a). Physical model investigations on coastal structures with shallow foreshores: 2d model tests with single and double-peaked wave energy spectra [Publisher: Deltares (WL)]. *H3608*. Retrieved January 5, 2024, from https://repository.tudelft.nl/islandora/object/uuid%3A1b4729de-2e86-4b8a-98d5-48d8e07d5902

Van Gent, M. R. A. (1999b). Wave run-up and wave overtopping for double peaked wave energy spectra [Publisher: Deltares (WL)]. *H3351*. Retrieved January 5, 2024, from https://repository.tudelft.nl/islandora/object/uuid%3A05632d4d-6823-4570-a8af-7adbe2598e8e

Van Gent, M. R. A., & Van der Werf, I. M. (2014). Rock toe stability of rubble mound breakwaters. *Coastal Engineering*, *83*, 166–176. https://doi.org/10.1016/j.coastaleng.2013.10.012

Vuik, V., Jonkman, S. N., Borsje, B. W., & Suzuki, T. (2016). Nature-based flood protection: The efficiency of vegetated foreshores for reducing wave loads on coastal dikes. *Coastal Engineering*, *116*, 42–56. https://doi.org/10.1016/j.coastaleng.2016.06.001

Vuik, V., Suh Heo, H. Y., Zhu, Z., Borsje, B. W., & Jonkman, S. N. (2018). Stem breakage of salt marsh vegetation under wave forcing: A field and model study. *Estuarine, Coastal and Shelf Science*, *200*, 41–58. https://doi.org/10.1016/j.ecss.2017.09.028

Willemsen, P. W. J. M., Borsje, B. W., Vuik, V., Bouma, T. J., & Hulscher, S. J. M. H. (2020). Field-based decadal wave attenuating capacity of combined tidal flats and salt marshes. *Coastal Engineering*, *156*, 103628. https://doi.org/10.1016/j.coastaleng.2019.103628

Zayed, A. I. (Ed.). (2019, August 30). *Handbook of function and generalized function transformations*. CRC Press. https://doi.org/10.1201/9780138752859

Zelt, J. A., & Skjelbreia, J. E. (1992). Estimating incident and reflected wave fields using an arbitrary number of wave gauges [Number: 23]. *Coastal Engineering Proceedings*, (23). https://doi.org/10.9753/icce.v23.%p

Zhang, X., & Nepf, H. (2021). Wave-induced reconfiguration of and drag on marsh plants. *Journal of Fluids and Structures*, *100*, 103192. https://doi.org/10.1016/j.jfluidstructs.2020.103192

Zhu, Z., Vuik, V., Visser, P. J., Soens, T., van Wesenbeeck, B., van de Koppel, J., Jonkman, S. N., Temmerman, S., & Bouma, T. J. (2020). Historic storms and the hidden value of coastal wetlands for nature-based flood defence [Number: 10 Publisher: Nature Publishing Group]. *Nature Sustainability*, *3*(10), 853–862. https://doi.org/10.1038/s41893-020-0556-z

A

Appendix: Construction

Multiple experiments were conducted with the same setup, see table A.1. This has lead to a combination of requirements for the setup, which needed to be taken into account with the total design.

Researcher	**Subject**
Dermentzoglou	scaling and wave dissipation over salt marsh
Muller	hydrodynamics and erosion at salt marsh edge and at the dike toe interface
Faber	hydrodynamics at salt marsh edge
Lakerveld	wave runup and overtopping

Table A.1: Division of subjects researched with experiment

The model is constructed from shuttering plywood ('betonplex'). For the cases without vegetation, regular plates are used. The vegetation plates are made by laser cutting holes in a plastic sheet with the desired dimensions, these are screwed on the wooden plates. The neoprene shoots are cut by a paper cutter jig which is set to the specified dimensions. These are placed in the holes and are secured by superglue. In this way, these plates can be swapped out and a variety of model variations can be tested.

(a) Construction of the vegetation plates

(b) Vegetation plates

Figure A.1: Vegetation plates

A.1. Positioning camera

The camera is placed parallel to the slope of the dike, in a 3D printed case. This is hard mounted to a frame which can be moved up and down. When the height is chosen it can be secured with a screw. Next to the camera, a cinematographic light is placed to adjust the light levels of the video. Unlike a regular AC light source, this kind of light maintains a consistent output without any flicker.

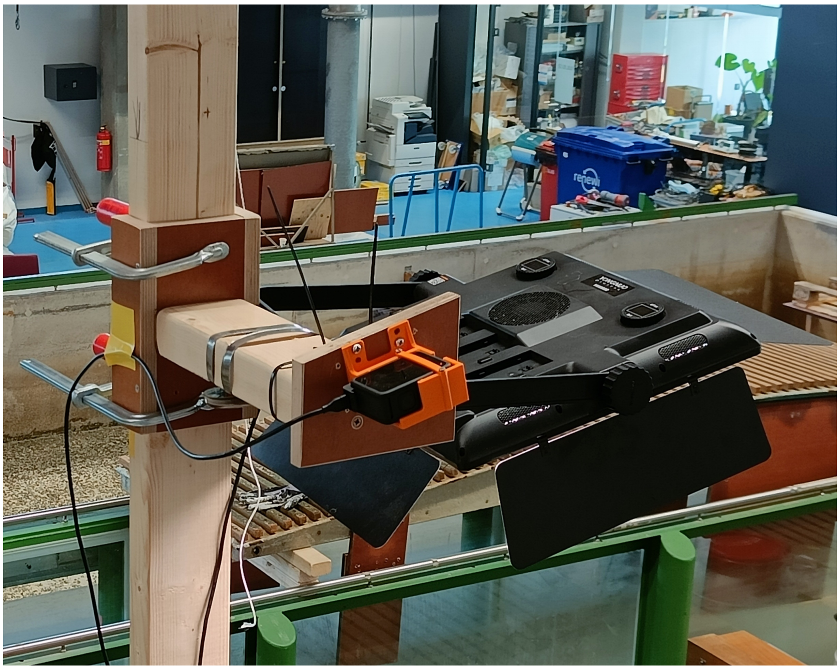

Figure A.2: Camera mount: The camera is mounted on a frame parallel to the dike slope, can be moved up and down and can be secured with a screw.

Two SICK LMS511 lidar laser scanners are used to record the water level along the flume (Hofland et al., 2015; Oosterlo et al., 2021). As the laser beam can only reflect on opaque materials, MagSpheres G25/60 are used as seeding to increase the reflectivity of the water surface. In Hofland et al. (2015) and Oosterlo et al. (2021), the wave run-up was measured with a similar laser scanner used in this experimental setup (see section 2.1.2). Application of this method did not result in satisfactory results, for the water was too thin and translucent on the dike slope, with the most likely explanation that the measurements were on a scale 1:10 instead of 1:1. As in Hofland et al. (2015) it was mentioned that run-up below 10cm was difficult to distinguish. In the paper, overtopping was assessed using virtual overtopping. For a further analysis, virtual overtopping could be used to measure overtopping rates.

A.2. Salt marsh model

See technical drawings on next pages

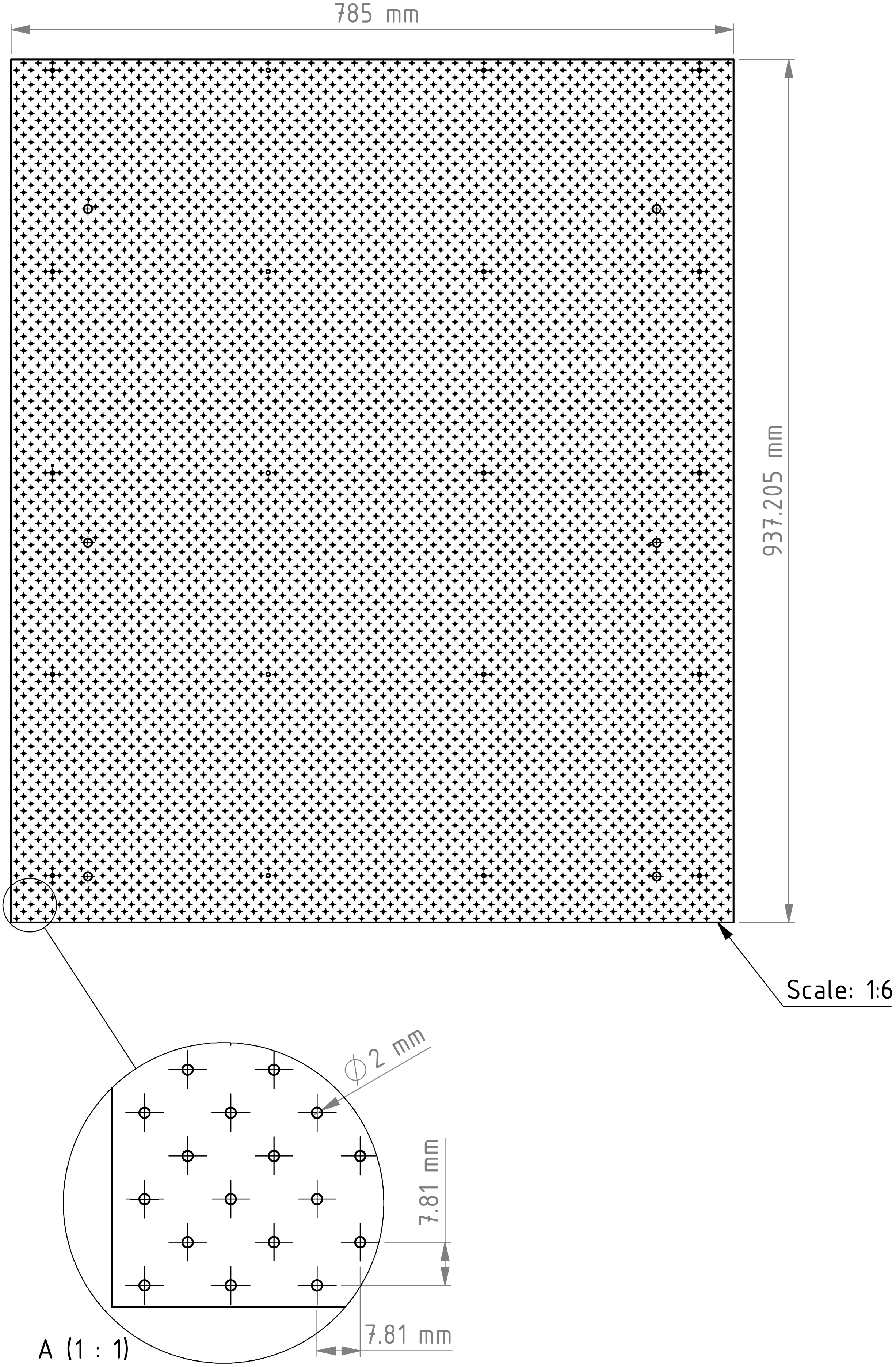
785 mm
937.205 mm
Scale: 1:6
ϕ 2 mm
7.81 mm
7.81 mm
A (1 : 1)

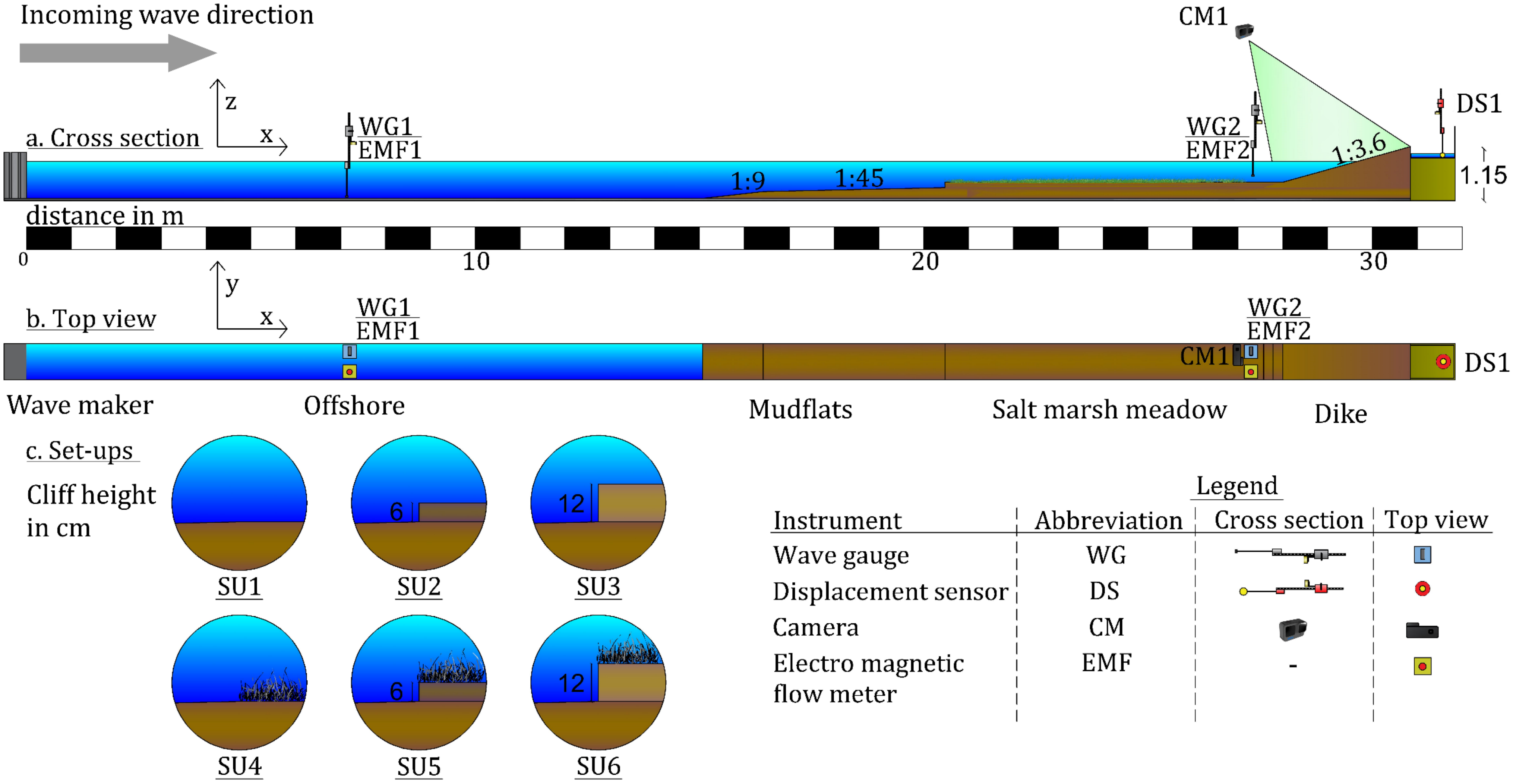
Incoming wave direction
CM1
DS1
a. Cross section
z
x
WG1
EMF1
WG2
EMF2
1:9
1:45
1:3.6
1.15
distance in m
0
10
20
30
b. Top view
y
x
WG1
EMF1
WG2
EMF2
CM1
DS1
Wave maker
Offshore
Mudflats
Salt marsh meadow
Dike
c. Set-ups
Cliff height
in cm
SU1
6
SU2
12
SU3
SU4
6
SU5
12
SU6
Legend
Instrument
Abbreviation
Cross section
Top view
Wave gauge
WG
Displacement sensor
DS
Camera
CM
Electro magnetic
flow meter
EMF
-

B

Appendix: Calibration

B.1. Wave gauges

Calibration of the wave gauges is done by raising and lowering the mount by a certain height and recording the corresponding output voltage. For each wave gauge the height and voltage are recorded. As the voltage output versus the water height is (ideally) linear, the difference in voltage can be directly related to a difference in wave height.

B.2. Time synchonization

The falling edge tFE of the light intensity of the signal present in the FOV of the camera is recorded and the frame number is notated. The timestamps relative to the start of the video are calculated by dividing the frame number by the FPS count. The time that the falling edge is turned off on DASYlab is equal to 5 seconds. Time is synchronized accordingly.

$$t = frame/fps \tag{B.1}$$

$$t_{cam,sync} = t_{cam,orig} - tFE + 5 \tag{B.2}$$

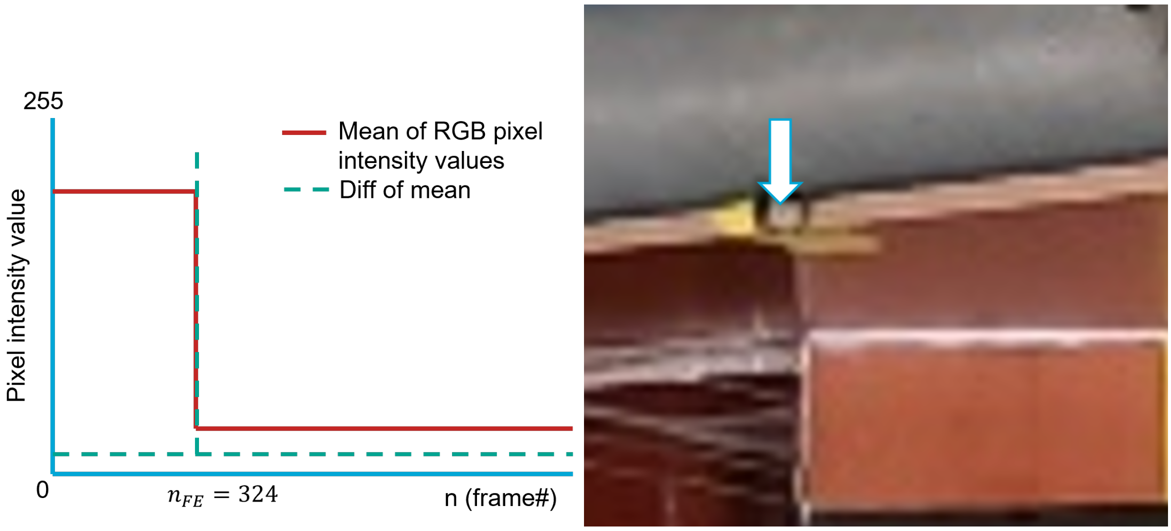

(a) Schematisation of signal of LED light

(b) LED light visible on camera

Figure B.1: Synchronization of wave run-up signal with the other instruments

B.3. Procedure

Every camera has a certain distortion due to the curvature of the lens. An internal calibration needs to be performed to remove this effect. This calibration gives a internal matrix and distortion coefficients. These can be used to undistort the image. This undistortion needs to be executed on every frame of the experiment data. Used reference: https://docs.opencv.org/4.x/dc/dbb/tutorial_py_calibration.html

The camera is mounted in a fixed position aligned with the slope of the dike. However, this alignment is not perfect due to physical limitations. To correct for this, a perspective transform can be performed. A chessboard pattern is placed on the slope of the dike which is filmed. This image can be transformed in a way that the camera is looking straigh on the plane. The cornerpoints are found of the physical chessboard pattern of the image. These corner points are matched with the same chessboard pattern corner points by using the function findHomography. A least squares fit is calculated and gives an perspective transformation matrix. This perspective transformation can be applied to every frame of the experiment data. Used reference: https://docs.opencv.org/4.x/d9/dab/tutorial_homography.html

The viewpoint from the camera onto the dike plane can now be considered flat. In this way a linear relationship between the pixel values an the actual distance along the plane can be made.

$$R_{u,diag} = b - a x_{image} \tag{B.3}$$

Where $R_{u,diag}$ is the diagonal reading of the real distance from the bottom of the dike without a cliff in millimeters and x_{image} is the distance in pixels from the left side of the image. $a = 2.1$ mm/px, and $b = 3635.022482$ mm

B.4. Parameters top camera

Table B.1: Matrices used in the calibration of the frames of the run-up camera video data

Internal camera matrix

$$\begin{bmatrix} f_x & 0 & c_x \\ 0 & f_y & c_y \\ 0 & 0 & 1 \end{bmatrix} = \begin{bmatrix} 1007.91395 & 0 & 969.792362 \\ 0 & 1008.1114 & 544.849325 \\ 0 & 0 & 1 \end{bmatrix}$$

Internal distortion parameters: k radial distortion, p tangential distortion

$$\begin{bmatrix} k_1 & k_2 & p_1 & p_2 & k_3 \end{bmatrix} = \begin{bmatrix} 0.01214238 & -0.00722643 & 0.00172313 & 0.00479434 & 0.00739411 \end{bmatrix}$$

External transformation matrix and procedure

$$\begin{bmatrix} 0.964936781 & 0.0172388219 & -1.13306871 \\ -0.0138724401 & 1.00580734 & -0.199503379 \\ -2.659\,408\,17 \times 10^{-5} & 1.538\,270\,67 \times 10^{-5} & 1 \end{bmatrix}$$

$$\Rightarrow dst(x,y) = src\left(\frac{M_{11}x+M_{12}y+M_{13}}{M_{31}x+M_{32}y+M_{33}}, \frac{M_{21}x+M_{22}y+M_{23}}{M_{31}x+M_{32}y+M_{33}}\right)$$

B.5. Overtopping box

Two overtopping box dimensions were used during the experiment, as due to the low overtopping rates a higher resolution could be obtained by making the box smaller.

	Dimensions of the top of the box	Volt to mm	Volt to mL
SU1, SU4	337 x 745 mm	$\Delta U = 1$ V $\equiv -42.5$ mm	-11936.7625
SU2, SU3, SU5, SU6	120 x 745 mm	$\Delta U = 1$ V $\equiv -16.356$ mm	-1462.2264

Table B.2: Overtopping box calibration

C

Appendix: Plots

C.1. Wave characteristics

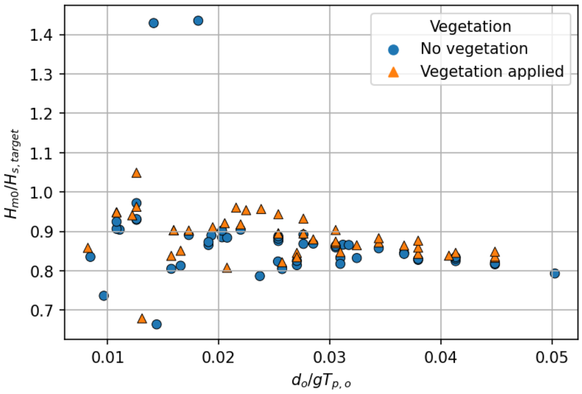

Figure C.1: Influence of d_o/gT_p on the measured wave heights versus target values

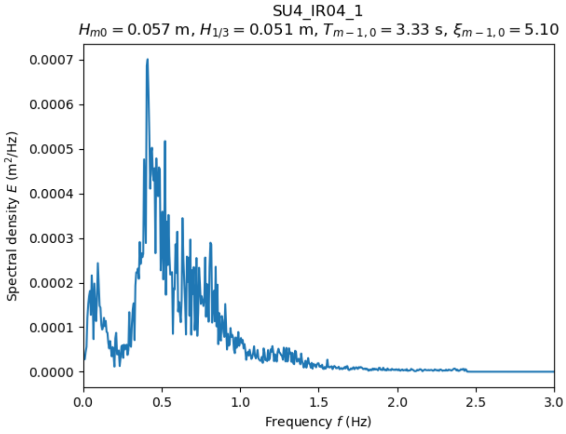

Figure C.2: Spectrum at the toe of the dike. Wave energy is significantly reduced, so the low frequencies are more dominant in determining wave characteristics.

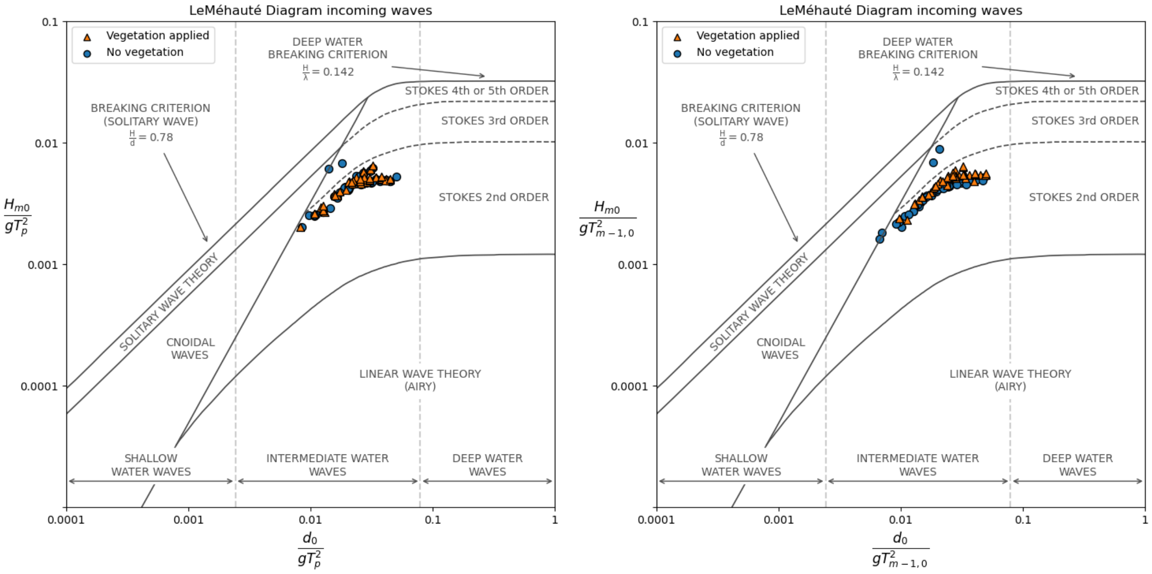

(a) T_p (offshore) **(b)** $T_{m-1,0}$ (offshore)

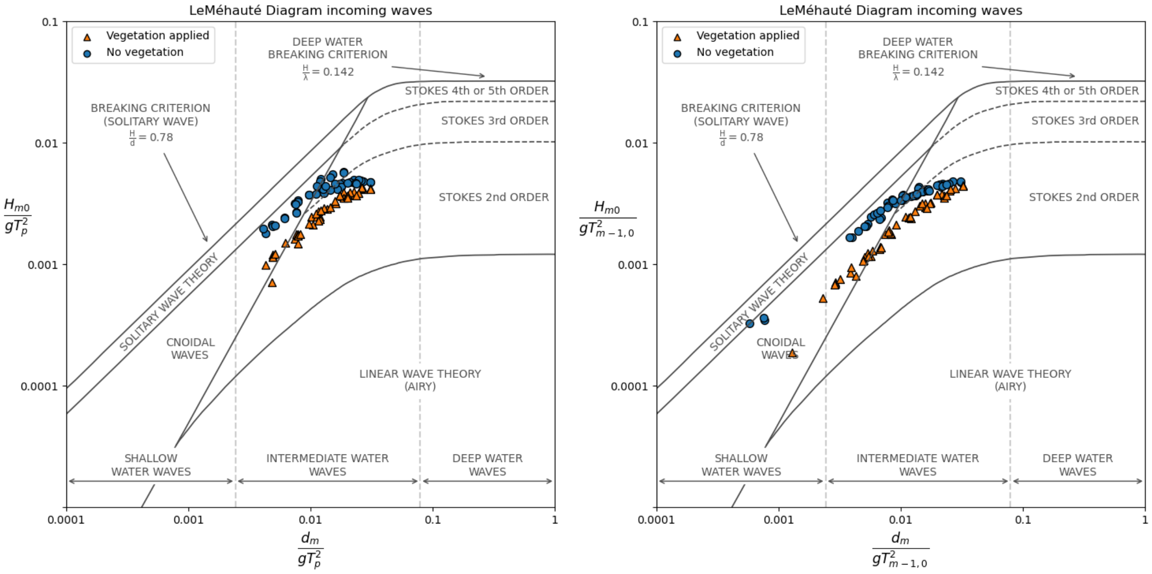

(c) T_p (dike toe) **(d)** $T_{m-1,0}$ (dike toe)

Figure C.3: The incoming waves offshore and at the toe of the dike, plotted on a Le Méhauté diagram. Waves are separated by tests using vegetated and unvegetated conditions. A clear distinction can be observed between these conditions at the toe of the dike, which is not visible at the offshore location

(a) Offshore wave characteristics using T_p (b) Offshore wave characteristics using $T_{m-1,0}$

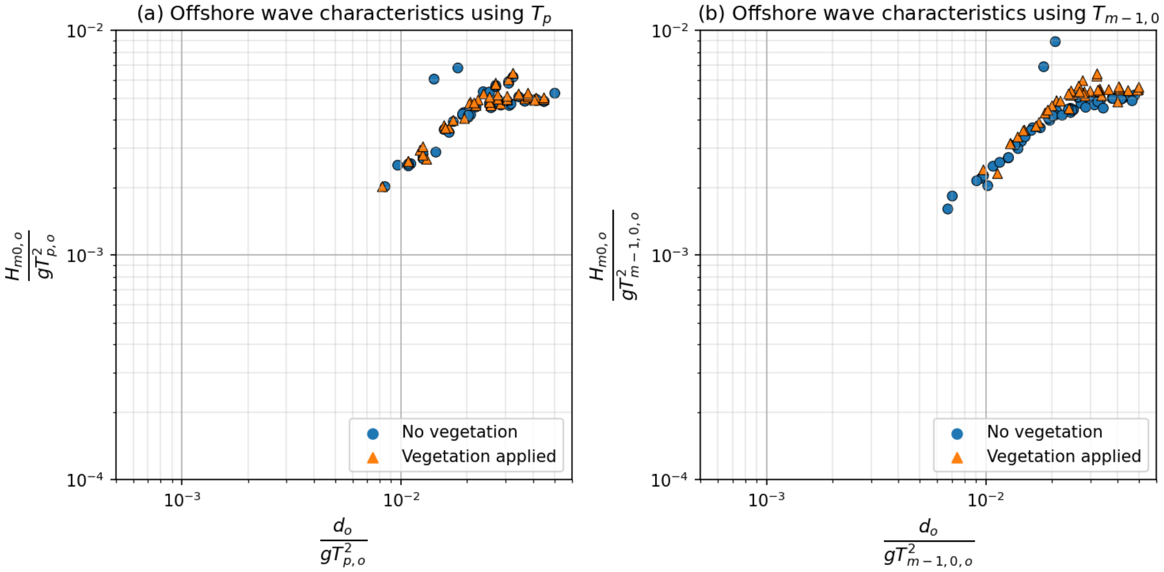

(c) Wave characteristics at dike toe using T_p (d) Wave characteristics at dike toe using $T_{m-1,0}$

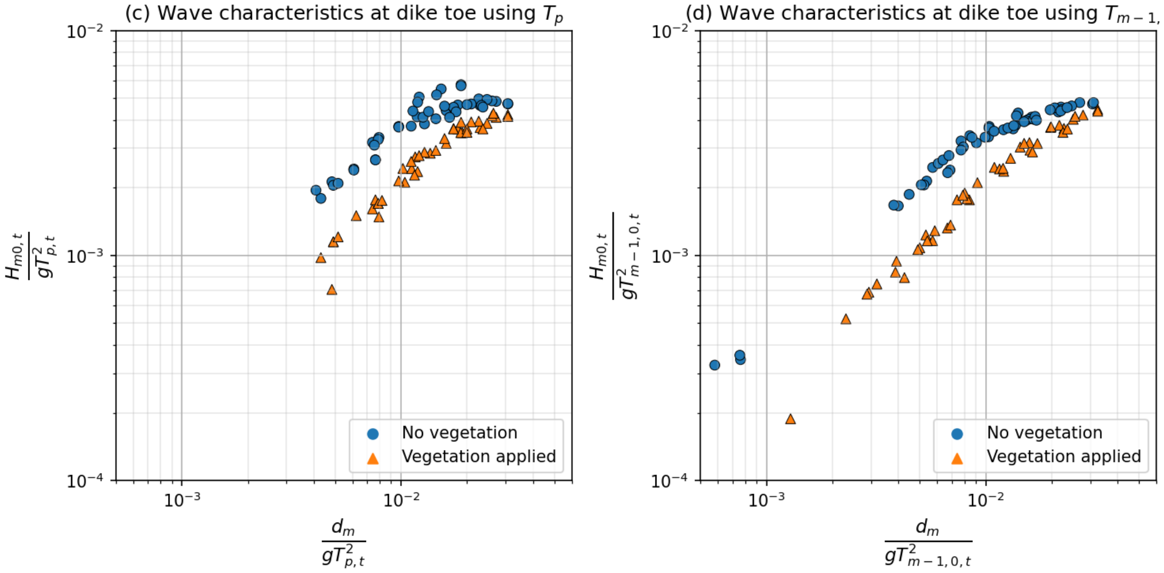

Figure C.4: Wave characteristics plot using a logarithm

A depth dependency of the relation between H_{m0} and $H_{1/3}$ can be seen (figure C.6). Moreover, for higher Ursell numbers this dependency is less, as the wave responds more nonlinear. These higher Ursell numbers are generally found in the cases without vegetation. This could be due to that less wave breaking has taken place in comparison with the vegetated cases, as vegetation enhances wave breaking. This lack in vegetation results in more shoaling (figure C.7b and figure C.8b). An average difference in H_{m0} of 4-5cm between the tests without and with vegetation is observed for d_m lower than 0.40m. Higher than this the differences between vegetation and no vegetation are less distinguishable (figure C.8b).

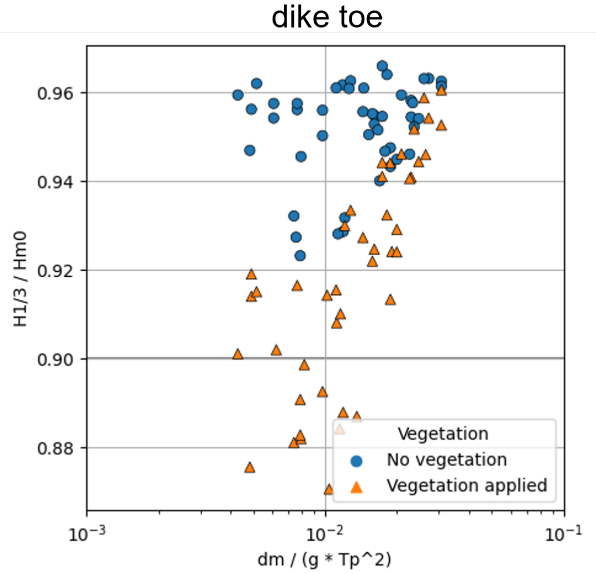

Figure C.5: Zoom in of figure 3.5

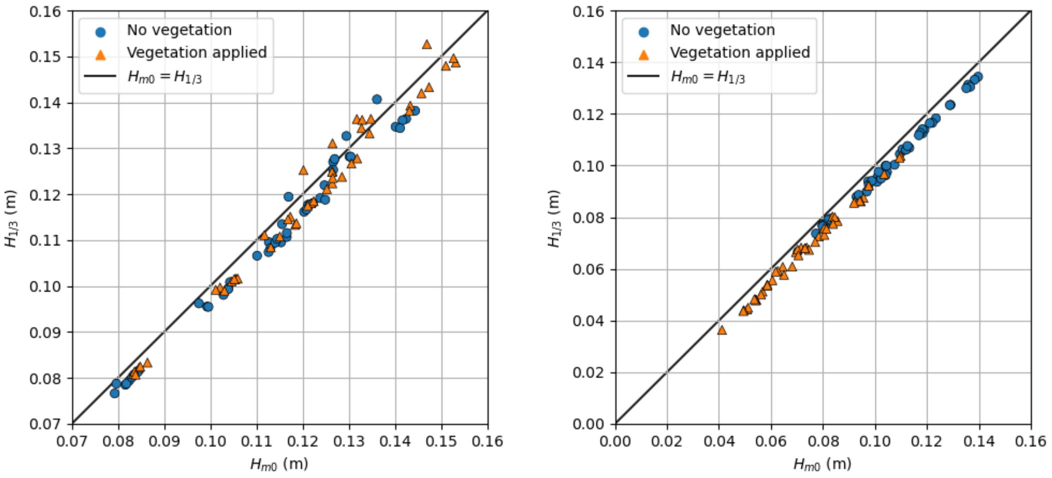

(a) Offshore conditions

(b) Toe of dike. When using a linear fit, the slope = 0.994, intercept=-0.005m

Figure C.6: The measured values of H_{m0} are plotted against $H_{1/3}$. In deep water conditions they should be the same. As both locations are in intermediate waters there is a deviation from the line depicting equal values.

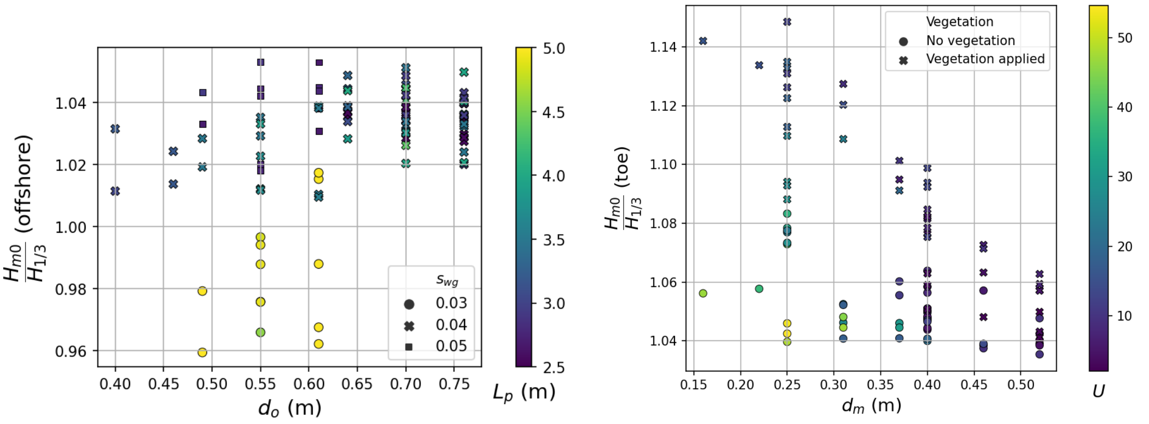

(a) Offshore conditions. Wave length dependence is plotted with a colormap. The reduction factor ranges between 1.01 to 1.06 (1 to 6% increase) for cases with a low wave length. For higher wave lengths (yellow) $H_{1/3}$ is higher than H_{m0}

(b) Waves at the toe of the dike. Ursell number dependence is plotted with a colormap. In lower water depths, cases with vegetation have an higher $H_{m0}/H_{1/3}$ ratio in comparison with cases without vegetation

Figure C.7: Water depth plotted against the difference factor between H_{m0} and $H_{1/3}$ at two locations.

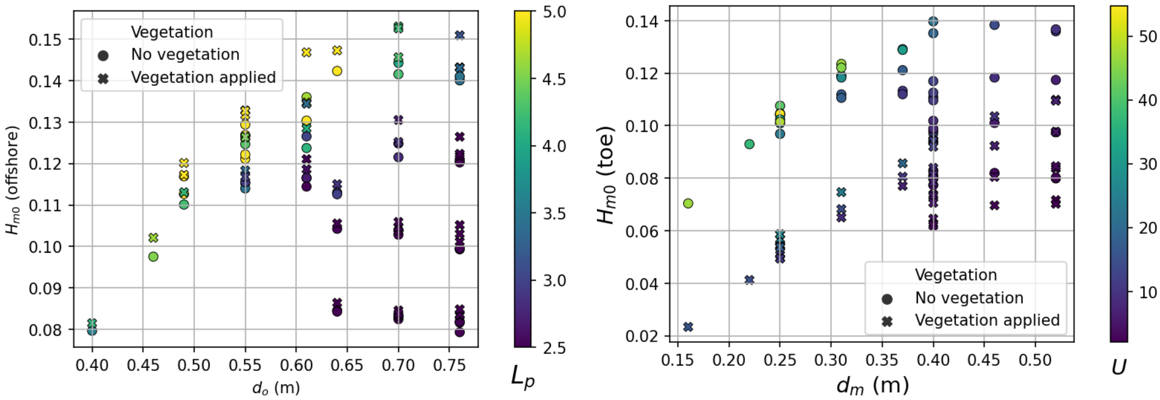

(a) Influence of depth on wave height offshore

(b) Influence of depth on wave height at the toe of the dike

Figure C.8: H_{m0} offshore and at the toe of the dike, both given in meters. Wave heights between cases with and without vegetation are similar offshore but show a clear deviation at the toe. This shows similar behavior to figure C.3c and figure C.3d

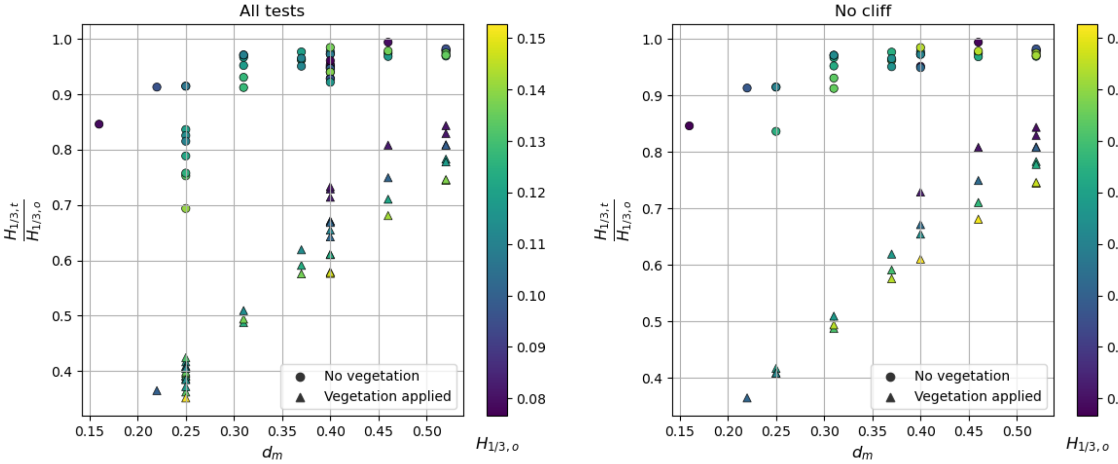

(a) All tests

(b) No cliff ($h_c = 0$m)

Figure C.9: Change in $H_{m0,o}$ compared at the dike toe and offshore for every water depth on the salt marsh

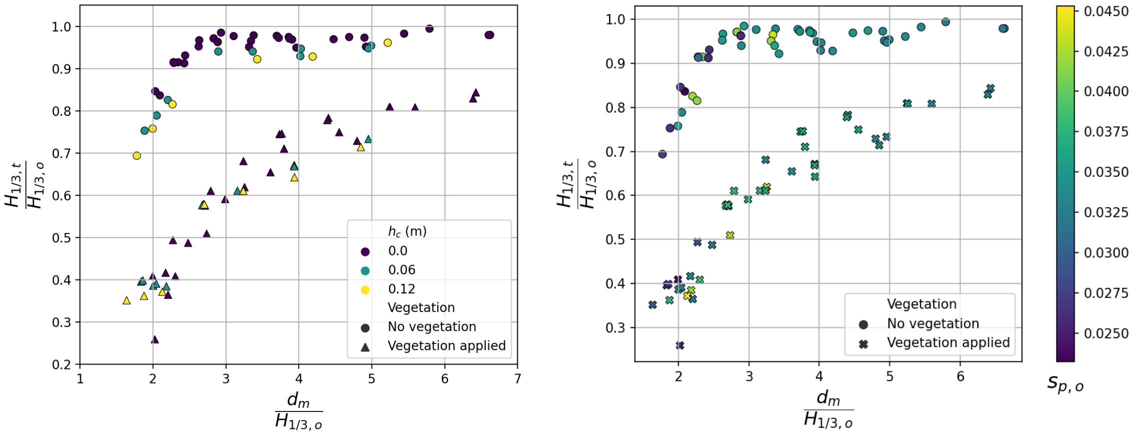

(a) The cliff reduces the wave height even further by around 4%. For $H_s > 2.5$ the salt marsh without vegetation does not reduce the incoming wave height drastically, but does for lower values.

(b) A color map of the peak offshore wave steepness is given. For lower $d_m/H_{1/3}$ tests with different wave steepnesses have been tested. There is not a clear correlation between a given offshore peak wave steepness and the reduction in wave height.

Figure C.10: Reduction factor between the wave height at the toe and offshore. $d_m/H_{1/3}$ is used to make the relation dimensionless. Vegetation reduces the incoming wave height more than without vegetation. Vegetation has always a reducing factor in the tested cases. The wave height reduction is not only due to to a reduction in perceived water depth (which would only place the vegetated cases more to the right as d_m increases)

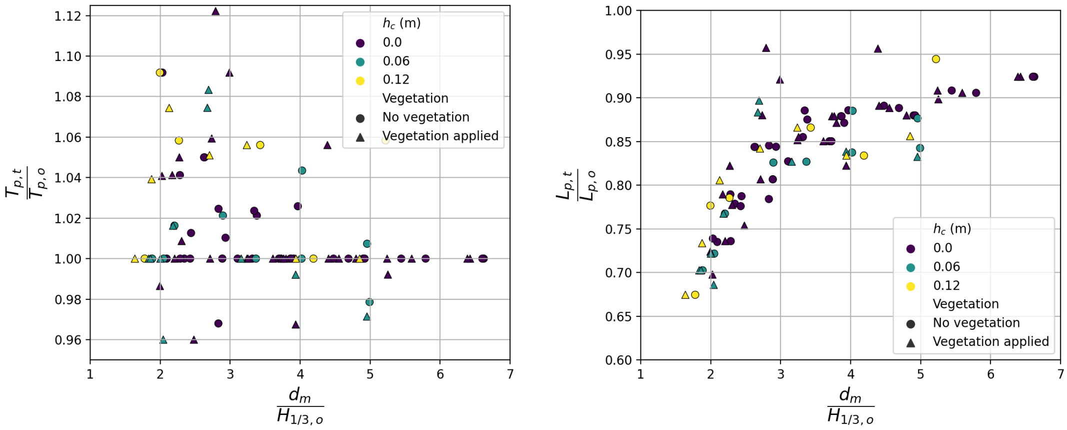

(a) Peak period

(b) Peak wave length

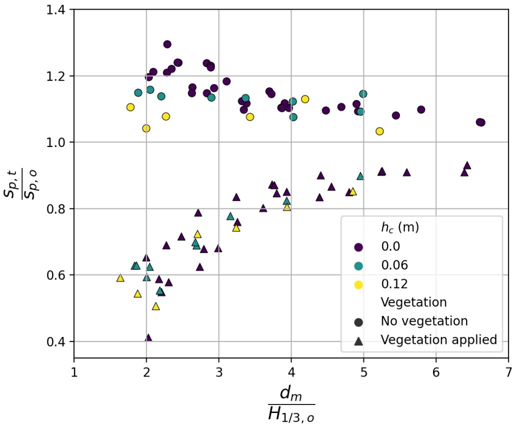

(c) Wave steepness

Figure C.11: Changes in peak parameters. The change in peak wave steepness does differ for cases with and without vegetation. The change in peak wave length is similar for cases with and without vegetation. Hence, this change is primarily dependent on the change in wave height.

C.2. Comparison in wave characteristics

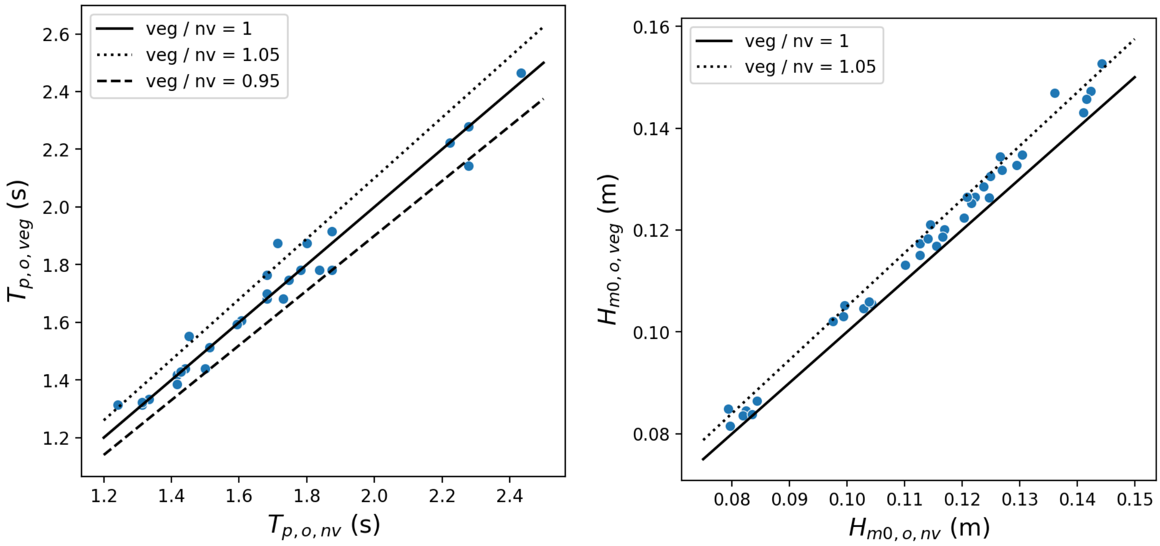

(a) Comparison with Tp

(b) Comparison with Hm0

Figure C.12: Comparison of measurements with and without vegetation

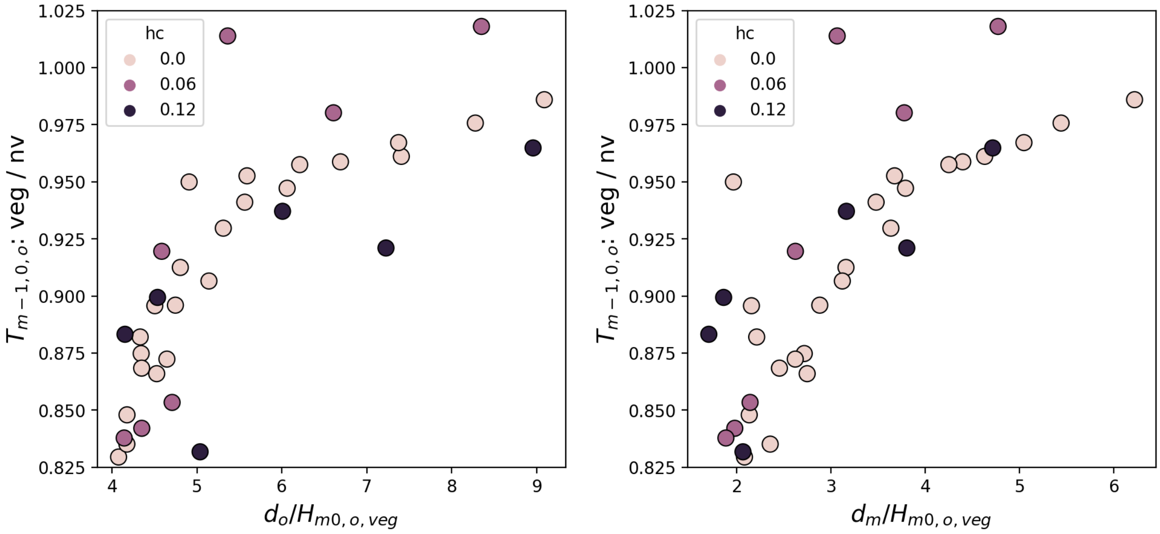

(a) Offshore depth

(b) Salt marsh depth

Figure C.13: Comparison with Tm1

C.3. Wave run-up

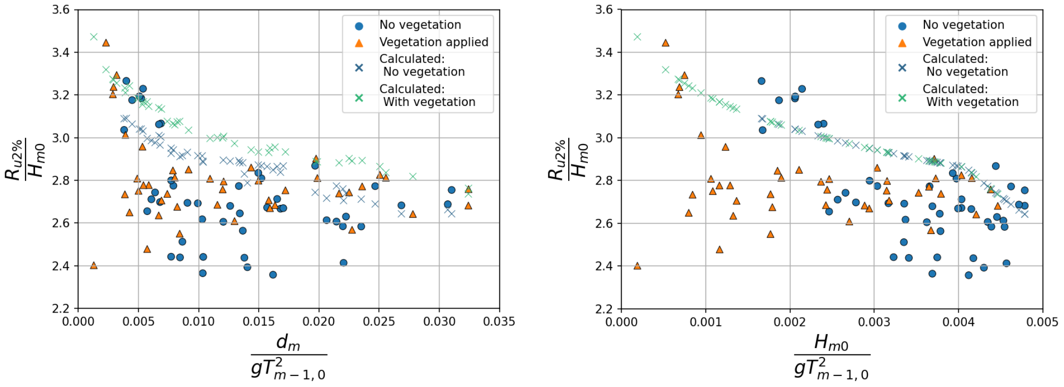

(a) Depth and wave period dependency. The calculated values follow as similar pattern to figure C.3d. However, measurements are lower than predicted, showing a less clear lines.

(b) Wave height and wave period dependency. This is can be seen as an alternative version of figure 3.18. Where some points align with the equation, but most points are lower than predicted

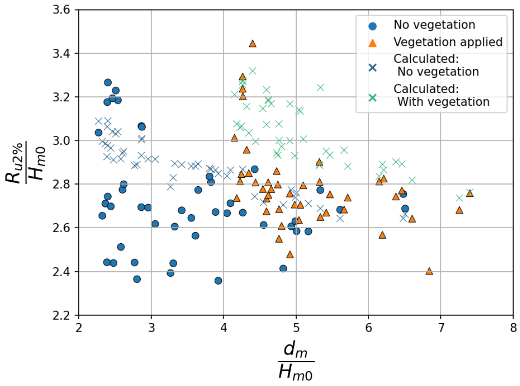

(c) Wave height and depth dependency. There is not a real correlation found.

Figure C.14: Comparison of calculated parameters using TAW/EurOtop equation for a given dimensionless ratio based on the LeMehaute diagram figure C.3. The wave parameters at the toe of the dike are used.

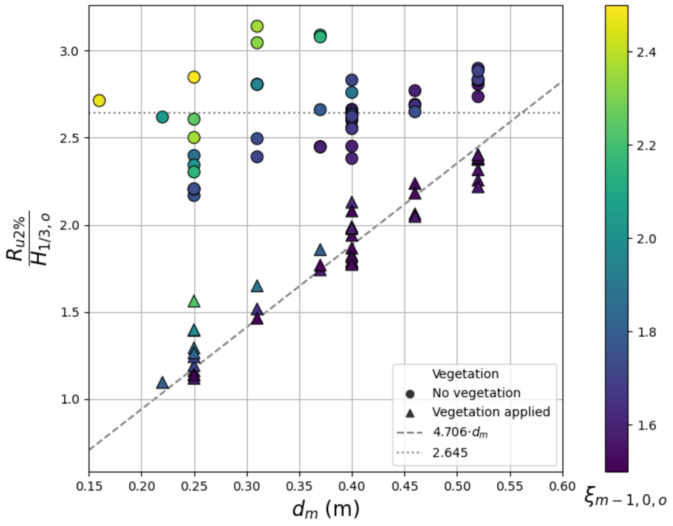

Figure C.15: Linear fit

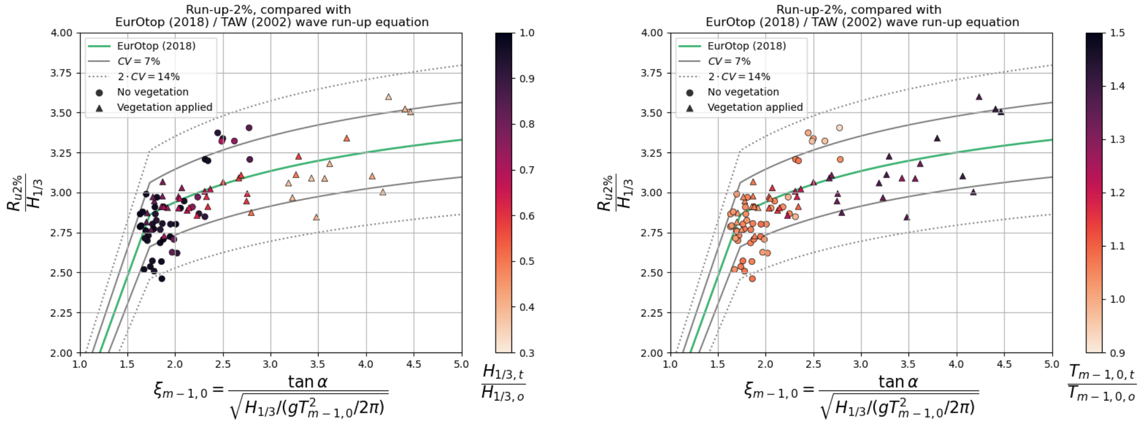

(a) Influence of the change in wave height

(b) Influence of the change in spectral wave period

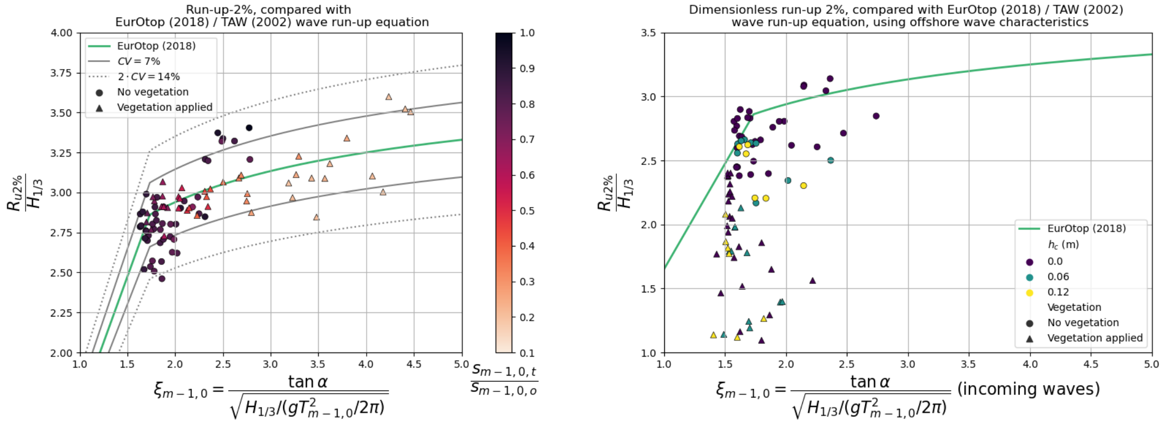

(c) Influence of the change in wave steepness

(d) $\xi_{m-1,0}$ calculated using dike slope (1./3.6) and offshore wave characteristics.

Figure C.16: Effect of change in wave characteristics on dimensionless wave run-up

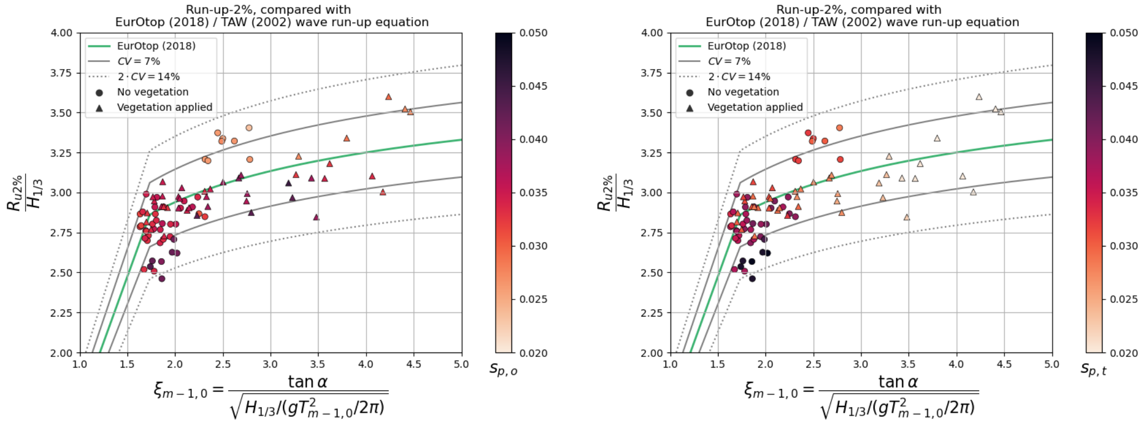

(a) $s_{p,o}$ offshore. Offshore peak wave steepness seems to be correlated with the deviation with equation (3.4)

(b) $s_{p,t}$ toe. Peak wave steepness at the dike toe seems to be less correlated.

Figure C.17: Comparison wave run-up vs Iribarren parameter at the toe of the dike. The peak wave steepness is plotted using a colormap. The EurOtop (2018) and TAW (2002) formula is calculated using the displayed definitions, and plotted to compare the measurements. A coefficient of variation $CV = 7\%$ (TAW, 2002) is used to depict the exceedance. $2 \cdot CV$ corresponds with the $2\sigma = 95.45\%$ confidence bands

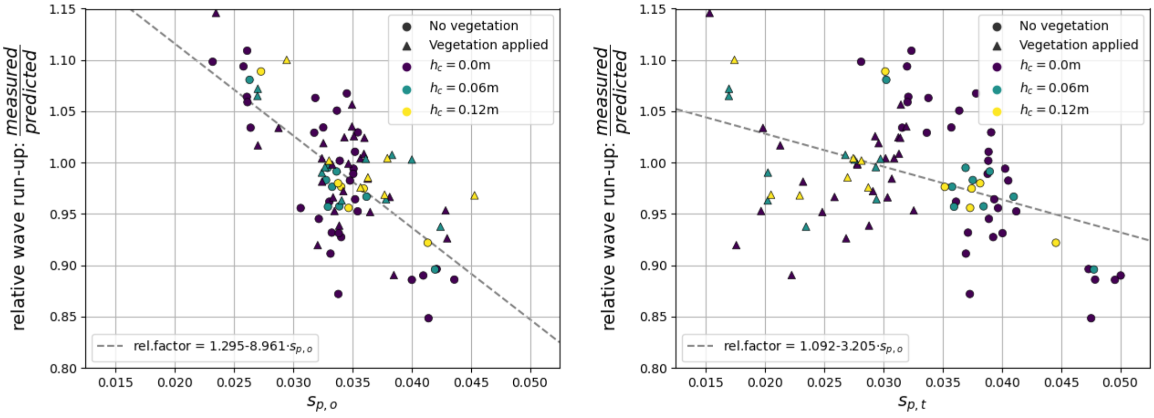

(a) $s_{p,o}$ offshore

(b) $s_{p,t}$ toe

Figure C.18: Correlation between $s_{p,o}$ and the difference factor between measured and predicted relative wave run-up ($R_{u2\%}/H_{1/3}$) values using EurOtop (2018) and TAW (2002) formula

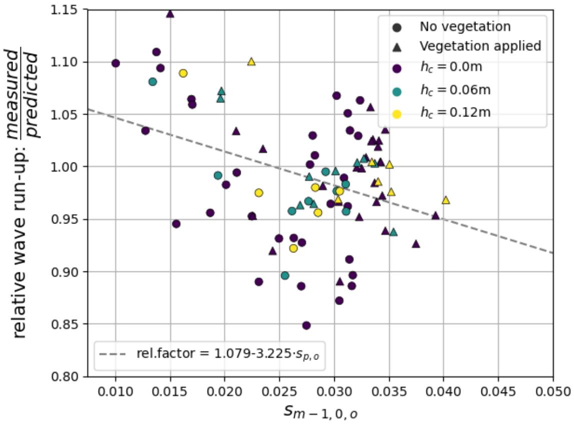

Figure C.19: Influence with $s_{m-1,0,o}$

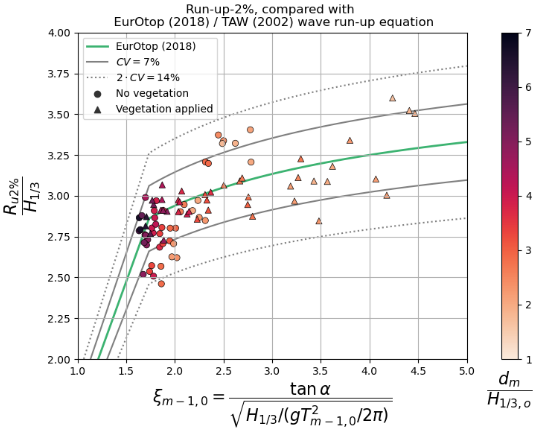

Figure C.20: Influence of depth

D

Appendix: Wave overtopping

If the wave run-up exceeds the crest height of the dike, the water tops over the crest of the dike. This wave overtopping occurs in a total 10 tests. There are several ways in which overtopping is expressed throughout literature (overview given in EurOtop (2018), or TAW (2002)). A straightforward way to describe overtopping is through its volume and (average) velocity.

The individual overtopping volumes are calculated by measuring the differences of the water level in the overtopping box before and after an event. The use of velocity sensors on the crest of the dike is tough. At the dike crest the conditions are dry to wet, instruments such as an EMF require constant wet conditions to operate well. Hence, due to these physical constraints, the calibrated video footage is used to estimate the front velocity.

D.1. Average overtopping rates

The voltages of the overtopping box displacement sensor are converted to water levels using the calibration function described in appendix B.

The total volume of overtopping can be converted to an average overtopping rate (table D.1). Two methods to define the beginning and end of the overtopping can be made, one starting when the first wave hits the dike until the last wave hits the dike (t_{tot}), the second one beginning at the first overtopping event, and stopping at the last overtopping event (t_{fl}). This leads to an increase in average overtopping rate between 1.18 to 5 times between the two.

The decrease in overtopping rate is a factor 0.05. This is due to the significant decrease in wave run-up height experienced by the dike. As 2 tests using vegetation experienced overtopping, this factor is only an indication of the reduction.

Table D.1: Total overtopping volumes and resulting average overtopping rate for every test

Test ID	V_{tot} **(mL)**	t_{tot} **(s)**	t_{fl} **(s)**	V_{pm} **(mL/m)**	q_{tot} **(mL/s/m)**	q_{fl} **(mL/s/m)**
SU1-IR18-1	339	1830	1453	426	0.233	0.293
SU1-IR26-1	2650	1647	1391	3333	2.024	2.396
SU1-IR27-1	7051	1788	1549	8869	4.962	5.726
SU1-IR27-2	7401	1746	1547	9309	5.331	6.018
SU2-IR08-1	32	1613	522	40	0.025	0.077
SU2-IR09-1	233	1827	1257	293	0.160	0.233
SU3-IR08-1	117	1636	305	147	0.090	0.483
SU3-IR09-1	3727	1755	1361	4688	2.671	3.445
SU4-IR27-1	235	1940	574	296	0.152	0.515
SU4-IR27-2	176	1843	663	221	0.120	0.334

The overtopping rate is plotted on Figure 5.14 of EurOtop (2018) (figure D.1). Which depicts the relation between the relative (average) overtopping rate and the relative freeboard. The relative freeboard is high in comparison with the dataset, due to the nature of the wave setup. Most tests have a lower relative overtopping rate than predicted. This is most likely due to the low amount of overtopping events during the experiment. Tests with higher amounts of overtopping events show a closer alignment with the predicted value. However, this could also be a similar result which was observed for wave run-up.

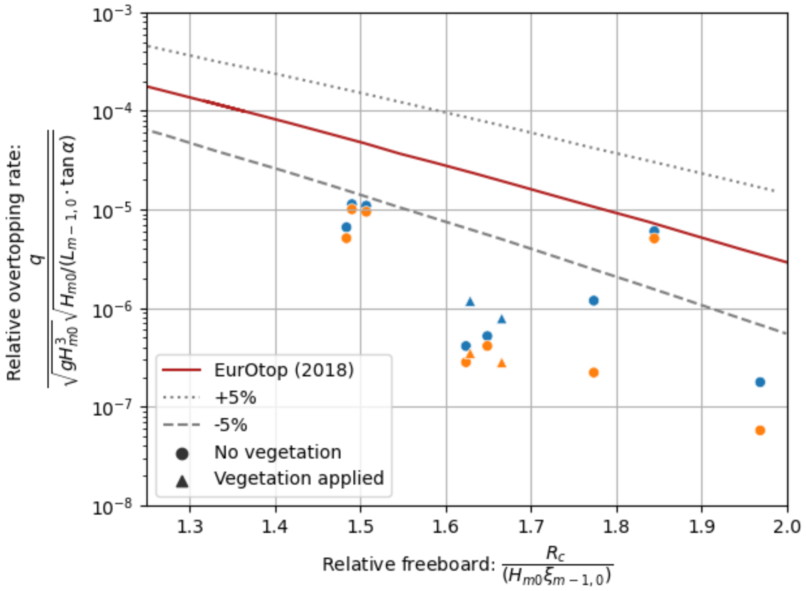

Figure D.1: Comparison with Figure 5.14 of EurOtop (2018), orange and blue coloring represent the two estimates for q, using t_{tot} and t_{fl} respectively. The overtopping rate is lower in most cases than predicted. This is likely due to the limited amount of overtopping events during the tests, however could also have similar origins as which can be seen in the wave run-up analysis.

D.2. Individual overtopping volumes

Each overtopping event causes oscillations due to the impacts of the incoming water which causes movement of the surface of the water of the overtopping box. These can be used to track the amount of overtopping events by calculating a moving standard variation, which is calculated over a moving window of 5 seconds. A high value of the moving standard deviation is a found to be a good measure to indicate an overtopping event, because the standard deviation in an area where these oscillations are present is higher than in an area where there is little water movement. These oscillations however do hinder an accurate reading of the water level, which is needed to calculate the overtopping volumes, therefore the signal needs to be smoothed out. This is done by applying a moving mean of the signal with a window size of 5s.

As the displacement sensor outputs voltages in a certain resolution, the volumetric readings have also a resolution accordingly. This can be seen as a step like result on very small scale. For SU1 and SU4 the resolution of the overtopping box is equal to 120 mL per step, as the overtopping box was quite large relative to the incoming volumes. For experiments SU2, SU3, SU5 and SU6 a smaller overtopping box was used, giving a higher resolution equal to 15 mL per step. Overtopping events are selected manually by subtracting a point before and after the event, giving a volume for that certain event.

The flow velocities can give further insight into the (average) momentum of the overtopping event. These flow velocities are measured using the video data. As the time of the overtopping occurrence is known from the overtopping box signal, the corresponding camera footage can be found of the relevant event at that given time. This footage is calibrated using the procedure described in appendix B. As the run-up signal is only measured on the matte black part of the dike slope, the run-up event which causes overtopping has a chance to be not present in this area. To account for this, the peak of the run-up which causes this overtopping event is hand selected on the frame. For each event, 10 frames before the water tops over the dike's edge, the position of the peak which causes overtopping is selected for each following frame up until it tops over. Following this, the pixel coordinates can be converted to

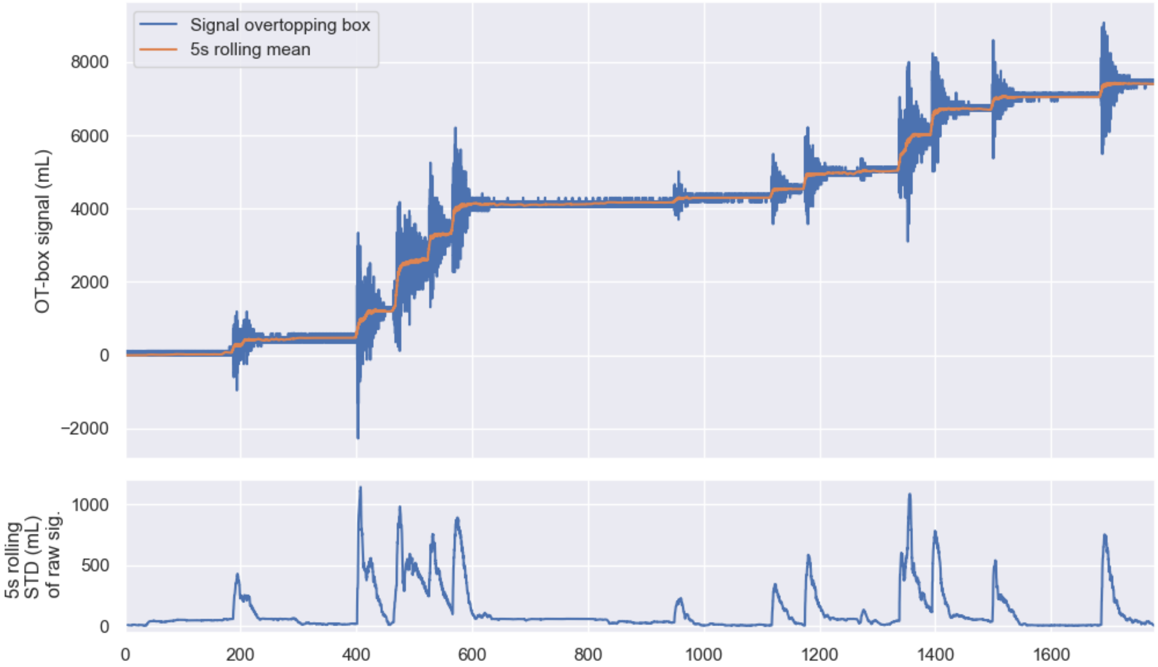

Figure D.2: The signal measuring the volume of the overtopping box. The rolling mean of 5s is plotted and the rolling standard deviation of 5s is plotted of this signal. Overtopping events can be distinguished by the jump in signal and the increased oscillations. The amount of oscillations is captured with the rolling standard deviation.

experimental coordinate system using appendix B. The average velocity can then be calculated with a linear regression of these coordinates, as the time and distance of these coordinates is known. With this, the volume of each overtopping event and speed of the overtopping water is determined.

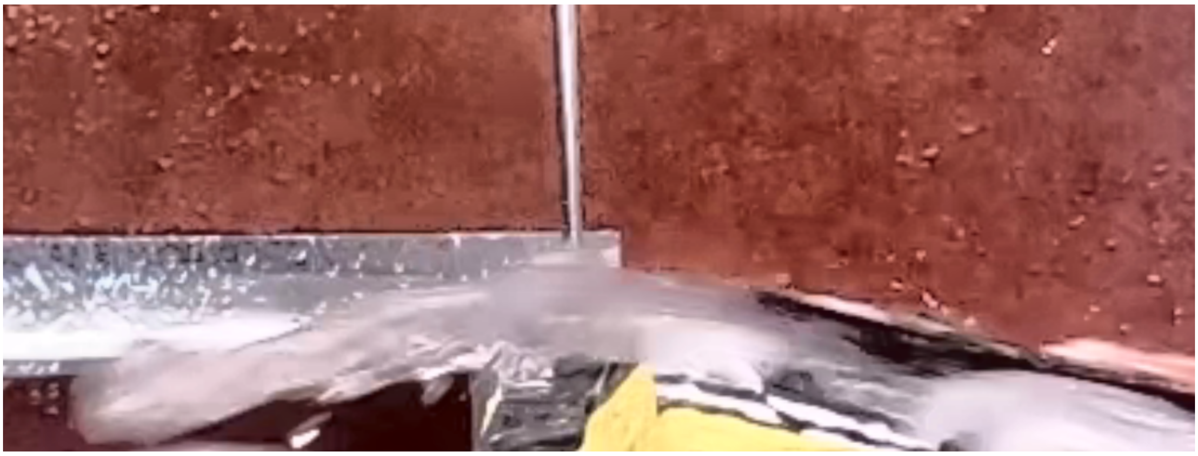

Figure D.3: Side view of an overtopping event at the crest of the dike model. The water moves from right to left from the dike to the overtopping box.

table D.2 depicts an overview for each experiment. Overtopping velocities range from 1 to 2 m/s. The largest individual overtopping volumes decrease with a factor 0.10. As only a small dataset is present, further analysis on this overtopping data will not be done.

Individual overtopping volumes were estimated from the overtopping box signal. As there is some error in the estimation of the individual volumes, they do not add up precisely to the total overtopping volume for that test. Two estimations have been made, the first is a subtraction signal just after the overtopping event of the signal just before. The second is only using the signal value after an overtopping event and subtracting this from the previous value just after the previous overtopping event.

Differences are due to the resolution of the measurements of the overtopping box.

Table D.2: The largest individual overtopping volumes and largest overtopping velocities measured for each experiment

Test ID	No.	Largest volume		Largest velocity	
	events	$V_{ind,maxvol}$ (mL)	$u_{ind,maxvol}$ (m/s)	$V_{ind,maxu}$ (mL)	$u_{ind,maxu}$ (m/s)
SU1-IR18-1	2	223	1.460	223	1.460
SU1-IR26-1	6	1286	1.724	147	1.850
SU1-IR27-1	13	1157	1.830	910	2.039
SU1-IR27-2	16	1373	1.659	544	2.414
SU2-IR08-1	1	37	1.187	37	1.187
SU2-IR09-1	4	116	1.263	64	1.325
SU3-IR08-1	2	101	1.200	101	1.200
SU3-IR09-1	23	1105	1.702	287	2.210
SU4-IR27-1	2	162	1.636	162	1.636
SU4-IR27-2	3	80	1.458	80	1.458

Table D.3: Individual volumes

		TestID	SU3-IR09-1
		Tot. volume difference (mL)	3727
Event	**OT volume (mL)**		**Velocity**
time (s)	**Est. 1**	**Est. 2**	**top (m/s)**
107.95	186	184	1.394
182.38	21	21	1.209
200.63	492	492	1.481
300.19	187	187	1.659
313.37	264	264	1.442
368.90	28	28	1.297
415.86	73	77	1.274
431.52	119	120	1.246
486.17	34	34	1.133
501.65	287	287	2.210
580.77	90	86	1.298
755.99	113	115	1.386
788.98	37	37	1.174
865.09	84	83	1.008
898.06	53	52	1.226
952.52	110	108	1.695
1047.59	26	25	1.164
1067.32	115	114	1.533
1102.60	109	110	1.413
1284.90	101	103	1.043
1364.77	63	63	1.152
1408.30	1105	1105	1.702
1755.97	28	31	1.123

TestID			SU1-IR18-1
Tot. volume difference (mL)			339
Event time (s)	**OT volume (mL) Est. 1**	**Est. 2**	**Velocity top (m/s)**
421.51	116	116	1.080
1822.19	218	223	1.460

TestID			SU1-IR26-1
Tot. volume difference (mL)			2650
Event time (s)	**OT volume (mL) Est. 1**	**Est. 2**	**Velocity top (m/s)**
302.86	239	240	1.814
430.50	101	100	1.198
531.72	718	721	1.828
741.96	149	147	1.850
1370.34	154	185	1.291
1633.28	1275	1286	1.724

TestID			SU1-IR27-1
Tot. volume difference (mL)			7051
Event time (s)	**OT volume (mL) Est. 1**	**Est. 2**	**Velocity top (m/s)**
207.46	372	491	1.846
291.72	135	130	1.287
404.62	698	706	1.885
467.83	911	910	2.039
528.86	791	787	1.570
569.86	1163	1157	1.830
952.33	79	110	1.267
1121.05	86	93	1.118
1178.00	390	392	1.553
1341.59	1113	1112	1.670
1398.14	553	559	1.954
1502.06	239	240	1.372
1690.24	280	280	1.658

TestID			SU1-IR27-2
Tot. volume difference (mL)			7401
Event time (s)	**OT volume (mL) Est. 1**	**Est. 2**	**Velocity top (m/s)**
168.00	53	26	1.210
186.99	245	245	1.428
203.66	176	176	1.225
401.23	720	748	1.777
464.35	1367	1373	1.659
525.43	660	724	1.639
566.33	810	822	1.714
948.87	132	184	1.708
1117.09	241	241	1.471
1174.68	429	429	1.941
1270.80	55	53	1.325
1337.97	544	544	2.414
1352.28	449	449	1.720
1394.38	699	706	1.671
1498.72	333	324	1.392
1686.28	363	363	1.692

TestID			SU2-IR08-1
Tot. volume difference (mL)			32
Event time (s)	**OT volume (mL) Est. 1**	**Est. 2**	**Velocity top (m/s)**
1280.46	28	37	1.187

TestID			SU2-IR09-1
Tot. volume difference (mL)			233
Event time (s)	**OT volume (mL) Est. 1**	**Est. 2**	**Velocity top (m/s)**
231.36	111	116	1.263
304.77	25	24	0.993
1443.24	66	64	1.325
1556.80	30	29	1.058

TestID			SU3-IR08-1
Tot. volume difference (mL)			117
Event time (s)	**OT volume (mL) Est. 1**	**Est. 2**	**Velocity top (m/s)**
964.83	95	101	1.200
1155.92	15	15	1.124

TestID			SU4-IR27-1
Tot. volume difference (mL)			235
Event time (s)	**OT volume (mL) Est. 1**	**Est. 2**	**Velocity top (m/s)**
952.63	63	68	1.291
1394.54	166	162	1.636

TestID			SU4-IR27-2
Tot. volume difference (mL)			176
Event time (s)	**OT volume (mL) Est. 1**	**Est. 2**	**Velocity top (m/s)**
956.66	84	80	1.458
1398.00	20	40	1.424
1499.54	65	65	1.335

E

Appendix: Wave run-up variation along width

The way the wave run-up was determined by the algorithm, lends itself to explore the variability of the run-up across width (transverse direction in the flume). To accomplish this, a parallel process, with minor adjustments to the original is made. The isolated (moving) water surface representing run-up obtained after the application of the Gaussian filter (figure 2.11, step e) can be used to get representation along the transverse direction of the wave run-up for every frame.

In order to obtain this tracking of wave run-up along the width, the original procedure is applied to the whole array representing the moving water surface in a 2D way. Hence, similar to the original procedure, a threshold is applied to the array representing the moving water surface. In this case this is done on the whole 2D array (figure E.1). Also similar to the original procedure, the indices of the leftmost edge created by the threshold can be used to obtain the position corresponding with the run-up signal level (see also figure 2.18, equation (2.20)). The threshold is increased to $\kappa_V = 64$ in comparison with threshold in the original case, by the use of the same calibration procedure described before.

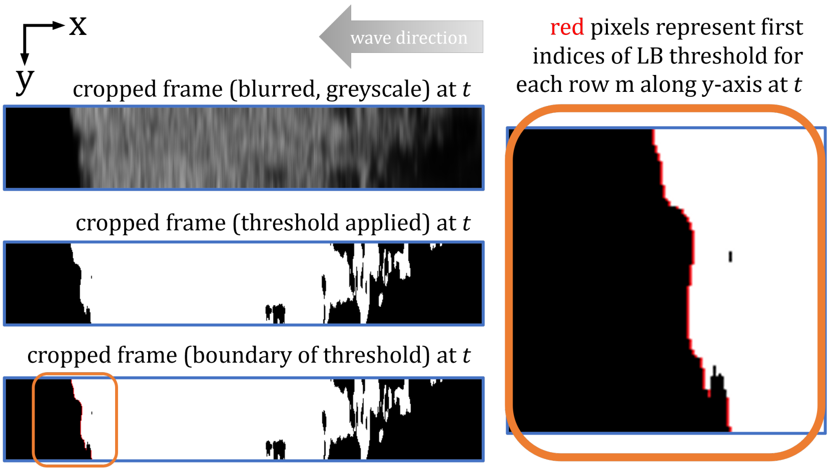

Figure E.1: The edge of the isolated moving water is detected by applying a threshold to the image. This is the same as in figure 2.18, but executed for every row. In this way the left side of the boundary between the water and the dike (depicted as black and white) is traced (depicted as the red line).

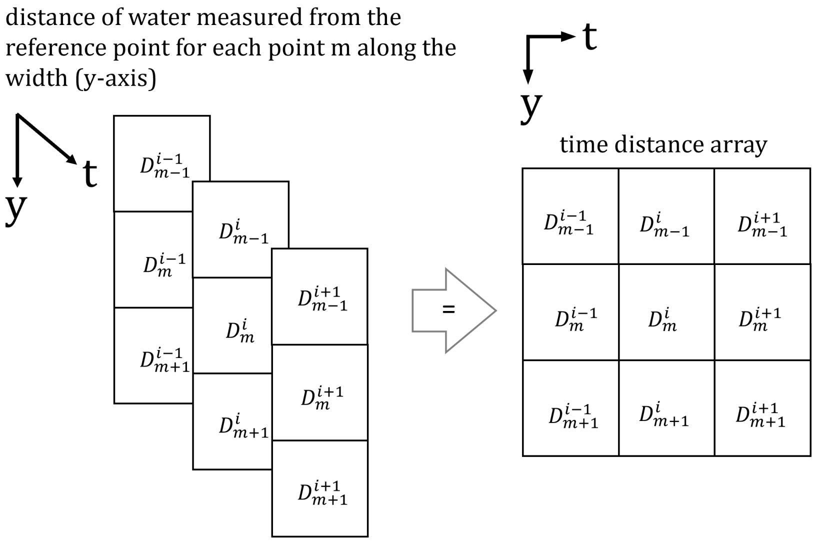

Figure E.2: The array resulting from obtaining a representation of the wave run-up height, is a 1D-array for every time index. This 1D array can be displayed as a time index i and space index m, resulting in a 2D view.

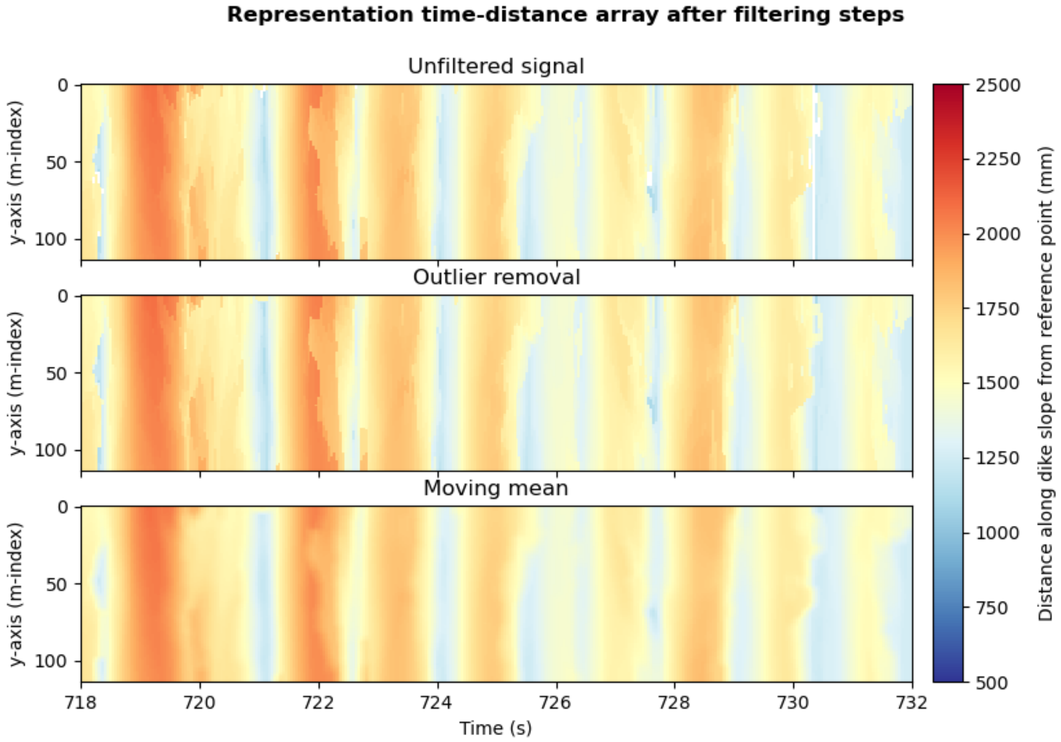

Figure E.3: The 2D-array (time × space) depicting the wave run-up signal along the width, is filtered using the outlier removal from Box 2.2 in two dimensions. After this an moving mean is applied similar to equation (2.26). These filters remove outliers which are deemed inaccurate. The data which is used in the depiction is of SU4-IR23, run 1

As the indices represent the same dimensions along the surface of the dike slope, these indices can be converted to measurements over the diagonal with equation (2.21). As shown in section 2.3.1 and figure 2.19, applying a outlier detection and removal algorithm (Box 2.2) is necessary in this procedure to remove outliers. Moreover by not calculating the median along the y-direction this procedure is even more prone to outliers. In this case, the filter is applied to the whole time and space domain (figure E.2, figure E.3) $(\mathrm{med}(\zeta_{m-2}^{i-2},\ldots,\zeta_{m+2}^{i+2}))$. The filter uses a median filter with size 5x5 ($\Delta t \times \Delta y = 0.23$s $\times 10.5$mm), and removes spikes which have a deviation greater than 1 standard deviation of the filtered array. A moving mean is applied using a 5x5 area ($\Delta t \times \Delta y = 0.23$s $\times 10.5$mm) for the same reasons as mentioned in section 2.3.1 to the signal as well $(\mathrm{mean}([\zeta_{rs}]_{m-2}^{i-2},\ldots,[\zeta_{rs}]_{m+2}^{i+2}))$.

With the filters applied to the signal, a representation of the run-up signal along the width (transverse direction of the flume) is obtained for every time index. With this several parameters according to the variability of the waterline across the width can be obtained. Two ways can be used to describe this variability:

1. Observe the variability of the waterline with a moving reference frame: From this point the waterline can be thought of a line changing shape over time, not taking the absolute height into account.
2. Observe the variability of the waterline from a static position: From this point of view the line will pass a certain height, where the area of passing this line can be quantified, akin to virtual overtopping concept introduced in Hofland et al. (2015), although in 2D.

For this thesis, the variability of the waterline with a moving reference frame is chosen. This can be obtained by converting the time-distance array into a time-run-up signal array with equation (2.22). From this the standard deviation along the width can be found, as well as the max, min and mean, see figure E.4.

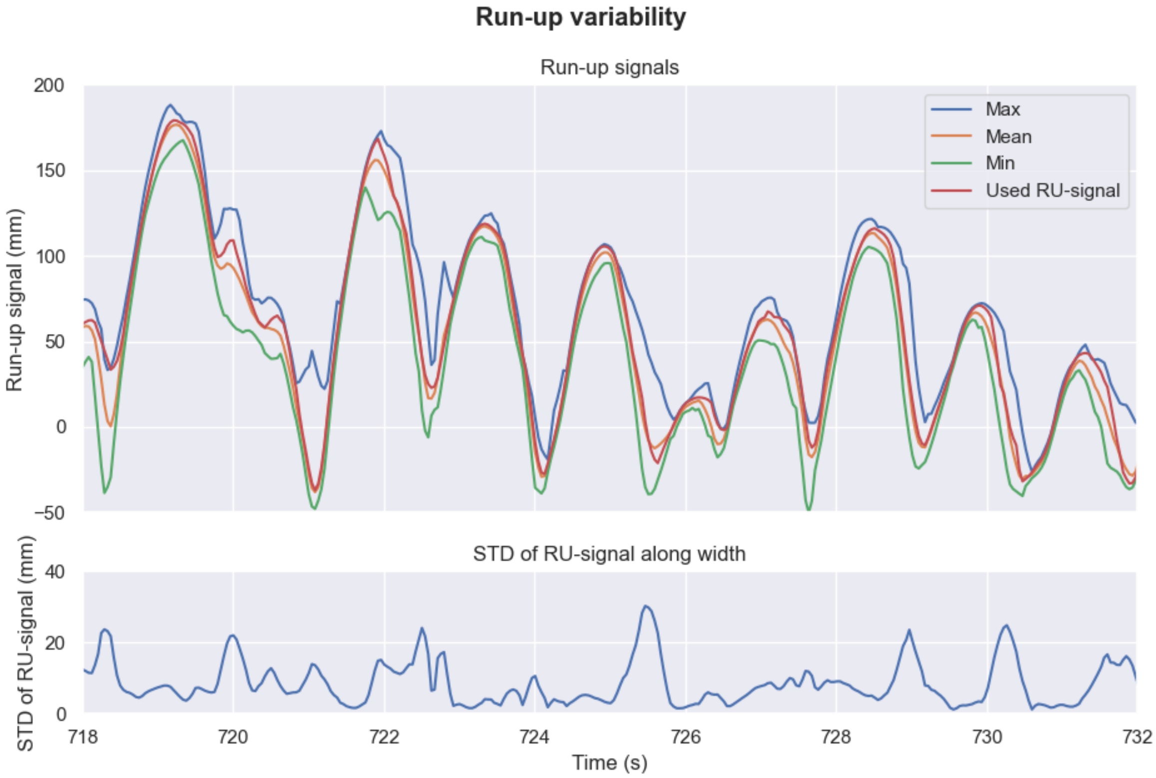

Figure E.4: The variation along the width of the dike slope (transverse direction of the flume) of the run-up signal, of SU4-IR23, Run 1. The minimum, mean and maximum along this direction are given, as well as the used run-up signal which resembles the median. The standard deviation along the width for every time index is plotted underneath the graph. A larger deviation between the maximum and minimum of the signal gives a higher standard deviation for that point.

When a wave transforms into run-up, the incoming wave transforms somewhat linearly over the width into wave run-up. When the maximum of the run-up of that wave is reached, it transforms into wave run-down. Due to small differences in surface tension the straightness of the top of the water will reduce and the run-down becomes more turbulent.

This can be shown when comparing the calculated variation along width with the derivative of the run-up signal. This derivative is calculated using a midpoint method using a 4 point distance (0.16s):

$$\frac{\Delta z}{\Delta t} = \frac{z(t_{i+2}) - z(t_{i-2})}{4/f_s} \tag{E.1}$$

If this derivative is plotted against time and the standard deviation along the width is plotted against time, the peaks of the standard deviation line up with the troughs of the derivative. This was also observed during the calibration and validation procedure, when the tests were done by hand. There was no real dividing line depicting the distinction between water and surface visible as the run-down was very turbulent.

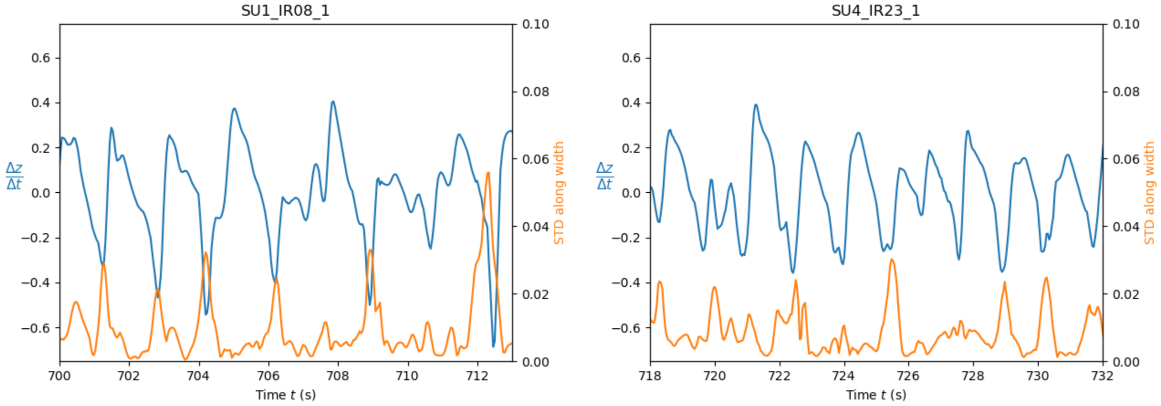

(a) **(b)**

Figure E.5: The troughs of the derivative of run-up signal are correlated with the peaks in the standard deviation along width. This can be seen by similarities for the same time. The troughs of the derivative of the run-up signal correspond with wave run-down. Wave run-down has shows higher turbulence than run-up.

For all peaks in the run-up signal, the corresponding standard deviation along the width is found. When analyzing at a set of peaks versus these standard deviations, there is no correlation found. The median of all these standard deviations is calculated for each set. If this median is plotted against the run-up 2%, there is a weak correlation visible. This gives an indication in the general variation along the width of measurements in the conducted flume tests (figure E.6). On average this is around 8 to 10mm. This means that each reading of a given peak in a wave run-up signal in the measured flume experiments has a standard deviation of about 8 to 10mm.

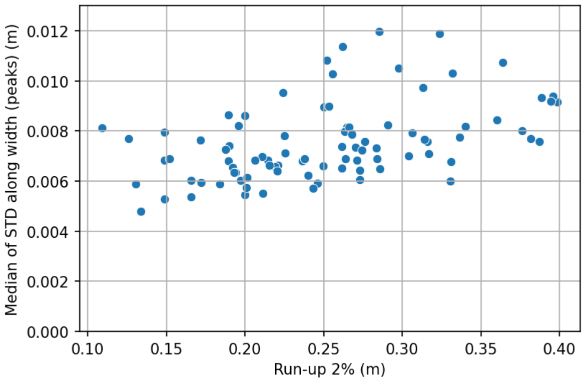

Figure E.6: The median of all standard deviation along the width for each detected run-up. This gives an indication in the general variation along the width of measurements in the conducted flume tests.

F

Appendix: Information about tests

Table F.1: Used experiment IDs in the comparing the wave run-up results to literature. The measurements for the smallest water levels were deemed unreliable.

SU1	**SU1**	**SU2 and SU3**	**SU4**	**SU4**	**SU5 and SU6**
SU1-IR03-1	SU1-IR15-1	SU2-IR03-1	SU4-IR03-1	SU4-IR15-1	SU5-IR03-2
SU1-IR04-2	SU1-IR16-1	SU2-IR04-1	SU4-IR04-1	SU4-IR16-1	SU5-IR03-3
SU1-IR05-2	SU1-IR17-1	SU2-IR05-1	SU4-IR05-1	SU4-IR17-1	SU5-IR04-2
SU1-IR06-1	SU1-IR18-1	SU2-IR06-1	SU4-IR06-1	SU4-IR18-1	SU5-IR04-3
SU1-IR06-2	SU1-IR20-1	SU2-IR06-2	SU4-IR07-1	SU4-IR20-1	SU5-IR05-2
SU1-IR07-1	SU1-IR21-1	SU2-IR07-1	SU4-IR08-1	SU4-IR21-1	SU5-IR06-1
SU1-IR08-1	SU1-IR22-1	SU2-IR07-2	SU4-IR09-1	SU4-IR22-1	SU5-IR07-2
SU1-IR08-2	SU1-IR22-2	SU2-IR08-1	SU4-IR12-1	SU4-IR23-1	SU5-IR08-1
SU1-IR09-1	SU1-IR23-1	SU2-IR09-1	SU4-IR13-1	SU4-IR24-1	SU5-IR09-1
SU1-IR11-1	SU1-IR23-2	SU3-IR03-1	SU4-IR14-1	SU4-IR24-2	SU5-IR09-2
SU1-IR12-1	SU1-IR24-1	SU3-IR04-1		SU4-IR25-1	SU6-IR03-1
SU1-IR12-2	SU1-IR24-2	SU3-IR05-1		SU4-IR25-2	SU6-IR04-1
SU1-IR13-1	SU1-IR25-1	SU3-IR06-1		SU4-IR26-1	SU6-IR05-1
SU1-IR13-2	SU1-IR26-1	SU3-IR07-1		SU4-IR26-2	SU6-IR06-1
SU1-IR14-1	SU1-IR27-1	SU3-IR08-1		SU4-IR27-1	SU6-IR07-1
SU1-IR14-2	SU1-IR27-2			SU4-IR27-2	SU6-IR08-1
					SU6-IR09-1

Table F.2: Overview of all experiments conducted. 2×45 tests are conducted, these include tests with and without vegetation. IDs without vegetation displayed at the left and ID's with vegetation displayed at the right (as they have the same wave conditions). Virtual cliff heights are used for SU1 and SU4 to compare with the other setups.

No Veg.		**Shared hydrodynamic conditions**								**Veg.**	
SU	*IR*	d_m [cm]	H_s [cm]	s [%]	h_c [cm]	$h_{c,vir}$ [cm]	d_o [cm]	$L_{p,o}$ [m]	T_p [s]	*SU*	*IR*
1	1	0	8	4	0	0	24	2.00	1.42	4	1
1	2	10	12	4	0	0	34	3.00	1.77	4	2
1	3	25	14	4	0	0	49	3.50	1.78	4	3
1	4	25	14	3	0	0	49	4.67	2.27	4	4
1	5	25	14	5	0	0	49	2.80	1.50	4	5
1	6	40	10	4	0	0	64	2.50	1.32	4	6
1	7	40	12	4	0	0	64	3.00	1.48	4	7
1	8	40	14	4	0	0	64	3.50	1.66	4	8
1	9	40	16	4	0	0	64	4.00	1.83	4	9
1	10	6	8	4	0	6	30	2.00	1.32	4	10
1	11	16	12	4	0	6	40	3.00	1.68	4	11
1	12	31	14	4	0	6	55	3.50	1.72	4	12
1	13	31	14	3	0	6	55	4.67	2.18	4	13
1	14	31	14	5	0	6	55	2.80	1.46	4	14
1	15	46	10	4	0	6	70	2.50	1.30	4	15
1	16	46	12	4	0	6	70	3.00	1.46	4	16
1	17	46	14	4	0	6	70	3.50	1.62	4	17
1	18	46	16	4	0	6	70	4.00	1.79	4	18
1	19	12	8	4	0	12	36	2.00	1.26	4	19
1	20	22	12	4	0	12	46	3.00	1.61	4	20
1	21	37	14	4	0	12	61	3.50	1.68	4	21
1	22	37	14	3	0	12	61	4.67	2.10	4	22
1	23	37	14	5	0	12	61	2.80	1.43	4	23
1	24	52	10	4	0	12	76	2.50	1.29	4	24
1	25	52	12	4	0	12	76	3.00	1.44	4	25
1	26	52	14	4	0	12	76	3.50	1.60	4	26
1	27	52	16	4	0	12	76	4.00	1.76	4	27
2	1	0	8	4	6	0	30	2.00	1.32	5	1
2	2	10	12	4	6	0	40	3.00	1.68	5	2
2	3	25	14	4	6	0	55	3.50	1.72	5	3
2	4	25	14	3	6	0	55	4.67	2.18	5	4
2	5	25	14	5	6	0	55	2.80	1.46	5	5
2	6	40	10	4	6	0	70	2.50	1.30	5	6
2	7	40	12	4	6	0	70	3.00	1.46	5	7
2	8	40	14	4	6	0	70	3.50	1.62	5	8
2	9	40	16	4	6	0	70	4.00	1.79	5	9
3	1	0	8	4	12	0	36	2.00	1.26	6	1
3	2	10	12	4	12	0	46	3.00	1.61	6	2
3	3	25	14	4	12	0	61	3.50	1.68	6	3
3	4	25	14	3	12	0	61	4.67	2.10	6	4
3	5	25	14	5	12	0	61	2.80	1.43	6	5
3	6	40	10	4	12	0	76	2.50	1.29	6	6
3	7	40	12	4	12	0	76	3.00	1.44	6	7
3	8	40	14	4	12	0	76	3.50	1.60	6	8
3	9	40	16	4	12	0	76	4.00	1.76	6	9

G

Appendix: Overtopping manual

An assessment of dike dimensions has developed throughout history and is still developing. The crest height of the first modern dikes in the Netherlands were tested by using the *wave run-up* level. This is the level which the water contained in each incident wave reaches on the slope of the dike, measured vertically from still water level (SWL). The run-up level which is exceeded by 2% of the number of incident waves is called the wave run-up height ($R_{u,2\%}$), which is used for design. After the closing of the Zuiderzee with the building Afsluitdijk, the first tests of wave run-up were conducted at Delft Hydraulics (now Deltares). The results of tests were used to design dikes for the Noordoostpolder, where equation (G.1) was used to assess the height of the dikes, which was used until the 1980's.

$$R_{u2\%} = 8H_{m0,toe}\tan\alpha \tag{G.1}$$

Where $H_{m0,toe}$ is the spectral wave height of the incoming waves at the toe of the dike and α is the dike slope measured from the horizontal. The choice of why specifically the 2% value was chosen as an intermediary value between 1% and 5% as the first tests were conducted with 50 waves[1], and thus 2% value was the highest wave in the series. The formula is still correct if s = 0.040.

The current formula used for the wave run-up for gentle dike slopes is given in EurOtop (2018):

$$\frac{R_{u2\%}}{H_{m0,toe}} = a\gamma_b\gamma_f\gamma_\beta\xi_{m-1,0} \tag{G.2}$$

with a maximum of:

$$\frac{R_{u2\%}}{H_{m0,toe}} = b\gamma_f\gamma_\beta\left(c - \frac{1.5}{\sqrt{\gamma_b\xi_{m-1,0}}}\right) \tag{G.3}$$

Where a, b and c are coefficients, with mean values $\mu(a) = 1.65$, $\mu(b) = 1.0$ and $\mu(c) = 4.0$, with a standard deviation of $\sigma(a) = 0.10$, $\sigma(b) = 0.07$ and $\sigma(c) = 0.3$. Where γ_b is the factor related to the berm of the dike, γ_f the factor related to the surface friction on the slope of the dike and γ_β the factor related to the angle of incidence of the incoming waves perpendicular to the dike. $\xi_{m-1,0}$ is the Iribarren number or surf similarity parameter using the wave conditions at the toe of the dike. Instead of using the peak period T_p, which is commonly used to describe wave spectra, the spectral period $T_{m-1,0}$ is used for this number. This spectral period "gives more weight to longer periods in the spectrum than an average period and, independent of the type of spectrum, give similar wave run-up or overtopping for the same values of $T_{m-1,0}$ and the same wave heights. In this way, wave run-up and overtopping can be easily determined for bimodal and 'flattened' spectra, without the need for other difficult procedures".

Modern dikes are designed using dimensions obtained from wave overtopping formulae. *Wave overtopping* is the process were the wave run-up level exceeds the crest of the dike and causes water to flow over the crest of the dike. This type of overtopping is called green water overtopping. Splashes and wind spray generated from wave breaking and other turbulent phenomena are called white overtopping.

---

[1] Historically, the wave maker was manually driven by a person on a bike type drive. 50 waves was the physical limit to generate for each test, before rest was needed, thus the highest run-up value during the experiment was used

High levels of overtopping causes damage to the inner slope of the dike, resulting in dike failure. Design formulas are based on average discharges, however this does not represent the failure mechanism present on dikes. Large waves can cause a big overtopping volume which leads to erosion, whereas a lot of smaller waves give the same average discharges however do not cause severe erosion. Thus can be concluded that for a full understanding of wave attack the discharge distribution of each overtopping event is of importance. To obtain this individual overtopping discharge, the velocities and dimensions of the overtopping events need to be known.

H

Appendix: Video Processing Code

Water tracing

```
# -*- coding: utf-8 -*-
"""
Created on Sun May 14 11:05:21 2023

@author: Stijn Lakerveld

"""

import cv2
import numpy as np
from collections import deque
from scipy.ndimage import gaussian_filter1d
from tqdm import tqdm
from pathlib import Path

def image_process(queue, blur=5, gaus_filter=5):
    """


    Parameters
    ----------
    queue : deque type
        Moving window of frames.
    blur : int, optional
        Amount of blurring using the median blur. The default is 5.
    gaus_filter : int, optional
        Amount of blurring using the gaussian 1D blur. The default is 5.

    Returns
    -------
    image : array
        Black and white image of the variance of the moving window, blurred.

    """

    # Calculate the variance of the frames in the moving window, then takes the
    # mean of the colors to create a black and white variance image
    image = np.mean(np.var(np.array(queue),axis=0),axis=2)
    # Blur the image to reduce noise
    image = cv2.medianBlur(image.astype(np.uint8), blur)
    image = gaussian_filter1d(image, gaus_filter, axis=0)
    return image

def median_line(image, line_threshold):
    # Calculate median of the image values over the vertical
    line_median = np.median(image, axis=0)
    # Calculate boolean where the median is higher than the threshold
    is_line_over_threshold = line_median > line_threshold
```

```
    # Returns the first index of this boolean
    first_index = is_line_over_threshold.argmax()
    return first_index

def variable_line(image, line_threshold):
    # Calculate the boolean where the values of the image is higher than the threshold
    is_grid_over_threshold = image > line_threshold
    # Returns the first index of every vertical line over the horizontal axis of this boolean
    indexlist = is_grid_over_threshold.argmax(axis=1)
    return indexlist

def show_image(image, testid, medval, varval, colormed=(0,255,0), thickness=2,
               colorvar=(0,0,255), chaospar=100, show_median_line=True, show_variable_line=
                   True):
    '''
    Show image with selected lines

    Parameters
    ----------
    image : 2D-array or OpenCV color image
        Image that needs to be shown.
    testid : string
        Name of image to be displayed in window.
    medval : int
        Value of the median line that is displayed.
    varval : array of int
        Values of the variable line that needs to be displayed
    colormed : tuple, optional
        Color of the median line. The default is (0,255,0).
    thickness : int, optional
        Thickness of the median line. The default is 2.
    colorvar : tuple, optional
        Color of the variable line. The default is (0,0,255).
    chaospar : float, optional
        Value of maximum standard deviation for the variable line to be shown. The default is
             100.
    show_median_line : boolean, optional
        If this is True the median line will be shown. The default is True.
    show_variable_line : boolean, optional
        If this is True the variable line will be shown. The default is True.

    '''

    # Convert grayscale image to color to display it with colored lines
    if len(image.shape) == 2:
        image = cv2.cvtColor(image.astype(np.uint8),cv2.COLOR_GRAY2RGB)
    image_to_show = image.copy()
    # Show straight line using medval variable
    if show_median_line == True:
        cv2.line(image_to_show, [medval, 0], [medval, image_to_show.shape[0]], colormed,
            thickness)
    # Show variable line using the varval values
    if show_variable_line == True:
        coords = np.vstack([varval,np.arange(image.shape[0]).astype(int)])
        if np.std(varval) <= chaospar:
            cv2.polylines(image_to_show,[coords.T],False,colorvar,1,cv2.LINE_AA)
    cv2.imshow(testid, image_to_show.astype(np.uint8))
    return None

def main_process(filename, mtx, dist, warpmtx, timestart=0.0, maxsize=3,
                 hmin=0, hmax=-1, showimg=True, medthresh=40, varthresh=40,
                 medblur=5, gausfilt=5):
    """


    Parameters
    ----------
    filename : WindowsPath
        This is the path of the file made using pathlib.
    mtx : array of float64
        Camera matrix with size 3x3 of the video.
```

```
    dist : array of float64
        Distortion coefficients of the video.
    warpmtx : array of float64
        Transformation matrix to warp the video, this is defined by matching
        the chessboard on camera with cv2.findHomography.
    timestart : float, optional
        Start of the time array. The default is 0.0.
    maxsize : int, optional
        Size of the queue used in the variance calculation. The default is 3.
    hmin : int, optional
        Index of top row used in processing. The default is 0.
    hmax : int, optional
        Index of last row used in processing. The default is -1.
    showimg : string, optional
        Show live image processing.
        To only see median line use 'median'.
        To only see variable line use 'variable'.
        To see both lines use 'all'.
        To see the corresponding variance image add '_variance' to string
        To see no live image processing use 'no'. The default is 'all'.
    medthresh : int, optional
        Threshold of the median variance line. The default is 40.
    varthresh : int, optional
        Threshold of the variance line . The default is 40.
    medblur : int, optional
        Amount of blurring using the median filter. The default is 5.
    gausfilt : int, optional
        Amount of blurring using the gaussian filter. The default is 5.

    Returns
    -------
    vidtime : array of float64
        Timestamps for each frame.
    med_index : array of float64
        size = (1 x n.o.frames). Median line value for each frame.
    var_index : array of float64
        size = (hmax-hmin x n.o.frames). Variating line values for each frame.
    new_time : int
        The timestamp of the following step of the video after the last frame

    """

    if not isinstance(filename, Path):
        raise TypeError('filename must be of type WindowsPath')

    # Open video
    cap = cv2.VideoCapture(str(filename))

    # Helpful variables
    nom = filename.stem
    nof = int(cap.get(cv2.CAP_PROP_FRAME_COUNT))
    w   = int(cap.get(cv2.CAP_PROP_FRAME_WIDTH))
    h   = int(cap.get(cv2.CAP_PROP_FRAME_HEIGHT))
    fps = cap.get(cv2.CAP_PROP_FPS)
    print(f'Currentfile: {str(nom)} | Total frames: {nof} | FPS: {fps:.3f} | Starttime: {timestart}')

    # Create time array, median line array, variable line array and queue
    vidtime = np.arange(0, nof, dtype='float64')/fps + timestart
    newtime = vidtime[-1]+1./fps
    med_index = np.zeros_like(vidtime)
    var_index = np.zeros((len(med_index), hmax-hmin))
    q = deque()

    for i in tqdm(range(nof)):
        ret, frame = cap.read()

        if not ret:
          print("Ignoring empty camera frame.")
          # If loading a video, use 'break' instead of 'continue'.
          break
```

```

        # Undistort the frame with the intrinsic calibration parameters
        frame = cv2.undistort(frame, mtx, dist)
        # Perspective transformation with the extrinsic calibration matrix
        frame = cv2.warpPerspective(frame, warpmtx, (w, h))
        # The relevant area where the processing is applied to
        frame = frame[hmin:hmax]

        if len(q) and (q[-1]==frame).all():
            print('cont')
            continue

        # Create the queue / moving window of frames, and remove the oldest
        # frame if bigger than the specified maxsize
        q.append(frame)
        if len(q)>maxsize:
            q.popleft()

        # Process the image to obtain the variance of the queue/moving window
        var_image = image_process(q, blur=medblur, gaus_filter=gausfilt)
        # Find the median edge line of the variance image and save it to the array
        med_index[i] = median_line(var_image, medthresh)
        # Find the edge line for every pixel and save it to the array
        var_index[i] = variable_line(var_image, varthresh)

        # Section to see what the process is doing.
        # To see variance image replace 'frame' with var_image
        if showimg == 'all':
            show_image(frame, nom, med_index[i].astype(int), var_index[i].astype(int))
        if showimg == 'median':
            show_image(frame, nom, med_index[i].astype(int), var_index[i].astype(int),
                show_variable_line=False)
        if showimg == 'variable':
            show_image(frame, nom, med_index[i].astype(int), var_index[i].astype(int),
                show_median_line=False)
        if showimg == 'all_variance':
            show_image(var_image, nom, med_index[i].astype(int), var_index[i].astype(int))
        if showimg == 'median_variance':
            show_image(var_image, nom, med_index[i].astype(int), var_index[i].astype(int),
                show_variable_line=False)
        if showimg == 'variable_variance':
            show_image(var_image, nom, med_index[i].astype(int), var_index[i].astype(int),
                show_median_line=False)
        if showimg == 'no':
            continue

        # Shortest waittime for each frame
        if cv2.waitKey(1) == ord('q'):
            break

    # Close the total loaded video
    cap.release()
    cv2.destroyAllWindows()

    return vidtime, med_index, var_index, newtime
```

Signal Filtering

```
# -*- coding: utf-8 -*-
"""
Created on Tue May 14 15:35:19 2024

@author: stijn
"""

import numpy as np
import pandas as pd
from scipy.ndimage import median_filter, uniform_filter1d

pixels2diag = lambda x: 3635.022482 - 2.1 * x
```

```

def findExpInfo(excel, setup_name, revision):
    # Looks in the experiment excel file for the correct data
    tests = excel[excel['Experiment'] == setup_name]
    corr = tests[tests['Rev'] == revision]

    return corr.iloc[0]

def timeSync(sf, p2d, entries):
    # Synchronises the time to DASYlab data
    startframe = int(sf[sf['TestID'] == p2d]['Startframe'].values[0])
    t = np.arange(entries)/23.976024
    t = t - t[startframe] + 5

    return t

def upperAndLowerBound(data, zerothresh=1, upperthresh=1724):
    # Sets an upper and lower bound to the data, and replaces outliers with nan
    if zerothresh > 0:
        data[data < zerothresh] = np.nan
    if upperthresh > 0:
        data[data > upperthresh] = np.nan

    return data

def filterOutliersMedian(data, filterSize=5):
    # Detects outliers with median filter and replaces outliers with nan
    filtered = median_filter(data, size=filterSize)
    mask = np.abs(data - filtered) > np.nanstd(filtered)
    data[mask] = np.nan

    return data

def filterAndConvert(data, info):
    # Converts pixel data to actual measurements
    uplow = upperAndLowerBound(data)
    filt = filterOutliersMedian(uplow)
    diag = pixels2diag(filt)
    vertical = diag / (np.sqrt(1+3.6**2))
    if len(data.shape) == 1:
        return vertical - info['dm [cm]']*10 - info['hc [cm]']*10
    else:
        return vertical * (np.sqrt(1+3.6**2))

def convertParquet2CSV(testid, path_runup, path_offset, path_experiments_excel):
    # Load data
    df_offset = pd.read_csv(path_offset, sep=',')
    df_experiments = pd.read_excel(path_experiments_excel, sheet_name=0, index_col=0)
    info = findExpInfo(df_experiments, testid[:-2], float(testid[-1]))
    ru_data = pd.read_parquet(path_runup)

    # Select data
    mdata = ru_data.iloc[:, 1].to_numpy()

    # Syncronise time with other files
    ru_time = timeSync(df_offset, testid, len(ru_data['Time']))

    # Convert pixels to vertical measurements
    msig = filterAndConvert(mdata, info)

    # Interpolate signal
    ruout_inter = pd.Series(msig).interpolate()
    ruout_inter = ruout_inter.fillna(0).to_numpy()

    # Smooth signal
    ruout_smooth = uniform_filter1d(ruout_inter, 5)

    runupsignals = {
                    'time (s)': ru_time,
                    'runup-index (px)': mdata,
                    'runup-converted (mm)': msig,
```

```
                    'runup-filtered (mm)': ruout_smooth
                    }

    df_RU = pd.DataFrame(runupsignals)
    float_cols = ['time (s)', 'runup-converted (mm)', 'runup-filtered (mm)']
    df_RU[float_cols] = df_RU[float_cols].astype(float)
    df_RU['runup-index (px)'] = df_RU['runup-index (px)'].astype(int)

    return df_RU

testid = 'SU2_IR02_1'
runup_parquet_file = r'U:\LivingDikesTest\Living Dikes\Tests\Irregular\SU2_IR02\RU_SU2_IR02_1
    .parquet'
runup_offset_file = r'U:\LivingDikesTest\Living Dikes\Scripts\calib\runup_offset.csv'
excel_experiments_file = r'U:\LivingDikesTest\Living Dikes\Tests\Experiments.xlsx'
```

Obtaining metrics

```
# -*- coding: utf-8 -*-
"""
Created on Wed May 15 11:45:36 2024

@author: stijn
"""

import numpy as np
import pandas as pd
from scipy.signal import find_peaks
from python_subfunctions import zerocrossing as zc
from python_subfunctions import wave_spectrum as ws

Ldeepwater = lambda x: 9.81 * x**2 / (2 * np.pi)

def T2L(T, d, g=9.81, n=100):
    # Calculates the wave period
    if not d or not T:
        return 0
    else:
        L0 = g*T**2 / (2 * np.pi)
        L_old = L0
        for i in range(n):
            L_new = L0 * np.tanh((2*np.pi*d)/L_old)
            if np.abs(L_old - L_new) < 0.0000001:
                break
            L_old = L_new
        return L_new

def findExpInfo(excel, setup_name, revision):
    # Looks in the experiment excel file for the correct data
    tests = excel[excel['Experiment'] == setup_name]
    corr = tests[tests['Rev'] == revision]

    return corr.iloc[0]

def toePositions(nom):
    # Description of position of toe during experiments
    no = nom[2]
    if no == '1' or no =='4':
        wgpos = 27.36
    elif no =='2' or no =='5':
        wgpos = 27.36+0.216
    elif no =='3' or no =='6':
        wgpos = 27.36+0.216*2
    return wgpos

def checkOvertopping(testid, otexcel):
    # Check if overtopping and assign parameters
    names = ['SU1_IR18_1', 'SU1_IR26_1', 'SU1_IR27_1', 'SU1_IR27_2', 'SU2_IR08_1',
             'SU2_IR09_1', 'SU3_IR08_1', 'SU3_IR09_1', 'SU4_IR27_1', 'SU4_IR27_2']

```

```python
    if testid in names:
        OT = 'Y'
        sel = otexcel[otexcel.Test == testid]
        NOOT = len(sel)
        otdata = sel[['Event time (s)', 'Difference (mL)', 'Velocity top (m/s)']]
    else:
        OT = 'N'
        NOOT = 0
        otdata = np.nan

    return OT, NOOT, otdata

def calcSignificants(H, T):
    # Gives H1/3 and T1/3 using H and T values
    array = np.column_stack((H, T))
    sorted_array = array[np.argsort(array[:, 0])[::-1]]
    which = int(len(sorted_array) / 3)
    top3 = sorted_array[:which]
    return np.mean(top3[:,0]), np.mean(top3[:,1])

def calcPeakfreq(f, E, lim=(0.1, 5)):
    search = E.copy()
    search[f < lim[0]] = 0
    search[f > lim[1]] = 0
    return f[np.argmax(E)]

def getPercentile(runups, N, fraction, n_o_overtopping):
    # Calculates the percentile of a dataset using a total size different to the actual size
    index = N * fraction
    # Sort the array in descending order
    runups_sort = np.sort(runups)[::-1]
    # Determine the two closest indices
    index_below = int(np.floor(index))
    index_above = int(np.ceil(index))
    # Check to make sure indices are within array bounds
    if index_above >= len(runups_sort) or index_below < 0:
        raise ValueError("Hypothetical index is out of array bounds")
    if index <= n_o_overtopping:
        raise ValueError("Hypothetical index is smaller than number of overtopping events")

    # Get the two closest values from the array
    value_below = runups_sort[index_below]
    value_above = runups_sort[index_above]
    # Perform linear interpolation and return the result
    interpolated_value = (value_above - value_below) * (index - index_below) + value_below

    return interpolated_value

def calculateCDF(peaks, NW, noot=0):
    # Calculates the CDF with another size than the size of the dataset
    percentiles = np.arange(0.002, 0.90, step=0.001)
    ru_height = np.zeros_like(percentiles)

    for i, p in enumerate(percentiles):
        try:
            ru_height[i] = getPercentile(peaks, NW, p, noot)
        except ValueError:
            ru_height[i] = np.nan

    return percentiles, ru_height

def mainProcess(testid, experiments_excel, overtopping_excel, wavegauge_signal,
                runup_signal, fs_wg=200, fs_ru=23.976024, fftlength_minutes=3,
                height_dike=1.15, min_peak_height=0, min_peak_prominence=10,
                slope_dike = 1./3.6 ):

    # General info
    length = fftlength_minutes * 60 * fs_wg
    info = findExpInfo(experiments_excel, testid[:-2], float(testid[-1]))
    Rc = height_dike - info['d [cm]']/100.
    position_toe = toePositions(testid)
```

```
    # Load overtopping data
    OT, number_of_overtopping, overtopping_data = checkOvertopping(testid, overtopping_excel)

    # Wave gauge data
    wg_time = np.array(wavegauge_signal['t']).flatten()
    if testid == 'SU5_IR06_1':
        wg_offshore = wavegauge_signal['Etaig'][:, 2]
    else:
        wg_offshore = wavegauge_signal['Etaig'][:, 3]
    wg_toe = wavegauge_signal['Etaig'][:, -1]

    wg_lbcutoff_index = int(len(wg_time) * 0.1)
    wg_lbcutoff_time = wg_time[wg_lbcutoff_index]
    wg_hbcutoff_index = int(len(wg_time) * 0.9)

    wg_offshore_cut =  wg_offshore[wg_lbcutoff_index : wg_hbcutoff_index]
    wg_toe_cut = wg_toe[wg_lbcutoff_index : wg_hbcutoff_index]
    wg_time_lb = wg_time[wg_lbcutoff_index:]
    wg_time_lb_0 = wg_time_lb - wg_time_lb[0]
    wg_toe_lb = wg_toe[wg_lbcutoff_index:]

    zd_H_offshore, _, _, zd_T_offshore, _, _ = zc.zerodown(wg_offshore_cut, np.arange(0, len(wg_offshore_cut))/fs_wg)
    zd_H_toe, _, _, zd_T_toe, _, _ = zc.zerodown(wg_toe_cut, np.arange(0, len(wg_toe_cut))/fs_wg)

    H3_offshore, T3_offshore = calcSignificants(zd_H_offshore, zd_T_offshore)
    H3_toe, T3_toe = calcSignificants(zd_H_toe, zd_T_toe)

    E_offshore, f_offshore, _, _ = ws.wave_spectrum(wg_offshore_cut, length, fs_wg)
    E_toe, f_toe, _, _ = ws.wave_spectrum(wg_offshore_cut, length, fs_wg)
    Hm0_offshore, Tm1_offshore = ws.getHm0andTm1(f_offshore, E_offshore, 0, 5)
    Tp_offshore = calcPeakfreq(f_offshore, E_offshore)
    Hm0_toe, Tm1_toe = ws.getHm0andTm1(f_toe, E_toe, 0, 5)
    Tp_toe = calcPeakfreq(f_toe, E_toe)

    # Run-up data
    ru_time = runup_signal['time (s)'].to_numpy()
    ru_sig = runup_signal['runup-filtered (mm)'].to_numpy()
    ru_time_lb = ru_time[ru_time > wg_lbcutoff_time]
    ru_sig_lb = ru_sig[ru_time > wg_lbcutoff_time]
    _, _, _, _, nw, starts = zc.zerodown(wg_toe_lb, wg_time_lb_0)
    min_peak_distance = int(np.percentile(np.diff(starts), 1))

    ru_locs, _ = find_peaks(ru_sig_lb, height=min_peak_height, distance=min_peak_distance, prominence=min_peak_prominence)
    ru_peaks = ru_sig_lb[ru_locs]
    ru_peaks_noedit = ru_peaks.copy()
    ru_peaktime = ru_time_lb[ru_locs]

    if number_of_overtopping:
        bool_ru = np.full((len(ru_peaks)), False, dtype=bool)

        for i, t in enumerate(overtopping_data['Event time (s)']):
            try:
                j = np.where((ru_peaktime < t))[0][-1]
                bool_ru[j] = True
            except IndexError:
                continue

            ru_peaks[bool_ru] = Rc

    ru_dist_perc, ru_dist_height = calculateCDF(ru_peaks, nw, noot=number_of_overtopping)
    try:
        ru2p = getPercentile(ru_peaks, nw, 0.02, number_of_overtopping)
    except ValueError:
        ru2p = np.nan

    out = pd.Series(dtype='float')
```

```
    # General info
    out['ID'] = testid
    out['SU'] = int(testid[2])
    out['IR'] = int(testid[6:8])
    out['Rev'] = int(testid[-1])
    out['Comments'] = info['Comments']
    out['Veg'] = info['Vegetation']
    out['Lfs'] = position_toe - 15.07
    out['OT'] = OT
    out['NOOT'] = number_of_overtopping
    out['d'] = info['d [cm]']/100.
    out['dm'] = info['dm [cm]']/100.
    out['hc'] = info['hc [cm]']/100.
    out['Hs_wg'] = info['Hs [cm]']/100.
    out['s_wg'] = info['s [-]']
    out['Tp_wg'] = info['Tp [s]']

    # Run-up height
    out['ru2p'] = ru2p / 1000.

    # Wave info offshore
    out['Hm0_o'] = Hm0_offshore
    out['H3_o'] = H3_offshore
    out['Tm1_o'] = Tm1_offshore
    out['T3_o'] = T3_offshore
    out['Tp_o'] = Tp_offshore
    out['Lm1_o'] = Ldeepwater(Tm1_offshore)
    out['Lp_o'] = T2L(Tp_offshore, out['d'])
    out['sm1_o'] = Hm0_offshore / out['Lm1_o']
    out['sp_o'] = Hm0_offshore / out['Lp_o']
    out['xim1_o'] = slope_dike / np.sqrt(out['sm1_o'])
    out['xip_o'] = slope_dike / np.sqrt(out['sp_o'])
    out['xim1_H3_o'] = slope_dike / np.sqrt(H3_offshore / out['Lm1_o'])
    out['Up_o'] = Hm0_offshore * out['Lp_o']**2 / out['d']**3

    # Wave info dike toe
    out['Hm0_t'] = Hm0_toe
    out['H3_t'] = H3_toe
    out['Tm1_t'] = Tm1_toe
    out['T3_t'] = T3_toe
    out['Tp_t'] = Tp_toe
    out['Lm1_t'] = Ldeepwater(Tm1_offshore)
    out['Lp_t'] = T2L(Tp_toe, out['dm'])
    out['sm1_t'] = Hm0_toe / out['Lm1_t']
    out['sp_t'] = Hm0_toe / out['Lp_t']
    out['xim1_t'] = slope_dike / np.sqrt(out['sm1_t'])
    out['xip_t'] = slope_dike / np.sqrt(out['sp_t'])
    out['xim1_H3_t'] = slope_dike / np.sqrt(H3_toe / out['Lm1_t'])
    out['Up_t'] = Hm0_toe * out['Lp_t']**2 / out['dm']**3

    # Arrays
    arrays = pd.Series(dtype = 'object')

    arrays['H_zd_o'] = zd_H_offshore
    arrays['T_zd_o'] = zd_T_offshore
    arrays['H_zd_t'] = zd_H_toe
    arrays['T_zd_t'] = zd_T_toe
    arrays['E_o'] = E_offshore
    arrays['f_o'] = f_offshore
    arrays['E_t'] = E_toe
    arrays['f_t'] = f_toe
    arrays['ru_peaks'] = ru_peaks
    arrays['ru_peaks_noedit'] = ru_peaks_noedit
    arrays['ru_peaks_time'] = ru_peaktime
    arrays['ru_dist_perc'] = ru_dist_perc
    arrays['ru_dist_height'] = ru_dist_height

    return out, arrays
```